Material property targets for emerging nanomaterials to enable point-of-use and point-of-entry water treatment systems

Elvis A. Eugene, William A. Phillip, and Alexander W. Dowling*

Depatment of Chemical and Biomolecular Engineering, University of Notre Dame
Notre Dame, IN 46556

E-mail: adowling@nd.edu

Abstract

The scarcity of potable water is an imminent threat to at least half the world's population. Engineered nanomaterials (ENMs) have the potential to treat water from polluted sources to mitigate the scarcity of potable water. However, the performance demands on these materials in practical applications has not been studied in detail. This is but one of the challenges that hinder the widespread implementation of ENMs for water treatment. The emerging fit-for-purpose paradigm which encourages water treatment at the point-of-use (POU) or point-of-entry (POE) could lower the barrier for the use of ENMs in water technology by incorporating smaller, decentralized ENM-based treatment systems. This work develops a bottom-up and top-down modeling framework to facilitate the design of nanoporous membrane-based sorbents, a promising class of ENMs, for POU and POE water treatment applications. Langmuir isotherm and membrane structure-property calculations provide the multiscale link between molecular properties, including affinity, saturation capacity, and pore size, device design decisions, including membrane area and thickness, and system design decisions,

including sorbent mass and number of parallel modules. The framework predicts that for lead contaminants, existing materials are near molecular and systems limitations; improvements in the properties of adsorptive materials to treat lead will yield few benefits for POU and POE treatment systems. Moreover, the framework provides dimensionless formulas that apply to all adsorptive systems that exhibit (near) equilibrium behavior as an easy-to-use tool for the broader membrane science and environmental engineering communities to assess the feasibility of emerging materials to meet process demands. A case study regarding materials for arsenic removal demonstrates how to apply the modeling framework to calculate material properties targets and predict system performance for an arbitrary single-solute adsorption process. Finally, these dimensionless models are used to identify three distinct regions of relative performance between batch and semi-continuous processes. These results give caution to applying scale-up heuristics outside their valid region, which can lead to under- or over-design during bottom-up studies. The presented modeling framework is a crucial step to fully optimize engineered nanomaterials across material, device, and system scales.

Introduction

In the next three decades, more than half of the world's population will likely face scarcity of clean water for at least one month each year.[1] A myriad of pollutants and the vast complexity of the interactions between human and natural water systems prevents the development of a panacea water treatment technology. For example, contamination of potable water resources by trace quantities of metals such as lead and arsenic is prevalent across the globe.[2–4] Lead can enter water as it travels through lead-based plumbing networks,[5] and when ingested, it hinders cognitive development.[6] Chronic exposure to arsenic, which occurs naturally in groundwaters surrounded by rocks or soil rich in the metal leads to cancer and skin lesions.[7] While the problem of trace metallic contaminants is well known, regulatory bodies across the world are monitoring the increase in emerging contaminants (ECs) in global drinking

water sources.[8] Pharmaceutical and personal care products (PPCPs) are one such class of ECs that can enter the water cycle through the excretions of humans and animals.[9] The concentration of PPCPs in the environment is not legally regulated, because of which most conventional water treatment plants do not separate PPCPs from water. The effect of PPCP contamination in drinking water on human health is not yet well known. However, even in small doses, they have been shown to have detrimental effects on aquatic life, which leads researchers to believe that they could be a cause for long term ecological stress and toxicity.[10] Effluents from wastewater plants also add nitrogen and phosphorus to aquatic and marine systems, which results in eutrophication[11] that leads to deleterious effects in water treatment systems and threatens water security.[12] Pathogens like antibiotic-resistant coliform bacteria which cause health issues such as gastroenteritis in humans may also enter the drinking water cycle via improperly treated or disposed of sewage and agricultural drainage into surface and groundwaters.[13]

Engineered nanomaterials (ENMs) possess physical and chemical properties that are different from their macroscale precursors, which can be tailored to create new technological solutions that address limitations of existing water treatment systems, e.g., inabilities to economically treat emerging contaminants.[14,15] Examples of such materials include ultrathin iron oxychloride (FeOCl) nanosheets which demonstrate high selectivity in adsorbing lead from aqueous solutions;[16] Magnetite (Fe_3O_4) nanocrystals which possess high specific surface area and can remove large quantities of arsenic from water;[17] metal-organic frameworks (MOFs) which have controlled, permanent, pore sizes and are useful in the removal of PPCPs from water;[8] silver (Ag) and graphene oxide (GO) nanoparticles which have antibacterial properties and are effective even against antibiotic-resistant strains.[18,19] Despite the promise of ENMs, several challenges hinder their widespread use in water treatment applications. While the performance of ENMs in controlled, ideal, synthetic polluted water conditions is well studied, their performance in the real world with multiple contaminants whose compositions vary over time is yet to be determined.[20] By extension, detailed process design and

systems engineering analyses are needed to understand how to optimally utilize ENMs in a real-world end-user application. The feasibility of sustainable, defect-free production of ENMs at the large scale is yet to be assessed.[21] With regards to sustainability, the efficient regeneration of ENMs for repeated use and the safe disposal of generated waste streams must also be addressed.[22]

The emerging fit-for-purpose (FFP) paradigm of water treatment[23] provides opportunities to tackle some of the challenges faced by conventional water treatment technologies. In the FFP paradigm, decentralized water treatment systems close to the point-of-use (POU) or at the point-of-entry (POE) of communities such as villages or housing complexes incorporate regenerative treatment technologies to provide water tailored to use specification. Potable and non-potable water (say, for landscape irrigation) are treated in different modular units using a suitable technology option. Individual modules in FFP water treatment systems will see less throughput than their centralized analogs, which could enable the economical incorporation of small quantities of ENMs into water treatment systems. Resource recycling such as the recovery of nitrogen and phosphorus from human excreta[24,25] will be a critical contributor to the cost-effectiveness of FFP systems. Recycling reduces the amount of wastewater generated, thereby lowering the cost and energy required for its treatment. The sale of recovered nutrients can provide additional revenue which may be used to offset the costs associated with an ENM-based POU or POE water treatment system.

Yet, there is a consensus that improving material properties alone is not sufficient to realize next-generation water treatment systems.[20,23,26] Multidisciplinary research integrating materials-, computational-, data-sciences, and molecular-to-systems design frameworks is needed to create breakthrough fit-for-purpose water technologies. Holistic computational frameworks that utilize techniques from process systems engineering can overcome the challenges inhibiting the development of ENM-based FFP water treatment technologies by explicitly linking material properties to application-specific goals.[27] In the bottom-up approach, holistic computational frameworks can unite competing objectives and metrics across molec-

ular, material, device, system, and infrastructure scales to identify material characteristics that significantly influence operating parameters for next-generation water treatment systems. Systems-level studies using emerging materials can also identify optimum process vessel and network configurations that maximally utilize characteristic properties of the candidate material for water treatment. Infrastructure level design can optimize the location of centralized nanomaterial regeneration and waste recycling or disposal units to meet sustainability goals. In the top-down approach, holistic computational frameworks enable inverse design by predicting material properties required for a desired system or infrastructure level goal. This paper develops both bottom-up predictions of ENMs in adsorption systems as well as top-down analysis to set quantitative material property targets needed to meet overall system design goals.

Adsorptive nanoporous membranes are an emerging class of nanomaterials whose promise arises from their multifunctional nanostructure, which is controlled during synthesis to target specific contaminants such as lead.[28] Once depleted, these membranes can be reused after regeneration using external stimuli such as pH swings.[28,29] Their ability to selectively extract contaminants from water and their reusability makes adsorptive nanoporous membranes an attractive option for integration into FFP water treatment systems. Furthermore, a high density of nanopores in the membrane enables very low mass-transfer resistance when compared with conventional packed bed adsorption. Readily scalable techniques used in the synthesis of these membranes also promote their consideration in the implementation of sustainable FFP water treatment systems.[30,31] Despite their promise, no detailed studies of adsorptive membrane materials in a POU or POE context have been performed. The objective of this paper is to present a generalized bidirectional molecular-to-systems scale analysis framework for adsorptive treatment systems.

The unfortunate conflux of several factors increased the corrosivity of water transmitted in the pipelines of Flint, Michigan,[32] leading to ingress of lead in the water supply, resulting in elevated blood lead levels in children, likely causing long-term health consequences.[33]

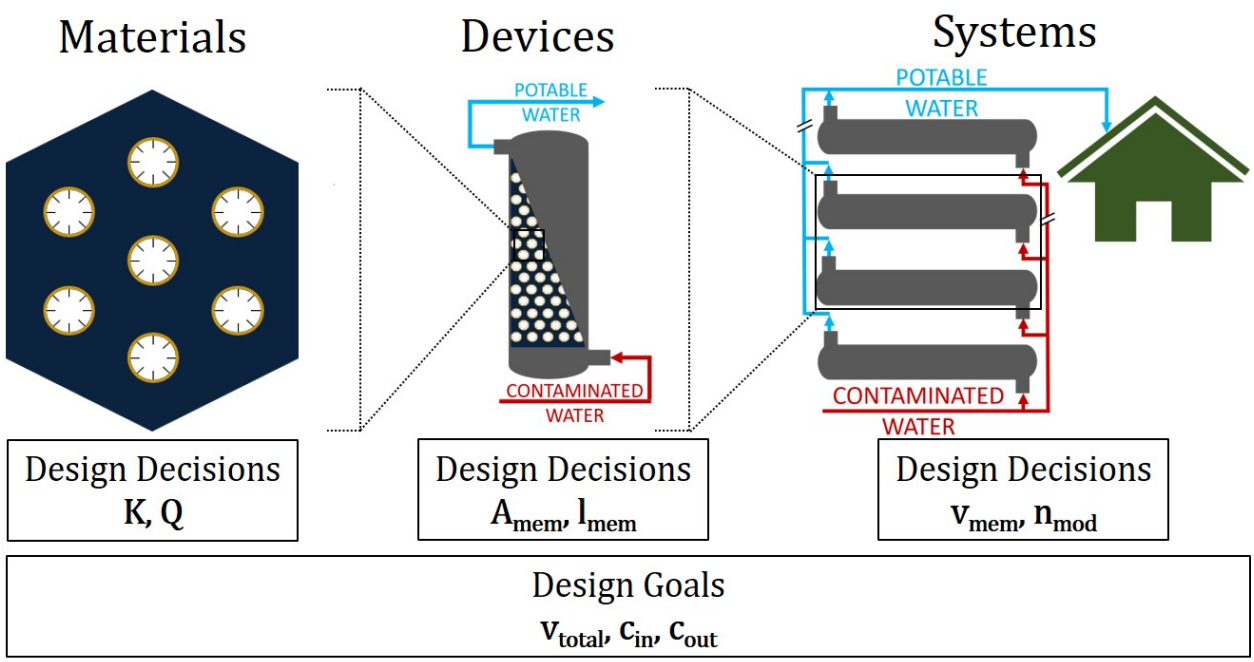

Figure 1: This work proposes multiscale mathematical models to rapidly screen and design adsorptive nanoporous membranes for contaminant (e.g., lead, arsenic) removal. The **overall design goal** is to treat v_{total} volume of water from an inlet contamination concentration c_{in} to an acceptable concentration c_{out}. The bidirectional framework simultaneously considers the **materials scale** characteristics binding affinity K and saturation capacity Q, **device scale** decisions including membrane area A_{mem} and thickness l_{mem}, and **systems scale** decisions including membrane volume v_{mem} and number of parallel modules n_{mod}. In **bottom-up mode**, we consider an existing or hypothetical material (K and Q are given) and predict the device and system scale performance. In **top-down mode**, we determine the material scale properties K and Q required to meet system scale goals such as utilization of less than 10 kg of engineered nanomaterials.

Conventional design techniques for adsorption-based treatment systems already rely on equilibrium models.[26] These models are often empirical correlations[34] or are fit from scale-up (bench to pilot-scale) studies. However, this work presents a modeling framework for the design of adsorptive nanoporous membrane-based modular water treatment systems by directly linking systems performance to material properties (see Fig. 1). By explicitly considering different goals at the materials, devices, and systems scales, macromolecular and process constraints are directly integrated into a multiscale mathematical model. Using a top-down approach, the feasible materials design space which includes the membrane properties of

saturation capacity, binding affinity, and porosity is defined. In conjunction, the process parameters such as flow rate and contaminant concentration of the source and treated water are considered. Bottom-up analysis shows that materials possessing the properties needed to enable next-generation water treatment systems already exist but need to be analyzed from a systems or infrastructure level perspective to maximally utilize material properties, e.g., deployed in hybrid water treatment systems with an adsorptive polishing step. Dimensionless extensions to the models and framework allow the analysis of an arbitrary single-solute adsorptive separations process, not restricted to lead removal from water. This framework also provides insight into the competitive behavior of adsorption processes operated in batch and semi-continuous mode. Mathematical definitions for regions where one process configuration behaves superior to the other are provided, along with their implications during scale-up studies. Extensions to the completed analysis utilizing alternate isotherm models and kinetic effects are planned.

The remainder of this article is structured as follows. First, the Methods section enumerates the assumptions and mathematical models that form the basis of this work. Next, the Results and Discussion section presents three case studies: (i) material property targets are derived for POU removal of lead; (ii) batch and semi-continuous processes are compared, revealing conditions where common scale-up heuristics fail; (iii) top-down and bottom-up analyses of arsenic removal illustrate the versatility of the generalized modeling framework. Finally, conclusions and future work are presented.

Methods: Mathematical Model

This section (i) defines the batch and semi-continuous process configurations, (ii) enumerates key assumptions, (iii) derives system scale mathematical models for both configurations, (iv) defines structure-property equations that link material and device scales, and (v) defines module design equations that link device and system scales.

Process configurations for adsorption process: batch and semi-continuous

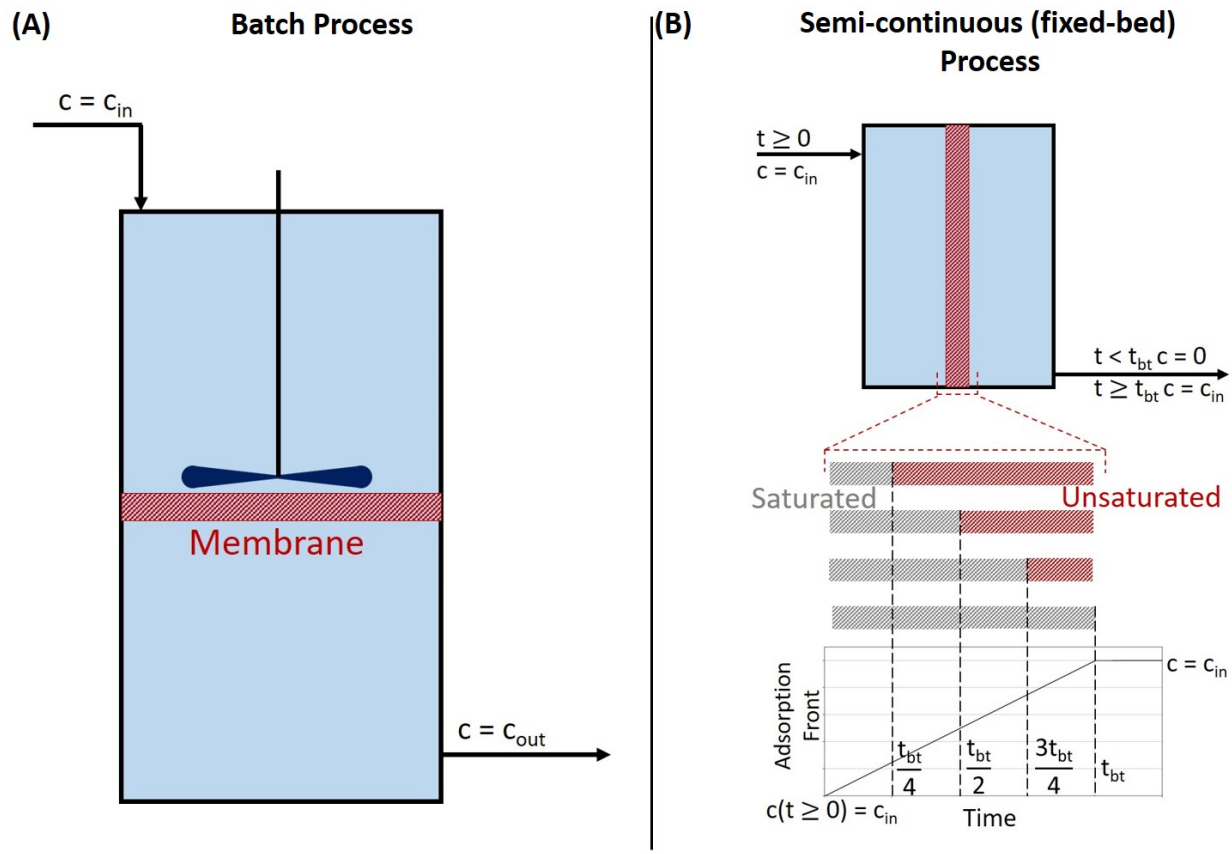

Figure 2: Schematic representation of batch (A) and semi-continuous (B) operating modes of the adsorptive treatment process. **(A)** When operating in **batch mode**, at the start of the process contaminated water with concentration c_{in} is allowed to equilibrate with the adsorptive membrane inside a well-mixed tank. At the end of the process, the concentration of the contaminant in water c_{out} is in equilibrium with the solute bound to the sorbent. **(B)** In the **semi-continuous mode**, at the beginning of the process ($t \geq 0$), contaminated water with concentration c_{in} starts to flow across the membrane at a constant flow rate. Under the model assumptions, till the membrane attains breakthrough at time t_{bt}, the contaminant in the water is adsorbed by the membrane, resulting in treated water leaving the membrane module containing no dissolved solute. The membrane is saturated with the contaminant at breakthrough. No adsorption occurs after t_{bt} and the water leaving the membrane module has the same concentration as that at the inlet, c_{in}.

This analysis considers the two operating modes for the adsorption process shown in Fig. 2: batch and semi-continuous. Batch adsorption is convenient to treat small quantities of solutions, for example, in the pharmaceutical industries or in laboratory settings where

it is frequently employed to characterize sorbent properties.[35] Batch processes operate until equilibrium, which is governed by an isotherm relationship. Since the final concentration of the solution is in equilibrium with the solute bound to the sorbent surface, batch processes offer the advantage of treating the solution to the exact specification of the intended application. However, the volume of a stirred-tank (see Fig. 2(A)) is directly proportional to the volume of treated solution, making batch adsorption impractical for large scale applications.

As a consequence, adsorption processes are operated in fixed or packed-bed mode, hereafter referred to as semi-continuous mode. In this mode, the solution to be treated is allowed to flow over the adsorbent at a constant flow rate (Fig. 2(B)). Ideally, this dynamic process over-treats the solution to remove nearly all of the contaminant(s) until breakthrough. At breakthrough, the adsorbent is entirely saturated, and adsorption stops, necessitating the regeneration of the sorbent. A key advantage of semi-continuous systems is they require orders of magnitude smaller equipment than an equivalent batch process.

Assumptions

Key modeling assumptions are listed below.

Sorbent structure

We assume the adsorptive membranes have an isotropic structure with a constant pore diameter over its cross-section. The porosity of the membrane is $\varepsilon = 0.3$. We assume that the materials used to form the solid matrix of the sorbents have density $\rho_{mat} = 1.0$ g cm^{-3}. This gives a sorbent density of $\rho_{mem} = (1-\varepsilon) \times \rho_{mat} = 0.7$ g cm^{-3}. All values are consistent with recent literature.[28,29,31]

Sorbent isotherm

The equilibrium loading q of the membrane is related to the concentration of the treated water c using the Langmuir isotherm:

$$q = \frac{KQc}{1 + Kc} \tag{1}$$

In Eq. (1), the binding affinity K and saturation capacity Q are structure-dependent properties of the membrane sorbent.

Process design

We assume that the membrane is fully regenerated at the beginning of the process, i.e., $q(t = 0) = 0$. We neglect mass transfer effects. We note that in practice, semi-continuous adsorption is governed by mass transfer resistances which give rise to time- and spatially-varying concentration profiles in the bed. Since we neglect mass transfer effects in the semi-continuous process, the sorbent is saturated at breakthrough and must be regenerated. The batch process models assume (i) feed water for treatment is maintained as a well-mixed solution in the tank and (ii) the process stops when water reaches the desired outlet concentration c_{out}.

Module design

In designing modules, we assume that the membranes are manufactured as spiral wound or pleated modules with a maximum thickness of $l_{sp} = 1$ mm. We assume that each module has a constant membrane area of $A_{mem} = 30$ m^2.[36] The thickness of the membrane in the module is governed by process requirements. We assume that n_{mod} number of parallel membrane modules will be used when the process requirement cannot be met by the limits set by l_{sp} and A_{mem}.

Household requirements for point-of-use (POU) application

We consider two point-of-use systems to treat water with inlet lead contaminant concentrations of $c_{in} = 100$ ppb, similar to levels measured in Flint, Michigan.[37] The goal is to produce water at or below the limit prescribed by the United States Environmental Protec-

tion Agency (US-EPA), i.e., $c_{out} = 15$ ppb of lead.[38] We assume a small household uses 30 m^3 per year of water for consumtion.[39] In the first design, $\mathbf{POU_{24}^{C}}$, we consider regeneration after $t_{total} = 24$ months. In the second design, $\mathbf{POU_{6}^{C}}$, we consider regeneration after $t_{total} = 6$ months. Both designs assume that water is supplied at a standard household pressure such that the pressure drop across the membrane is $\Delta P = 65$ psi. We use superscript ^{C} to indicate that the point-of-use system is operated in semi-continuous mode. We use $\mathbf{POU_{24}^{B}}$ and $\mathbf{POU_{6}^{B}}$ to identify batch-mode equivalents of $\mathrm{POU_{24}^{C}}$ and $\mathrm{POU_{6}^{C}}$, respectively.

Batch process models as baseline representations of laboratory experiments

We start with the solute mass conservation equation for the batch process:

$$v_{total}\left(c_{in} - c_{out}\right) = (1-\varepsilon) v_{mem} \frac{K Q^{B} c_{out}}{1 + K c_{out}} \tag{2}$$

In Eq. (2), v_{total} and v_{mem} are the quantity of water to be treated and volume of the adsorbent required for the process, respectively. The superscript ^{B} indicates a batch process. Eq. (2) is rearranged to obtain the material property target model for the batch process:

$$Q^{B} = \frac{1}{1-\varepsilon} N_{BV}\left(c_{in} - c_{out}\right) \frac{1 + K c_{out}}{K c_{out}}, \qquad N_{BV} = \frac{v_{total}}{v_{mem}} \tag{3}$$

In Eq. (3), ε is the void fraction of the membrane and N_{BV} is number of bed volumes treated. Q^{B} is in volume basis and can be converted to a mass basis by dividing with the sorbent density ρ_{mem}. Thus Eq. (3) gives the relationship between material characteristics K, Q and operational parameters v_{mem}, c_{in}, and c_{out}.

We generalize the batch process model by introducing the dimensionless binding affinity

$\overline{K}$, saturation capacity $\overline{Q}$ and removal ratio r:

$$\overline{K} = Kc_{in} \qquad \overline{Q} = \frac{Q}{c_{in}} \qquad r = \frac{c_{in}}{c_{out}} \tag{4}$$

Substituting Eq. (4) into Eq. (3) gives the dimensionless material property targets:

$$\overline{Q^B} = \frac{1}{1-\varepsilon} N_{BV} \left(1 - \frac{1}{r}\right) \frac{r + \overline{K}}{\overline{K}} \tag{5}$$

We rearrange Eqs. (3) and (5) to compute the number of bed volumes N_{BV}^B that can be treated by a batch process before regeneration:

$$N_{BV}^B = \frac{(1-\varepsilon)\, Q^B K c_{out}}{(c_{in} - c_{out})\,(1 + K c_{out})} = \frac{(1-\varepsilon)\, \overline{Q^B}\, \overline{K}}{\left(1 - \frac{1}{r}\right)\left(r + \overline{K}\right)} \tag{6}$$

In the results section, we perform a sensitivity analysis of Eq. (5) with respect to N_{BV} and $\overline{K}$ to compute the material design space. We emphasize that because Eq. (5) is dimensionless, it is independent of the specific adsorbent, contaminant, and design goals, and is thus broadly applicable to all adsorption-based processes. In the Supporting Information, we report sensitivity analysis figures of Eq. (3) which defines the material design space for $\mathrm{POU}_6^{\mathrm{B}}$ and $\mathrm{POU}_{24}^{\mathrm{B}}$, and of Eq. (6) to enable the reader to quickly compute material property targets for their application and system of interest.

Semi-continuous process models for water treatment systems

Semi-continuous adsorption processes overcome the limitations of a batch process by offering nearly complete solute removal up to breakthrough utilizing smaller equipment. The models for the semi-continuous adsorption process are derived from the conservation equation:[40]

$$\left[1 + \beta \frac{\partial q(c)}{\partial c}\right] \frac{\partial c}{\partial t} + V \frac{\partial c}{\partial z} = 0 \tag{7}$$

In Eq. (7), z is the spatial coordinate normalized by the thickness of the membrane sorbent. β and V are the phase ratio and interstitial velocity, respectively:

$$\beta = \frac{1-\varepsilon}{\varepsilon} \qquad V = \frac{v_{total}}{\varepsilon\ A_{mem}\ t_{total}} \tag{8}$$

In Eq. (8) t_{total} is the time available to treat v_{total} m^3 of water before regenerating the membrane. Solving the conservation equation (7) gives the breakthrough time:

$$t_{bt} = \frac{l_{mem}}{V}\left(1 + \beta\frac{q(c_{in})}{c_{in}}\right) \tag{9}$$

We highlight that the membrane must be regenerated as soon as the treated water concentration exceeds c_{out}. However, since we assume no mass transfer effects, the sorbent will be regenerated once it achieves breakthrough.

Next, we extend the conventional conservation equations for the semi-continuous process to a material property target model. Substituting the Langmuir isotherm in Eq. (1) into Eq. (9) and rearranging gives material property target equation for the semi-continuous adsorption process:

$$Q^C = \frac{1}{1-\varepsilon} \times (N_{BV} - \varepsilon) \times \frac{1 + Kc_{in}}{K} \qquad \forall\ N_{BV} > \varepsilon \tag{10}$$

As before, Q^C can be converted from a volume basis to a mass basis using the density of the sorbent. Substituting Eq. (4) into Eq. (10) gives the more general, dimensionless semi-continuous material property relationship:

$$\overline{Q^C} = \frac{1}{1-\varepsilon}\,(N_{BV} - \varepsilon)\,\frac{1+\overline{K}}{\overline{K}} \qquad \forall\ N_{BV} > \varepsilon \tag{11}$$

Eq. (10) and Eq. (11) are valid only for $N_{BV} > \varepsilon$, which corresponds to an operating assumption that the quantity of water treated by the adsorbent is greater than the pore volume of the membrane sorbent. We can rearrange Eq. (10) and Eq. (11) to compute the number of

bed volumes N_{BV}^{C} that can be treated by a semi-continuous process before regeneration:

$$N_{BV}^{C} = \frac{(1-\varepsilon)\, Q^{C} K}{1 + K c_{in}} + \varepsilon = \frac{(1-\varepsilon)\, \overline{Q^{C}}\, \overline{K}}{1 + \overline{K}} + \varepsilon \tag{12}$$

In the results section, we use the sensitivity analysis of Eq. (10) with respect to material property K and operating parameter N_{BV} to define the feasible material design space for $\mathrm{POU}_{24}^{\mathrm{C}}$ and $\mathrm{POU}_{6}^{\mathrm{C}}$. We also use Eq. (11) to show the sensitivity of $\overline{Q^{C}}$ with respect to material property $\overline{K}$ and operating parameters N_{BV} and r to define the material design space for a generic adsorption process. Extensive results are given in the Supporting Information to empower the reader to calculate material property targets for both batch and semi-continuous systems for their application and material of choice.

Material constraints

Eqs. (3) and (10) give minimum saturation capacities Q for a given binding affinity K and separation specifications N_{BV} and r based on a macroscopic mass balance and thermodynamic equilibrium. We now consider the restrictions based on structure-property relationships. Specifically, the saturation capacity is limited by the amount of solute that fits into the pores, which can be estimated based on a monolayer of coverage and the molar volume of the solute:

$$Q \leq \frac{4\varepsilon}{d_p} \frac{1}{(\pi N_A)^{\frac{1}{3}}} \left(\frac{4}{3\, \overline{v_s}} \right)^{\frac{2}{3}} \tag{13}$$

where d_p is the pore diameter of the membrane, N_A is Avogadro's number, and $\overline{v_s}$ is the molar volume of the contaminant solute.

Moreover, the minimum pore diameter d_p is constrained by the typical applied pressure and required process flow:

$$d_p \geq \left(\frac{N_{BV}}{t_{total}} \frac{128 \mu l_{mem}^{2}}{N \pi \Delta P} \right)^{\frac{1}{4}} \tag{14}$$

In Eq. (14), μ is the viscosity of the solution, N is the number of pores per unit area of the

membrane, and ΔP denotes the pressure drop available for the treatment process.

In the results section, we show how Eqs. (10), (13) and (14) define a more restricted feasible material design space.

Number of parallel modules

The minimum number of parallel membrane modules (n_{mod}) is:

$$n_{mod} = \left\lceil \frac{v_{mem}}{A_{mem} l_{sp}} \right\rceil \tag{15}$$

In Eq. (15), $\lceil \cdot \rceil$ is the ceiling function which rounds up a fraction to the next highest integer. Recall that l_{sp} is the maximum thickness of membrane in a spiral wound or pleated module. We assume the final membrane thickness is equal in each of the parallel modules:

$$l_{mem} = \frac{v_{mem}}{A_{mem} n_{mod}} \leq l_{sp} \tag{16}$$

Results and Discussion

Eqs. (10), (13) and (14) are first used to identify the feasible design space for $\mathrm{POU}_{24}^{\mathrm{C}}$ and $\mathrm{POU}_{6}^{\mathrm{C}}$. Next, the dimensionless models in Eqs. (5) and (11) are used to illustrate the need for caution in predicting the scaled-up performance of materials characterized in laboratories and quantify criteria needed for accurate performance predictions. Finally, a generic adsorption process is analyzed using the dimensionless models.

Case study: Point-of-use (POU) water treatment using adsorptive membranes

Eqs. (6) and (12) were applied to calculate the required mass to deploy nine recently-reported sorbents (***A*** - ***I***) in POU water treatment systems to treat lead contamination. These results,

shown in Table 1, are easy to calculate. Therefore, Eqs. (6) and (12) gives a straightforward way to quickly determine if a new material is well-suited for a given application.

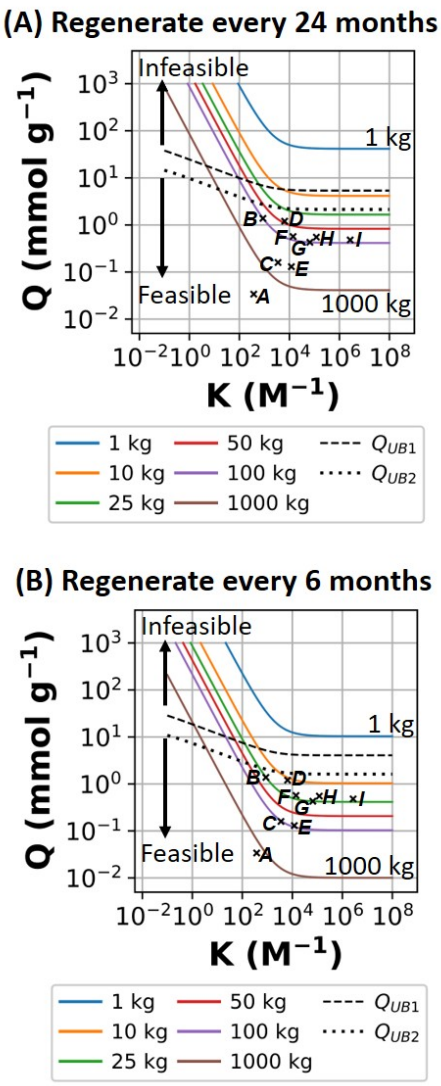

Figure 3: Material property targets for semi-continuous adsorption $\mathrm{POU}_{24}^{\mathrm{C}}$ (top, A) and $\mathrm{POU}_{6}^{\mathrm{C}}$ (bottom, B) systems for lead removal. Binding affinity K and saturation capacity Q are material properties in the Langmuir isotherm Eq. (1). The **solid colored contours** show the required Q and K to meet the separation specifications with 1 kg to 1000 kg of total adsorbent mass. These curves were computed by sensitivity analysis of Eq. (10) with respect to the binding affinity K and required amount of membrane v_{mem}. The **dashed lines** display the upper bound on saturation capacity determined by the process and material constraints implied by Eq. (10), Eq. (13), and Eq. (14). Details of their calculation are provided in the SI. Upper bounds Q_{UB1} (dashes) and Q_{UB2} (dots) correspond to membrane thicknesses $l_{mem} = 0.1$ mm and 1 mm, respectively. The **letters *A* to *I*** correspond with the materials summarized in Table 1.

Table 1: The properties of existing lead adsorbents ***A*** to ***I*** were utilized to predict the material mass required for deployment in point-of-use water treatment systems operated in batch and semi-continuous operating modes using Eqs. (6) and (12), respectively. Recall $\mathrm{POU}_{24}^{\mathrm{C}}$ and $\mathrm{POU}_{6}^{\mathrm{C}}$ are sized to treat the water consumption in a two-person US household with regeneration every 24 and 6 months, respectively. As such, $\mathrm{POU}_{24}^{\mathrm{C}}$ requires 4 times as much of the same adsorbent as $\mathrm{POU}_{6}^{\mathrm{C}}$. Moreover, material ***D***, whose binding affinity is an order of magnitude greater than that of ***B*** requires less than half of the quantity of ***B*** for $\mathrm{POU}_{24}^{\mathrm{C}}$. At low binding affinity K, the quantity of sorbent required for batch adsorption is greater than semi-continuous adsorption. With increasing binding affinity K, a crossover point is observed at which both operating modes require identical quantities of sorbent. When K is increased beyond the crossover point, the batch process requires less sorbent than the semi-continuous process. This crossover behavior is explained subsequently. *The Supporting Information describes each material in detail.

Legend identifier	Material*	K (M^{-1})	Q (mmol g^{-1})	$\mathrm{POU}_{24}^{\mathrm{C}}$ (kg)	$\mathrm{POU}_{24}^{\mathrm{B}}$ (kg)	$\mathrm{POU}_{6}^{\mathrm{C}}$ (kg)	$\mathrm{POU}_{6}^{\mathrm{B}}$ (kg)	Reference
A	SI-APTS-EDTA	3.8×10^{2}	3.4×10^{-2}	7.5×10^{3}	4.0×10^{4}	1.9×10^{3}	9.8×10^{3}	Gomes et al.[41]
B	PI-PS-PASH	8.7×10^{2}	1.4	1.0×10^{2}	4.3×10^{2}	25	1.1×10^{2}	Weidman et al.[28]
C	PS-EDTA resin	3.5×10^{3}	1.6×10^{-1}	4.1×10^{2}	1.1×10^{3}	1.0×10^{2}	2.7×10^{2}	Wang et al.[42]
D	Psf-Terp	6.4×10^{3}	1.2	46	93	11	23	Zhang et al.[43]
E	EDTA-PCF	1.2×10^{4}	1.3×10^{-1}	3.7×10^{2}	5.8×10^{2}	93	1.4×10^{2}	Tanhaei et al.[44]
F	EDCMS	1.4×10^{4}	5.7×10^{-1}	83	123	21	31	Ren et al.[45]
G	Magnetic Fe_3O_4 yeast treated with EDTA dianhydride	6.6×10^{4}	4.3×10^{-1}	99	99	25	25	Xu et al.[46]
H	Fe_3O_4@SiO_2–EDTA	1.2×10^{5}	5.5×10^{-1}	77	71	19	18	Liu et al.[47]
I	Mag-Ligand	2.7×10^{6}	4.8×10^{-1}	86	73	22	18	Huang and Keller[48]

Fig. 3 juxtaposes two fundamental phenomena that constrain the adsorptive system design. The colored contours show the required sorbent mass as a function of material properties K and Q arising out of the conservation relationship Eq. (10). In contrast, the black dashes/dots show the size limitations related to membrane thickness (pressure drop), pore diameter d_p, and saturation capacity Q. The area below the dashed lines forms the feasible design space for a POU water treatment system. This figure yields three key findings:

- $\mathrm{POU}_6^{\mathrm{C}}$ (Fig. 3(B)) can be realized by using sorbents with lower saturation capacity Q when compared with $\mathrm{POU}_{24}^{\mathrm{C}}$ (Fig. 3(A)), because the sorbent is regenerated 4-times more frequently in the former process. This observation is apparent from Fig. 3(B) for $\mathrm{POU}_6^{\mathrm{C}}$ in which the mass contours have been shifted vertically downwards when compared with the contours in Fig. 3(A) for $\mathrm{POU}_{24}^{\mathrm{C}}$.

- The asymptote observed in the mass lines at high binding affinity K is defined by the contaminant concentration in the feed c_{in}, and hence starts from the same K in Figs. 3(A) and (B). The asymptote demonstrates limited benefits to $\mathrm{POU}_{24}^{\mathrm{C}}$ and $\mathrm{POU}_6^{\mathrm{C}}$ by improvements in binding affinity K in this application. For solutes present at lower concentrations, improvements in binding affinity may be necessary.

- The black dots in Fig. 3 show the bound on the feasible saturation capacity Q calculated as a function of pore size and membrane thickness using Eq. (13). Using thinner membranes allows the use of smaller pore diameters and this increases the upper bound on saturation capacity Q up to the black dashes. However, there may be minimal scope to improve on this upper bound as a finite pore diameter is required for the adsorption of the contaminant.

These findings have several implications in the design of adsorptive water treatment systems. While material $\boldsymbol{D}$ is the most promising, at least 46 kg is required for $\mathrm{POU}_{24}^{\mathrm{C}}$, which is regenerated every 24 months, or 11 kg for $\mathrm{POU}_6^{\mathrm{C}}$, which is regenerated 4 times as frequently. Material constraints (dashed lines) prevent using less than 10 kg of an adsorbent

for this application, suggesting a treatment system using $\boldsymbol{D}$ would need to be regenerated more frequently than every 6 months. Conservative estimates of weight of sorbent and module footprint impose a practical limitation of no more than 100 kg of membrane in the POU application to maximize user convenience; this precludes the use of materials $\boldsymbol{A}$, $\boldsymbol{C}$, and $\boldsymbol{E}$ for $\mathrm{POU}_{24}^{\mathrm{C}}$ as seen in Fig. 3(A) and material $\boldsymbol{A}$ for $\mathrm{POU}_{6}^{\mathrm{C}}$, shown in Fig. 3(B). Lead mitigation is challenging because contamination can come from the distribution system which necessities point-of-use treatment. But for other contaminants (e.g., those in rivers or groundwater), point-of-entry (POE) of housing communities or industrial parks with parallel trains of sorbent modules may be the most feasible application.

Most striking, Fig. 3 shows there is virtually no opportunity to improve $\mathrm{POU}_{24}^{\mathrm{C}}$ nor $\mathrm{POU}_{6}^{\mathrm{C}}$ from improvements in material properties K and Q. This suggests novel adorption-based lead mitigation technologies in the fit-for-use paradigm are not limited by innovations at the materials scale. Instead, device and systems scale studies of existing materials incorporating higher-order effects such as mass transfer limitations will prove beneficial in developing novel water treatment systems. These studies are envisioned to provide insights into the optimal utilization of material characteristics while accounting for their limitations. For example, the sustainable operation of the sorbents will require them to be regenerated and reused. Regeneration processes typically occur under harsh operating conditions (high temperature, low pH). Therefore, it is likely that centralized regeneration plants catering to multiple POU or POE systems will be needed to ensure safety and cost-efficiency of the regeneration process, so that the consumer may swap out depleted adsorbent modules with fresh modules, similar to a propane tank switch. Thus, realizing the fit-for-purpose paradigm of water treatment systems will also see a key role played by infrastructure level design for the location of POE or POU systems, regeneration plants, and the interconnections among these units and their connection to the existing water network.

Need for caution in scaling up laboratory performance of materials to systems level

Recall, Eqs. (5) and (11) are non-dimensional and apply to all adsorptive processes operated in batch and semi-continuous modes. These equations predict the required saturation capacity $\overline{Q}$ as a function of other material properties and operating parameters. Fig. 4 shows sensitivity analysis of Eqs. (5) and (11) and reveals three distinct types of relative behavior between the batch and semi-continuous processes.

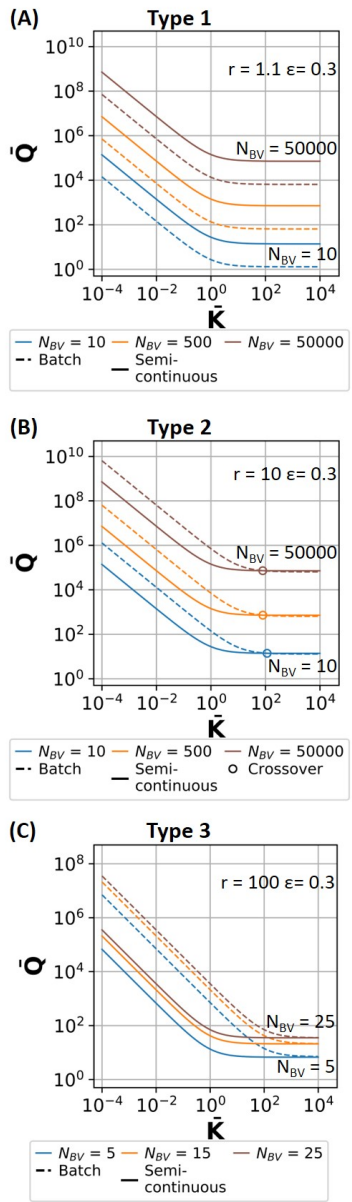

Figure 4: Binding affinity $\bar{K}$ targets are calculated as a function of saturation capacity $\bar{Q}$, and porosity of the adsorbent ε and operating parameters number of bed volumes processed N_{BV} and removal ratio r using Eqs. (5) and (11). This reveals three distinct regions for relative performance between the batch and semi-continuous processes. The **dashed contours** show Eq. (5) (batch process) and the **solid contours** show Eq. (11) (semi-continuous process). **(A)** At low removal ratios, **Type 1** behavior is observed. The batch process outperforms the semi-continuous process, i.e., the batch process requires a lower $\bar{Q}$ compared to a semi-continuous process at the same $\bar{K}$ and N_{BV}. **(B)** At moderate removal ratios, we observe **Type 2** behavior. At smaller $\bar{K}$, the semi-continuous process performs better, i.e., it requires smaller $\bar{Q}$ than the batch process at the same r and N_{BV}. At the crossover point denoted by the circle, the batch and semi-continuous processes perform identically. At $\bar{K}$ larger than the crossover point, the batch process is superior. **(C)** Finally, for large r we observe **Type 3** behavior. The semi-continuous process requires a lower $\bar{Q}$ compared to the batch process at all $\bar{K}$. The common heuristic that scaling-up from batch bench-scale experimental data to semi-continuous process will give the same or better performance is only valid in the Type 3 region.

- Fig. 4 (A) shows **Type 1** behavior: the batch process requires a lower saturation capacity $\overline{Q}$ than the semi-continuous process at the same binding affinity $\overline{K}$, bed volume N_{BV}, and removal ratio r. We caution the scale-up analysis of batch experiments in the type 1 regime, which occurs at small removal ratios r; the heuristic that semi-continuous process will always outperform a batch process is incorrect here. For example, a batch process with $\overline{Q} = 65$, $\overline{K} = 10^3$, and $r = 1.1$ can treat $N_{BV} = 500$ bed volumes. In contrast, a semi-continuous process at the same $\overline{Q}$, $\overline{K}$, only treats $N_{BV} = 46$ bed volumes under the same conditions.

- Fig. 4 (B) shows **Type 2** behavior: at low binding affinities $\overline{K}$, the semi-continuous process requires a smaller saturation capacity $\overline{Q}$ than the batch process to treat the same number of bed volumes N_{BV} at the same removal ratio r. At an intermediate $\overline{K}$, i.e., the crossover point, the batch and semi-continuous processes perform identically. At binding affinities larger than the crossover point, the batch process outperforms the semi-continuous process. That is, the batch process requires a smaller saturation capacity $\overline{Q}$ than the semi-continuous process for a specified $\overline{K}$, N_{BV} and r. Again, we caution against scale-up of batch experimental data at high binding affinities $\overline{K}$ that are near or beyond the crossover point. For example, a batch process with $\overline{Q} = 650$, $\overline{K} = 10^3$, and $r = 10$ can treat $N_{BV} = 500$ bed volumes. In contrast, a semi-continuous process at the same $\overline{Q}$, $\overline{K}$, only treats $N_{BV} = 450$ bed volumes under the same conditions.

- Fig. 4 (C) shows **Type 3** behavior: the semi-continuous process always outperforms the batch process. For a given $\overline{K}$ and large r, the semi-continuous process requires a lower saturation capacity $\overline{Q}$ than the batch process to treat N_{BV} bed volumes of water. In this regime, the scale-up heuristic applies. Note that the difference in performance between batch and semi-continuous is greatest at small binding affinities $\overline{K}$. Fig. 4(C) shows that scaling-up an adsorptive process based on batch experiments will result in

an over-design 12% at $\overline{K} = 10^3$. Specifically, a batch process will treat $N_{BV} = 25$ bed volumes using a sorbent with $\overline{Q} = 38$, $\overline{K} = 10^3$ and $r = 100$. On the other hand, a semi-continuous process using the same material with identical $\overline{Q}$ and $\overline{K}$ will treat $N_{BV} = 28$ bed volumes.

Analysis of Eqs. (5) and (11) gives the following boundaries between the Type 1, Type 2, and Type 3 regimes:

$$\begin{array}{ccc} \text{Type 1} & \text{Type 2} & \text{Type 3} \\ \frac{\varepsilon}{N_{BV}} < 2 - r & 2 - r < \frac{\varepsilon}{N_{BV}} < \frac{1}{r} & \frac{\varepsilon}{N_{BV}} > \frac{1}{r} \end{array} \tag{17}$$

In the Supporting Information, Eq. (17) is derived and it is shown that it is mathematically impossible to observe a fourth regime where the semi-continuous process is inferior to the batch process at low binding affinity $\overline{K}$, there is a crossover point, and the semi-continuous process becomes superior to the batch process at high binding affinity. Using sensitivity analysis, it was verified that Eq. (17) matches graphical results and accurately predicts the location of the crossover point in Fig. 4. These formulas give researchers and practitioners a quick means to check if their experimental data fall in the Type 3 regime and the scale-up heuristic is guaranteed to hold.

Both **Type 1** and **Type 2** behaviors may appear to contradict engineering intuition; one often expects semi-continuous processes, which benefit from implicit staging effects of packed beds, will always perform at par with or better than an equivalent batch process. However, the semi-continuous process operates at an unsteady state. While in operation, a front of saturated sorbent propagates across the thickness of the bed. This saturated front is defined by the location where the sorbent is in equilibrium with the feed concentration c_{in}. For the ideal case considered here, the front appears as a step function translating across the bed. At locations ahead of the front, the concentration of solute in solution is nearly zero, the semi-continuous processes over-treats the solution, i.e., c_{out} is below the prescribed contaminant threshold. When breakthrough is achieved, defined as when the saturated front

reaches the end of the bed, c_{out} crosses the acceptable contaminant limit, requiring immediate regeneration. In contrast, batch adsorption is an equilibrium process. The concentration of the solution in batch adsorption is in equilibrium with the adsorbed solute as governed by the Langmuir isotherm Eq. (1) or a similar model. The equilibrium process ensures the product solution is at the exact specification requirements of the end-user application and prevents over-treatment. At large r, the equilibrium loading for c_{in} is much larger than c_{out} and the advantage of the semi-continuous process outweighs the penalty from over-treatment. But at small r, this advantage is greatly diminished and the batch process is superior. Realizing these competing advantages resolves the paradox of Type 1 and Type 2 behaviors. To further contrast batch and semi-continuous systems, consider $\lim_{c_{out}\to 0} r = \infty$. For a batch system, $\lim_{r\to\infty} \overline{Q^B} = \infty$ per Eq. (5). Yet, for a semi-continuous system, $\overline{Q^C}$ is independent of r per Eq. (11). This is because the modeling framework (currently) assumes transport limitations are negligible and all contaminant is adsorbed, i.e., $c_{out} = 0$, before breakthrough. For many environmental applications, there is no known "safe" level of contaminants and this over-treating is beneficial.

The above analysis demonstrates the need to be cautious about which operating regime a material is being characterized in. This analysis also emphasizes the need to conduct bench-scale demonstrations in unsteady-state, continuous operating modes to judge the systems-level performance of novel materials accurately. While more arduous than material characterization in batch mode, dynamic experiments coupled with advanced computational techniques such as nonlinear regression and dynamic optimization have the potential to bridge the gap between fundamental scientific knowledge and technology development.

Material property targets for an arbitrary adsorption process

The dimensionless material property relationships Eqs. (5) and (11) coupled with bed volume calculations Eq. (6) and (12) facilitate rapid bottom-up and top-down analysis of any adsorptive treatment system. The design of a point-of-entry (POE) water treatment system

for the removal of arsenic from water is presented to highlight the ease and general nature of the calculations.

Arsenic occurs in the earth naturally and enters groundwater through erosion, from industrial runoff,[49] as the decomposition product of some PPCPs,[8] and is detrimental to human health if consumed. The goal of this study is to quickly determine the potential systems-level performance of emerging arsenic adsorbents recently reported in literature. An inlet concentration $c_{in} = 140$ ppb and an outlet concentration $c_{out} = 10$ ppb are considered based on literature[38,50] which gives $r = 14$. Starting with binding affinity K and saturation capacity Q values reported in literature, an assumed sorbent porosity $\varepsilon = 0.3$ and density $\rho_{mem} = 0.7$ g cm $^{-3}$, the dimensionless material properties $\overline{K}$ and $\overline{Q}$ are calculated using Eq. (4). Using $\overline{K}$, $\overline{Q}$, r, and ε alone, the number of bed volumes N_{BV} is calculated using Eqs. (6) and (12). From the results in Table 2 and Fig. 5, it is seen that material $\boldsymbol{e}$ treats the most bed volumes among the screened adsorbents. However, none of the screened arsenic adsorbents are capable of treating 10^4 bed volumes of water, which is typical of POE arsenic treatment systems deployed in villages in India.[50] Material $\boldsymbol{e}$ requires about an order of magnitude improvement in saturation capacity Q to meet this requirement. These calculations are consistent with Sarkar et al.,[51] which use a combination of precipitation followed by a polishing adsorption step to remove arsenic from water.

Table 2: Alternative materials were screened for the design of a point-of-entry (POE) adsorptive water treatment system for the removal of arsenic from water. Based on the process requirements c_{in}=140 ppb and c_{out}=10 ppb and assumed material properties $\varepsilon = 0.3$ and $\rho_{mem} = 1.0$ g cm $^{-3}$ the dimensionless material properties $\bar{K}$ and $\bar{Q}$ were calculated using Eq. (4). Eqs. (6) and (12) were then used to calculate the number of bed volumes that can be treated by the sorbent in batch and semi-continuous operating modes. Material ***e*** is the most promising as it can treat 3200 bed volumes of water before regeneration. However, none of the screened materials come close to treating 10^4 bed volumes of water typical of a point-of-entry (POE) system deployed in villages in India.[50] The approach to similar number of bed volumes treated by the batch and semi-continuous adsorption processes at high $\bar{K}$ is explained by the crossover phenomena observed in type 2 scale-up behavior. *The Supporting Information describes each material in detail.

Legend identifier	Material*	K (M^{-1})	Q (mmol g^{-1})	$\overline{K}$ (−)	$\overline{Q}$ (−)	N_{BV}^{C} (−)	N_{BV}^{B} (−)	Reference
a	H90	8.2×10^{2}	4.6×10^{-1}	1.5×10^{-3}	1.7×10^{5}	1.9×10^{2}	14	Chutia et al.[52]
b	MAHS	3.6×10^{3}	6.6×10^{-1}	6.8×10^{-3}	2.5×10^{5}	1.2×10^{3}	90	Beker et al.[53]
c	HAX1	2.8×10^{4}	1.74×10^{-1}	5.2×10^{-2}	6.5×10^{4}	2.2×10^{3}	1.8×10^{2}	Gifford et al.[54]
d	ARM	4.1×10^{5}	1.7×10^{-2}	7.7×10^{-1}	6.5×10^{3}	2.0×10^{3}	2.6×10^{2}	Altundoğan et al.[55]
e	Copper (II) oxide nanoparticles	3.0×10^{6}	1.5×10^{-2}	5.6	5.4×10^{3}	3.2×10^{3}	1.2×10^{3}	Goswami et al.[56]

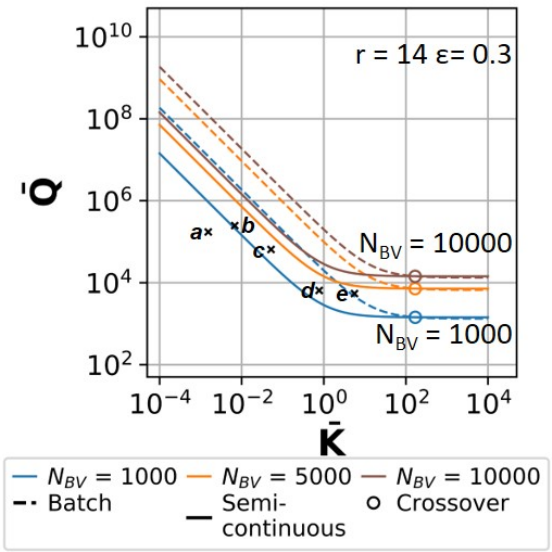

Figure 5: Dimensionless material property targets enable the rapid screening of alternative adsorbents for a given treatment. In an arsenic removal case study, we see that none of the screened adsorbents (see Table 2) can treat 10^4 bed volumes of water before regeneration. To treat this quantity of water for arsenic contamination in a point-of-entry (POE) system requires about one order of magnitude improvement in the saturation capacity Q of material $\boldsymbol{e}$. If a material with desired properties for the target removal cannot be found, alternate technological options should be evaluated for this treatment.

Conclusions

This work proposes a mathematical modeling framework for the top-down design of generic adsorptive separation systems. Specifically, the calculation of quantitative binding affinity K, saturation capacity Q, and adsorbent quantity v_{mem} targets needed to enable transformative point-of-entry and point-of-use technologies to treat water contaminated with lead and arsenic was demonstrated. This generic framework may be used to set property targets to design materials for the removal of other contaminants such as organic mircopollutants[57] and PFAS[58] from water. This analysis shows that advances in material characteristics alone are insufficient to realize future paradigms of sustainable water treatment technologies. Device and systems-level studies with high-fidelity models (e.g., transport limitations) are needed to fully utilize available materials for deployment in fit-for-purpose technologies. Infrastruc-

ture level studies can also identify the optimal location of regeneration units, point-of-use, and point-of-entry systems, as well as their connection to each other and the existing water distribution network. While the assumptions made in the analysis seem restrictive, this work establishes the necessary infrastructure required for a multiscale engineering design framework; extensions to consider alternate isotherms and adsorption system dynamics such as mass transfer effects are planned. The bounds of the feasible material design space defined in this article are optimistic due to the simplifying assumptions and will shrink as this framework is augmented using paradigms from data-science and process systems engineering.

Associated content

The Supporting Information contains A) Figures for: i) sorbent isotherm, ii) breakthrough time analysis, iii) material property targets for the batch process, iv) dimensionless material property targets; B) Tables with descriptive names of sorbents studied; C) Derivations for mathematical definitions of regions exhibiting different types of relative behavior between batch and semi-continuous adsorption processes; D) Optimization problem formulation for the calculation of the upper bound on saturation capacity.

Computer codes to recreate all of the figures in this paper and Support Information are available at `https://github.com/dowlinglab/multiscale-adsorption-targets`.

References

(1) Boretti, A.; Rosa, L. Reassessing the projections of the World Water Development Report. *npj Clean Water* **2019**, *2*, 1–6.

(2) Mosaferi, M.; Yunesian, M.; Dastgiri, S.; Mesdaghinia, A.; Esmailnasab, N. Prevalence of skin lesions and exposure to arsenic in drinking water in Iran. *Science of the Total Environment* **2008**, *390*, 69–76.

(3) Borah, K.; Bhuyan, B.; Sarma, H. Lead, arsenic, fluoride, and iron contamination of drinking water in the tea garden belt of Darrang district, Assam, India. *Environmental Monitoring and Assessment* **2010**, *169*, 347–352.

(4) Harvey, P.; Handley, H.; Taylor, M. Identification of the sources of metal (lead) contamination in drinking waters in north-eastern Tasmania using lead isotopic compositions. *Environmental Science and Pollution Research* **2015**, *22*, 12276–12288.

(5) Schnoor, J. L. Recognizing Drinking Water Pipes as Community Health Hazards. *Journal of Chemical Education* **2016**, *93*, 581–582.

(6) Hanna-Attisha, M.; LaChance, J.; Sadler, R. C.; Schnepp, A. C. Elevated blood lead levels in children associated with the Flint drinking water crisis: A spatial analysis of risk and public health response. *American Journal of Public Health* **2016**, *106*, 283–290.

(7) Karagas, M.; Gossai, A.; Pierce, B.; Ahsan, H. Drinking water arsenic contamination, skin Lesions, and malignancies: A systematic review of the global evidence. *Current Environmental Health Reports* **2015**, *2*, 52–68.

(8) Dhaka, S.; Kumar, R.; Deep, A.; Kurade, M. B.; Ji, S.-W.; Jeon, B.-H. Metal-organic frameworks (MOFs) for the removal of emerging contaminants from aquatic environments. *Coordination Chemistry Reviews* **2019**, *380*, 330–352.

(9) Rivera-Utrilla, J.; Sánchez-Polo, M.; Ferro-García, M. Á.; Prados-Joya, G.; Ocampo-Pérez, R. Pharmaceuticals as emerging contaminants and their removal from water. A review. *Chemosphere* **2013**, *93*, 1268–1287.

(10) Ellis, J. Pharmaceutical and personal care products (PPCPs) in urban receiving waters. *Environmental Pollution* **2006**, *144*, 184–189.

(11) Tarpeh, W. A.; Wald, I.; Wiprchtiger, M.; Nelson, K. L. Effects of operating and design

parameters on ion exchange columns for nutrient recovery from urine. *Environmental Science: Water Research & Technology* **2018**, *4*, 828–838.

(12) Li, J.; Hansson, L. A.; Persson, K. M. Nutrient control to prevent the occurrence of cyanobacterial blooms in a eutrophic lake in Southern Sweden, used for drinking water supply. *Water* **2018**, *10*, 919.

(13) Reinthaler, F. F.; Posch, J.; Feierl, G.; Wüst, G.; Haas, D.; Ruckenbauer, G.; Mascher, F.; Marth, E. Antibiotic resistance of E. coli in sewage and sludge. *Water Research* **2003**, *37*, 1685–90.

(14) Mauter, M. S.; Elimelech, M. Environmental applications of carbon-based nanomaterials. *Environmental Science & Technology* **2008**, *42*, 5843–5859.

(15) Adeleye, A. S.; Conway, J. R.; Garner, K.; Huang, Y.; Su, Y.; Keller, A. A. Engineered nanomaterials for water treatment and remediation: Costs, benefits, and applicability. *Chemical Engineering Journal* **2016**, *286*, 640–662.

(16) Luo, J.; Sun, M.; Ritt, C. L.; Liu, X.; Pei, Y.; Crittenden, J. C.; Elimelech, M. Tuning Pb(II) adsorption from aqueous solutions on ultrathin iron oxychloride (FeOCl) nanosheets. *Environmental Science & Technology* **2019**, *53*, 2075–2085.

(17) Yavuz, C. T.; Mayo, J. T.; Yu, W. W.; Prakash, A.; Falkner, J. C.; Yean, S.; Cong, L.; Shipley, H. J.; Kan, A.; Tomson, M.; Natelson, D.; Colvin, V. L. Low-field magnetic separation of monodisperse Fe_3O_4 nanocrystals. *Science* **2006**, *314*, 964–967.

(18) Díez-Pascual, A. M. Antibacterial activity of nanomaterials. *Nanomaterials* **2018**, *8*, 359.

(19) Santhosh, C.; Velmurugan, V.; Jacob, G.; Jeong, S. K.; Grace, A. N.; Bhatnagar, A. Role of nanomaterials in water treatment applications: A review. *Chemical Engineering Journal* **2016**, *306*, 1116–1137.

(20) Mauter, M. S.; Zucker, I.; Perreault, F.; Werber, J. R.; Kim, J.-H.; Elimelech, M. The role of nanotechnology in tackling global water challenges. *Nature Sustainability* **2018**, *1*, 166–175.

(21) Werber, J. R.; Osuji, C. O.; Elimelech, M. Materials for next-generation desalination and water purification membranes. *Nature Reviews Materials* **2016**, *1*, 16018.

(22) Alvarez, P. J. J.; Chan, C. K.; Elimelech, M.; Halas, N. J.; Villagrán, D. Emerging opportunities for nanotechnology to enhance water security. *Nature nanotechnology* **2018**, *13*, 634.

(23) Zodrow, K. R.; Li, Q.; Buono, R. M.; Chen, W.; Daigger, G.; Duenas-Osorio, L.; Elimelech, M.; Huang, X.; Jiang, G.; Kim, J.-H.; Logan, B. E.; Sedlak, D. L.; Westerhoff, P.; Alvarez, P. J. J. Advanced materials, technologies, and complex systems analyses: Emerging opportunities to enhance urban water security. *Environmental Science & Technology* **2017**, *51*, 10274–10281.

(24) Tarpeh, W. A.; Udert, K. M.; Nelson, K. L. Comparing ion exchange adsorbents for nitrogen recovery from source-separated urine. *Environmental Science & Technology* **2017**, *51*, 2373–2381.

(25) Trimmer, J. T.; Cusick, R. D.; Guest, J. S. Amplifying progress toward multiple development goals through resource recovery from sanitation. *Environmental Science & Technology* **2017**, *51*, 10765–10776.

(26) Luo, J.; Crittenden, J. C. Nanomaterial adsorbent design: From bench scale tests to engineering design. *Environmental Science & Technology* **2019**, *53*, 10537 – 10538.

(27) Eugene, E. A.; Phillip, W. A.; Dowling, A. W. Data science-enabled molecular-to-systems engineering for sustainable water treatment. *Current Opinion in Chemical Engineering* **2019**, *26*, 122–130.

(28) Weidman, J. L.; Mulvenna, R. A.; Boudouris, B. W.; Phillip, W. A. Nanoporous block polymer thin films functionalized with bio-inspired ligands for the efficient capture of heavy metal ions from water. *ACS Applied Materials and Interfaces* **2017**, *9*, 19152–19160.

(29) Weidman, J. L.; Mulvenna, R. A.; Boudouris, B. W.; Phillip, W. A. Nanostructured membranes from triblock polymer precursors as high capacity copper adsorbents. *Langmuir* **2015**, *31*, 11113–11123.

(30) Zhang, Y.; Sargent, J. L.; Boudouris, B. W.; Phillip, W. A. Nanoporous membranes generated from self-assembled block polymer precursors: Quo Vadis? *Journal of Applied Polymer Science* **2015**, *132*, 41683–1–41683–17.

(31) Zhang, Y.; Mulvenna, R. A.; Boudouris, B. W.; Phillip, W. A. Nanomanufacturing of high-performance hollow fiber nanofiltration membranes by coating uniform block polymer films from solution. *Journal of Materials Chemistry A* **2017**, *5*, 3358–3370.

(32) Bellinger, D. C. Lead contamination in Flint-An abject failure to protect public health. *The New England Journal of Medicine* **2016**, *374*, 1101–1103.

(33) Gómez, H. F.; Borgialli, D. A.; Sharman, M.; Shah, K. K.; Scolpino, A. J.; Oleske, J. M.; Bogden, J. D. Blood lead levels of children in Flint, Michigan: 2006-2016. *Journal of Pediatrics* **2018**, *197*, 158–164.

(34) Clark, R. M. Evaluating the cost and performance of field scale granular activated carbon systems. *Environmental Science & Technology* **1987**, *21*, 573 – 580.

(35) Hersel, A. A.; Lepek, D. H.; Geankoplis, C. J. *Transport Processes and Separation Process Principles*, 5th ed.; 2018.

(36) Baker, R. W. *Membrane Technology and Applications*, 2nd ed.; John Wiley & Sons, Ltd, 2004.

(37) Some Flint water test sites still showing high lead levels. Accessed June, 2020; https://www.mlive.com/news/flint/2016/03/some_flint_water_test_sites_st.html.

(38) National primary drinking water regulations. United States Environmental Protection Agency. Accessed June, 2020; https://www.epa.gov/ground-water-and-drinking-water/national-primary-drinking-water-regulations#seven.

(39) WaterSense Statistics and Facts. United States Environmental Protection Agency. Accessed June, 2020; https://www.epa.gov/watersense/statistics-and-facts.

(40) Mazzotti, M.; Rajendran, A. Equilibrium theory – based analysis of nonlinear waves in separation processes. *Annual Review of Chemical and Biomolecular Engineering* **2013**, *4*, 119–141.

(41) Gomes, E. C. C.; Sousa, A. F. D.; Vasconcelos, P. H. M.; Melo, D. Q.; Diógenes, I. C. N.; Sousa, E. H. S. D.; Ronaldo, F.; San, R. A. S.; Longhinotti, E. Synthesis of bifunctional mesoporous silica spheres as potential adsorbent for ions in solution. *Chemical Engineering Journal* **2013**, *214*, 27–33.

(42) Wang, L.; Yang, L.; Li, Y.; Zhang, Y.; Ma, X.; Ye, Z. Study on adsorption mechanism of Pb(II) and Cu(II) in aqueous solution using PS-EDTA resin. *Chemical Engineering Journal* **2010**, *163*, 364–372.

(43) Zhang, Y.; Vallin, J. R.; Sahoo, J. K.; Gao, F.; Boudouris, B. W.; Webber, M. J.; Phillip, W. A. High-affinity detection and capture of heavy metal contaminants using block polymer composite membranes. *ACS Central Science* **2018**, *4*, 1697–1707.

(44) Tanhaei, B.; Ayati, A.; Bamoharram, F. F.; Sillanpää, M. Magnetic EDTA functionalized preyssler cross linked chitosan nanocomposite for adsorptive removal of Pb(II) ions. *CLEAN-Soil, Air, Water* **2017**, *45*, 1700328.

(45) Ren, Y.; Abbood, H. A.; He, F.; Peng, H.; Huang, K. Magnetic EDTA-modified chitosan/SiO_2/Fe_3O_4 adsorbent : Preparation , characterization , and application in heavy metal adsorption. *Chemical Engineering Journal* **2013**, *226*, 300–311.

(46) Xu, M.; Zhang, Y.; Zhang, Z.; Shen, Y.; Zhao, M.; Pan, G. Study on the adsorption of Ca^{2+} , Cd^{2+} and Pb^{2+} by magnetic Fe_3O_4 yeast treated with EDTA dianhydride. *Chemical Engineering Journal* **2011**, *168*, 737–745.

(47) Liu, Y.; Fu, R.; Sun, Y.; Zhou, X.; Ali, S.; Xu, X. Multifunctional nanocomposites Fe_3O_4@SiO_2-EDTA for Pb(II) and Cu(II) removal from aqueous solutions. *Applied Surface Science* **2016**, *369*, 267–276.

(48) Huang, Y.; Keller, A. A. EDTA functionalized magnetic nanoparticle sorbents for cadmium and lead contaminated water treatment. *Water Research* **2015**, *80*, 159 – 168.

(49) Podgorski, J. E.; Eqani, S. A. M. A. S.; Khanam, T.; Ullah, R.; Shen, H.; Berg, M. Extensive arsenic contamination in high-pH unconfined aquifers in the Indus Valley. *Science Advances* **2017**, *3*, e1700935.

(50) Sarkar, S.; Greenleaf, J. E.; Gupta, A.; Ghosh, D.; Blaney, L. M.; Bandyopadhyay, P.; Biswas, R.; Dutta, A. K.; Sengupta, A. K. Evolution of community-based arsenic removal systems in remote villages in West Bengal, India: Assessment of decade-long operation. *Water Research* **2010**, *44*, 5813–5822.

(51) Sarkar, S.; Gupta, A.; Biswas, R.; Deb, A.; Greenleaf, J.; SenGupta, A. Well-head arsenic removal units in remote villages of Indian subcontinent: Field results and performance evaluation. *Water Research* **2005**, *39*, 2196–2206.

(52) Chutia, P.; Kato, S.; Kojima, T.; Satokawa, S. Arsenic adsorption from aqueous solution on synthetic zeolites. *Journal of Hazardous Materials* **2009**, *162*, 440–447.

(53) Beker, U.; Cumbal, L.; Duranoglu, D.; Kucuk, I.; Sengupta, A. Preparation of Fe oxide nanoparticles for environmental applications: arsenic removal. *Environmental Geochemistry and Health* **2010**, *32*, 291–296.

(54) Gifford, M.; Hristovski, K.; Westerhoff, P. Ranking traditional and nano-enabled sorbents for simultaneous removal of arsenic and chromium from simulated groundwater. *Science of the Total Environment* **2017**, *601-602*, 1008–1014.

(55) Altundoğan, H.; Altundoğan, S.; Tümen, F.; Bildik, M. Arsenic adsorption from aqueous solutions by activated red mud. *Waste Management* **2002**, *22*, 357–363.

(56) Goswami, A.; Raul, P.; Purkait, M. Arsenic adsorption using copper (II) oxide nanoparticles. *Chemical Engineering Research and Design* **2012**, *90*, 1387–1396.

(57) Alsbaiee, A.; Smith, B. J.; Xiao, L.; Ling, Y.; Helbling, D. E.; Dichtel, W. R. Rapid removal of organic micropollutants from water by a porous β-cyclodextrin polymer. *Nature* **2016**, *529*, 190–194.

(58) Kumarasamy, E.; Manning, I. M.; Collins, L. B.; Coronell, O.; Leibfarth, F. A. Ionic fluorogels for remediation of per- and polyfluorinated alkyl substances from water. *ACS Central Science* **2020**, *6*, 487–492.

Graphical TOC Entry

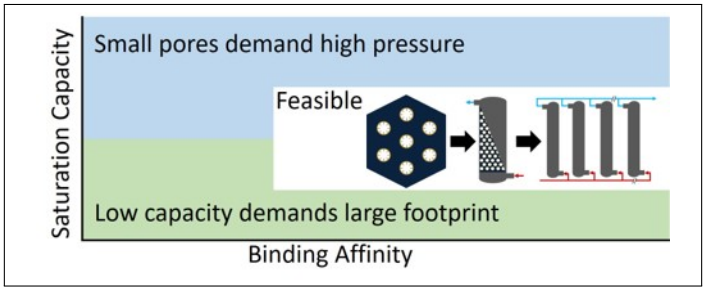

Supporting Information: Material property targets for emerging nanomaterials to enable point-of-use and point-of-entry water treatment systems

Elvis A. Eugene, William A. Phillip, and Alexander W. Dowling*

Depatment of Chemical and Biomolecular Engineering, University of Notre Dame
Notre Dame, IN 46556

E-mail: adowling@nd.edu

Derivations for the mathematical definitions of regions exhibiting different types of relative behavior between the batch and semi-continuous adsorption process

This work demonstrates different regions of relative behavior exhibited by adsorption processes operated in batch and semi-continuous operating modes, classified as Type 1, Type 2, and Type 3 behavior. This supporting information (i) derives for the mathematical conditions necessary to realize each type of behavior and (ii) proves so-called Type 4 behavior is mathematically impossible.

The dimensionless material property target equations for a batch and semi-continuous

process, Eqs. (5) and (11), respectively, form the basis of these derivations:

$$\overline{Q^B} = \frac{1}{1-\varepsilon} N_{BV} \left(1 - \frac{1}{r}\right) \frac{r + \overline{K}}{\overline{K}} \tag{S1}$$

$$\overline{Q^C} = \frac{1}{1-\varepsilon} \left(N_{BV} - \varepsilon\right) \frac{1 + \overline{K}}{\overline{K}} \quad \forall N_{BV} > \varepsilon \tag{S2}$$

Type 1: Batch always superior

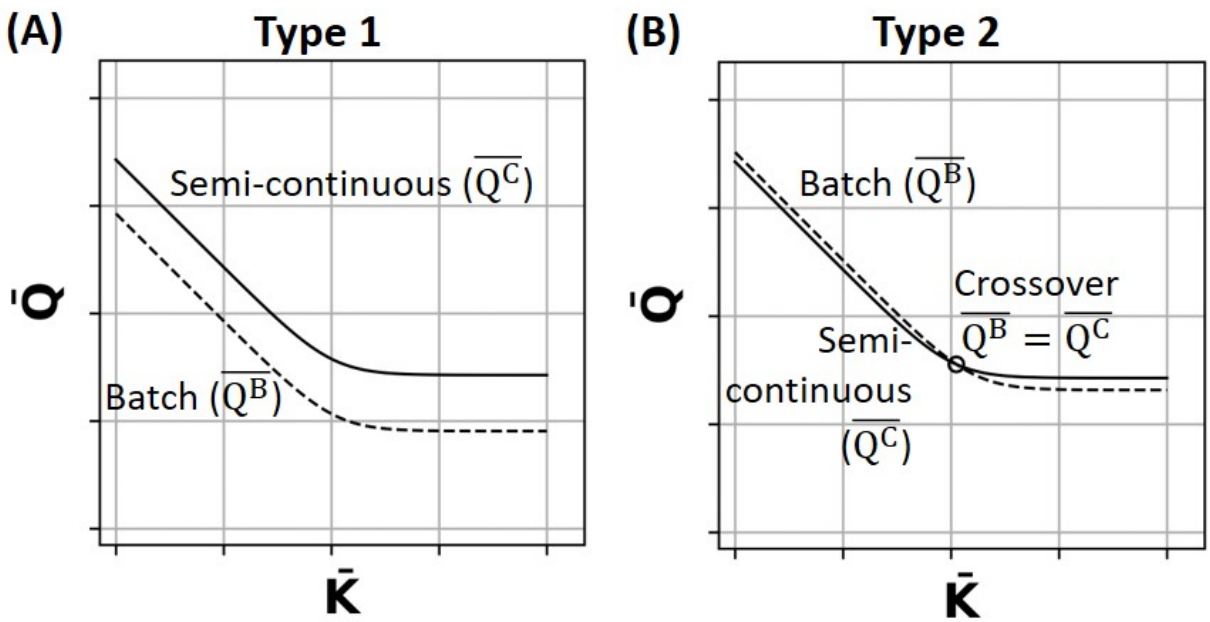

Figure S1: A schematic representation of Type 1 and Type 2 relative behavior between batch and semi-continuous process configurations for an adsorption process. **(A) Type 1** behavior: The batch process always requires a lower saturation capacity $\bar{Q}$ than the semi-continuous process at all values of N_{BV} and $\bar{K}$. This is mathematically expressed as as $\lim_{\bar{K}\to 0}(\bar{Q^C} - \bar{Q^B}) > 0$ and $\lim_{\bar{K}\to\infty}(\bar{Q^C} - \bar{Q^B}) > 0$. **(B) Type 2** behavior: The semi-continuous process requires a lower saturation capacity $\bar{Q}$ than the batch process at low binding affinity $\bar{K}$. At high $\bar{K}$, the batch process requires a lower saturation capacity $\bar{Q}$ than the semi-continuous process. A crossover point denoted by the circle exists where both processes operate identically. Mathematically this behavior is characterized as $\lim_{\bar{K}\to 0}(\bar{Q^C} - \bar{Q^B}) < 0$ and $\lim_{\bar{K}\to\infty}(\bar{Q^C} - \bar{Q^B}) > 0$. The crossover point is given by the solution of the equation $\bar{Q^C} - \bar{Q^B} = 0$.

In type 1 behavior, the semi-continuous process always requires a higher saturation capac-

ity $\bar{Q}$ than the batch process at all values of bed volume N_{BV} and binding affinity $\overline{K}$, as shown in Fig. S1(A). Using already defined models, the conditions to observe **type 1** system performance (see Fig. S1) can be written as:

$$\overline{Q^C} - \overline{Q^B} > 0 \quad \forall \ \overline{K} > 0 \tag{S3}$$

or equivalently:

$$\frac{\overline{Q^C}}{\overline{Q^B}} > 1 \quad \forall \ \overline{K} > 0 \tag{S4}$$

We consider two limiting conditions $\bar{K} \to 0$ and $\bar{K} \to \infty$:

$$\lim_{\overline{K} \to 0} \frac{\overline{Q^C}}{\overline{Q^B}} > 1 \qquad\qquad \lim_{\overline{K} \to \infty} \overline{Q^C} - \overline{Q^B} > 0 \tag{S5}$$

These limits are evaluated using Eqs. (S1) and (S2):

$$\lim_{\overline{K} \to 0} \frac{\overline{Q^C}}{\overline{Q^B}} \tag{S6}$$

$$= \lim_{\overline{K} \to 0} \frac{\frac{1}{1-\varepsilon}\left(N_{BV} - \varepsilon\right) \frac{1+\overline{K}}{\overline{K}}}{\frac{1}{1-\varepsilon} N_{BV} \left(1 - \frac{1}{r}\right) \frac{r+\overline{K}}{\overline{K}}} \tag{S7}$$

$$= \lim_{\overline{K} \to 0} \frac{\left(N_{BV} - \varepsilon\right)\left(1 + \overline{K}\right)}{N_{BV}\left(1 - \frac{1}{r}\right)\left(r + \overline{K}\right)} \tag{S8}$$

$$= \frac{\left(N_{BV} - \varepsilon\right)}{N_{BV}\left(1 - \frac{1}{r}\right) r} \tag{S9}$$

$$= \frac{\left(N_{BV} - \varepsilon\right)}{N_{BV}\left(1 - \frac{1}{r}\right) r} \tag{S10}$$

$$\Longrightarrow \boxed{\lim_{\overline{K} \to 0} \frac{\overline{Q^C}}{\overline{Q^B}} = \frac{\left(N_{BV} - \varepsilon\right)}{N_{BV}\left(r - 1\right)}} \tag{S11}$$

From this limit, we can derive a necessary condition for type 1 behavior:

$$\lim_{\overline{K}\to 0} \frac{\overline{Q^C}}{\overline{Q^B}} > 1 \tag{S12}$$

$$\implies \frac{(N_{BV} - \varepsilon)}{N_{BV}(r-1)} > 1 \qquad \text{(Note 1)} \tag{S13}$$

$$\implies N_{BV} - \varepsilon > N_{BV}(r-1) \tag{S14}$$

$$\implies 1 - \frac{\varepsilon}{N_{BV}} > r - 1 \tag{S15}$$

$$\boxed{\lim_{\overline{K}\to 0} \frac{\overline{Q^C}}{\overline{Q^B}} > 1 \implies 2 - r > \frac{\varepsilon}{N_{BV}}} \tag{S16}$$

Note 1: Multiplication of both sides by $N_{BV}(r-1)$ without changing the inequality conditions is allowed since $N_{BV} \geq 0$ and $r \geq 1$ which makes $N_{BV}(r-1) \geq 0$

Similarly:

$$\lim_{\overline{K}\to\infty} \left(\overline{Q^C} - \overline{Q^B}\right) \tag{S17}$$

$$= \lim_{\overline{K}\to\infty} \left(\frac{1}{1-\varepsilon}(N_{BV} - \varepsilon)\frac{1+\overline{K}}{\overline{K}} - \frac{1}{1-\varepsilon}N_{BV}\left(1 - \frac{1}{r}\right)\frac{r+\overline{K}}{\overline{K}}\right) \tag{S18}$$

$$= \lim_{\overline{K}\to\infty} \left(\frac{1}{1-\varepsilon}(N_{BV} - \varepsilon)\frac{\overline{K}\left(\frac{1}{\overline{K}}+1\right)}{\overline{K}} - \frac{1}{1-\varepsilon}N_{BV}\left(1 - \frac{1}{r}\right)\frac{\overline{K}\left(\frac{r}{\overline{K}}+1\right)}{\overline{K}}\right) \tag{S19}$$

$$= \lim_{\overline{K}\to\infty} \left(\frac{1}{1-\varepsilon}(N_{BV} - \varepsilon)\left(\frac{1}{\overline{K}}+1\right) - \frac{1}{1-\varepsilon}N_{BV}\left(1 - \frac{1}{r}\right)\left(\frac{r}{\overline{K}}+1\right)\right) \tag{S20}$$

$$= \frac{1}{1-\varepsilon}(N_{BV} - \varepsilon) - \frac{1}{1-\varepsilon}N_{BV}\left(1 - \frac{1}{r}\right) \tag{S21}$$

$$\implies \boxed{\lim_{\overline{K}\to\infty} \left(\overline{Q^C} - \overline{Q^B}\right) = \frac{1}{1-\varepsilon}(N_{BV} - \varepsilon) - \frac{1}{1-\varepsilon}N_{BV}\left(1 - \frac{1}{r}\right)} \tag{S22}$$

This limit gives a secondary necessary condition for type 1 behavior:

$$\lim_{\overline{K}\to\infty}\left(\overline{Q^C}-\overline{Q^B}\right)>0 \tag{S23}$$

$$\implies \frac{1}{1-\varepsilon}\left(N_{BV}-\varepsilon\right)-\frac{1}{1-\varepsilon}N_{BV}\left(1-\frac{1}{r}\right)>0 \qquad \text{Note 2a} \tag{S24}$$

$$\implies N_{BV}-\varepsilon-N_{BV}+\frac{N_{BV}}{r}>0 \tag{S25}$$

$$\implies \frac{N_{BV}}{r}-\varepsilon>0 \tag{S26}$$

$$\implies \frac{N_{BV}}{r}>\varepsilon \qquad \text{Note 2b} \tag{S27}$$

$$\implies \boxed{\lim_{\overline{K}\to\infty}\left(\overline{Q^C}-\overline{Q^B}\right)>0 \implies \frac{1}{r}>\frac{\varepsilon}{N_{BV}}} \tag{S28}$$

Note 2a: $0<\varepsilon<1 \implies \frac{1}{1-\varepsilon}>0$

Note 2b: $N_{BV}>0$

Recall Eqs. (S16) and (S28) provide two necessary conditions for type 1 behavior:

$$2-r>\frac{\varepsilon}{N_{BV}} \qquad \text{and} \qquad \frac{1}{r}>\frac{\varepsilon}{N_{BV}}$$

However:

$$2-r\leq\frac{1}{r} \qquad \forall\, r\geq 1 \tag{S29}$$

Recall $r>1$ by definition if $c_{out}<c_{in}$, i.e., any separation occurs. Thus $2-r$ is always less than $\frac{1}{r}$ and the two necessary conditions from Eqs. (S16) and (S28) simplify to a **single necessary condition for type 1 behavior**:

$$\frac{\varepsilon}{N_{BV}}<2-r \tag{S30}$$

Type 2: Semi-continuous superior - crossover - batch superior

In type 2 behavior, the semi-continuous process requires a lower saturation capacity $\bar{Q}$ than the batch process at low binding affinity $\overline{K}$. At high $\overline{K}$, the semi-continuous process requires

a higher saturation capacity than the batch process. A crossover point exists at which both processes perform identically. This behavior is shown in Fig. S1(B). Following the same steps as done earlier, the necessary conditions to observe **type 2** behavior are defined as:

$$\lim_{\overline{K}\to 0} \frac{\overline{Q^C}}{\overline{Q^B}} < 1 \tag{S31}$$

$$\lim_{\overline{K}\to \infty} \left(\overline{Q^C} - \overline{Q^B}\right) > 0 \tag{S32}$$

$$\overline{Q^C}\left(\hat{K}\right) = \overline{Q^B}\left(\hat{K}\right) \quad \text{for some} \quad \hat{K} \in (0, \infty) \tag{S33}$$

In Eq. (S33), $\hat{K}$ is the dimensionless binding affinity at which the batch and semi-continuous processes perform identically, i.e., the crossover point.

Eq. (S31) yields a necessary condition for type 2 behavior:

$$\lim_{\overline{K}\to 0} \frac{\overline{Q^C}}{\overline{Q^B}} < 1 \tag{S34}$$

$$\implies \frac{(N_{BV} - \varepsilon)}{N_{BV}(r-1)} < 1 \tag{S35}$$

$$\implies (N_{BV} - \varepsilon) < N_{BV}(r-1) \qquad \because N_{BV}(r-1) \geq 0 \tag{S36}$$

$$\implies 1 - \frac{\varepsilon}{N_{BV}} < r - 1 \tag{S37}$$

$$\lim_{\overline{K}\to 0} \left(\overline{Q^C} - \overline{Q^B}\right) < 0 \implies 2 - r < \frac{\varepsilon}{N_{BV}} \tag{S38}$$

Eq. (S32) is identical to Eq. (S28) and gives a second necessary condition for type 2 behavior:

$$\lim_{\overline{K}\to \infty} \left(\overline{Q^C} - \overline{Q^B}\right) > 0 \implies \frac{1}{r} > \frac{\varepsilon}{N_{BV}} \tag{S39}$$

Thus two necessary conditions for type 2 behavior are:

$$2 - r < \frac{\varepsilon}{N_{BV}} \qquad \text{and} \qquad \frac{1}{r} > \frac{\varepsilon}{N_{BV}}$$

Per Eq. (S29), $2 - r \leq \frac{1}{r}$ and these two conditions become a **single necessary condition**

for type 2 behavior:

$$2 - r < \frac{\varepsilon}{N_{BV}} < \frac{1}{r} \tag{S40}$$

Moreover, we can use Eqs. (S1), (S2), and (S33) to locate the crossover point $(\hat{K}, \hat{Q})$:

$$\boxed{\hat{Q} = \overline{Q^C}\left(\hat{K}\right) = \overline{Q^B}\left(\hat{K}\right)} \tag{S41}$$

$$\implies \frac{1}{1-\varepsilon}\left(N_{BV} - \varepsilon\right)\frac{1+\hat{K}}{\hat{K}} = \frac{1}{1-\varepsilon}N_{BV}\left(1 - \frac{1}{r}\right)\frac{r+\hat{K}}{\hat{K}} \tag{S42}$$

$$\implies \left(N_{BV} - \varepsilon\right)\left(1 + \hat{K}\right) = N_{BV}\left(1 - \frac{1}{r}\right)\left(r + \hat{K}\right) \tag{S43}$$

$$\implies N_{BV} + N_{BV}\hat{K} - \varepsilon - \varepsilon\hat{K} = N_{BV}\left(r + \hat{K} - 1 - \frac{\hat{K}}{r}\right) \tag{S44}$$

$$\implies N_{BV} + N_{BV}\hat{K} - \varepsilon - \varepsilon\hat{K} = N_{BV}r + N_{BV}\hat{K} - N_{BV} - N_{BV}\frac{\hat{K}}{r} \tag{S45}$$

$$\implies \hat{K}\left(-\varepsilon + \frac{N_{BV}}{r}\right) = N_{BV}\left(r - 1 - 1\right) - \varepsilon \tag{S46}$$

$$\implies \boxed{\hat{K} = \frac{N_{BV}\left(r-2\right) - \varepsilon}{N_{BV}/r - \varepsilon}} \tag{S47}$$

Type 3: Semi-continuous always superior

Type 3 behavior is when the semi-continuous process always requires a lower saturation capacity $\bar{Q}$ than the batch process at all values of bed volume N_{BV} and binding affinity $\overline{K}$, as shown in Fig. S2(A). This requires the following two limits are satisfied:

$$\lim_{\overline{K}\to 0}\frac{\overline{Q^C}}{\overline{Q^B}} < 1 \qquad \text{and} \qquad \lim_{\overline{K}\to\infty}\left(\overline{Q^C} - \overline{Q^B}\right) < 0 \tag{S48}$$

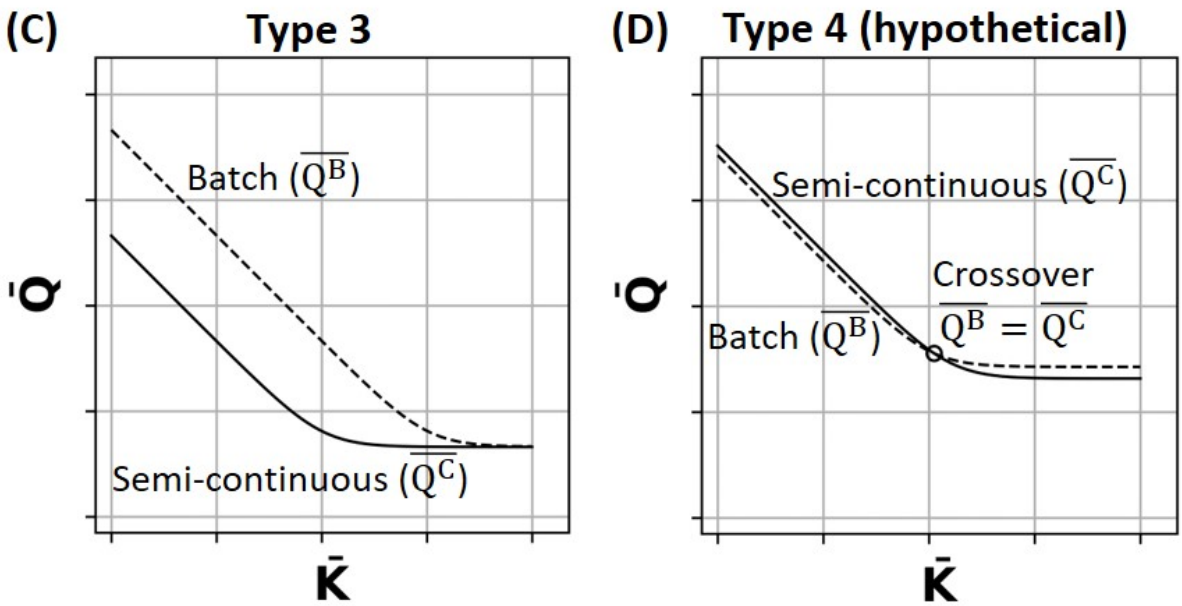

Figure S2: A schematic representation of Type 3 and Hypothetical Type 4 relative behavior between batch and semi-continuous process configurations for an adsorption process. **(A) Type 3** behavior: The batch process always performs worse than the semi-continuous process as the former always requires a higher saturation capacity $\bar{Q}$ than the latter at all values of N_{BV} and $\bar{K}$. Mathematically, this is expressed as as $\lim_{\bar{K}\to 0}(\bar{Q^C}-\bar{Q^B}) < 0$ and $\lim_{\bar{K}\to\infty}(\bar{Q^C}-\bar{Q^B}) < 0$. **(B) Type 4** behavior (hypothetical): The semi-continuous process requires a higher saturation capacity $\bar{Q}$ than the batch process at low binding affinity $\bar{K}$. At the crossover point denoted by the circle, that both processes will behave identically. At high $\bar{K}$, the batch process requires a higher saturation capacity $\bar{Q}$ than the semi-continuous process. Mathematically this behavior is characterized as $\lim_{\bar{K}\to 0}(\bar{Q^C} - \bar{Q^B}) > 0$ and $\lim_{\bar{K}\to\infty}(\bar{Q^C} - \bar{Q^B}) < 0$.

Following the same analysis as above, these limits give two necessary conditions:

$$\boxed{\lim_{\overline{K}\to 0} \frac{\overline{Q^C}}{\overline{Q^B}} < 1 \implies 2 - r < \frac{\varepsilon}{N_{BV}}} \tag{S49}$$

$$\lim_{\overline{K}\to\infty}\left(\overline{Q^C}-\overline{Q^B}\right)<0 \tag{S50}$$

$$\implies \frac{1}{1-\varepsilon}\left(N_{BV}-\varepsilon\right)-\frac{1}{1-\varepsilon}N_{BV}\left(1-\frac{1}{r}\right)<0 \tag{S51}$$

$$\implies \frac{1}{1-\varepsilon}\left(N_{BV}-\varepsilon-N_{BV}+\frac{N_{BV}}{r}\right)<0 \tag{S52}$$

$$\implies \frac{1}{1-\varepsilon}\left(\frac{N_{BV}}{r}-\varepsilon\right)<0 \tag{S53}$$

$$\implies \left(\frac{N_{BV}}{r}-\varepsilon\right)<0 \qquad \because\ \frac{1}{1-\varepsilon}\geq 0 \tag{S54}$$

$$\implies \frac{N_{BV}}{r}<\varepsilon \tag{S55}$$

$$\implies \boxed{\lim_{\overline{K}\to\infty}\left(\overline{Q^C}-\overline{Q^B}\right)<0 \implies \frac{1}{r}<\frac{\varepsilon}{N_{BV}}} \tag{S56}$$

Thus two necessary conditions for type 3 behavior are:

$$2-r<\frac{\varepsilon}{N_{BV}} \qquad \text{and} \qquad \frac{1}{r}<\frac{\varepsilon}{N_{BV}}$$

Per Eq. (S29), $2-r<\frac{1}{r}\ \forall r\geq 1$, thus:

$$\frac{\varepsilon}{N_{BV}}>\frac{1}{r}>2-r \tag{S57}$$

is a **single necessary condition to observe type 3 behavior**.

Hypothetical type 4: Batch superior - crossover - semi-continuous superior

Can a hypothetical type 4 relative behavior (see Fig. S2(B)), where the batch process requires a lower saturation capacity $\overline{Q}$ at low binding affinity $\overline{K}$, there is a crossover point, and the semi-continuous process requires a lower $\overline{Q}$ at high binding affinity, exist? The necessary

conditions to observe such type 4 behavior are:

$$\lim_{\overline{K}\to 0} \frac{\overline{Q^C}}{\overline{Q^B}} > 1 \qquad \text{and} \qquad \lim_{\overline{K}\to\infty} \left(\overline{Q^C} - \overline{Q^B}\right) < 0 \tag{S58}$$

These limits yield two necessary conditions:

$$\lim_{\overline{K}\to 0} \frac{\overline{Q^C}}{\overline{Q^B}} > 1 \implies \boxed{2 - r > \frac{\varepsilon}{N_{BV}}} \tag{S59}$$

$$\lim_{\overline{K}\to\infty} \left(\overline{Q^C} - \overline{Q^B}\right) < 0 \implies \boxed{\frac{1}{r} < \frac{\varepsilon}{N_{BV}}} \tag{S60}$$

However, per Eq. (S29) $2 - r \leq \frac{1}{r}\ \forall r \geq 1$. This implies there is no value for ε/N_{BV} that simultaneously satisfies both Eqs. (S59) and (S60). Therefore the necessary conditions for type 4 behavior are contradictory; it is **mathematically impossible to observe type 4 behavior** (under the model assumptions).

First derivative analysis

Next, we define a scaled difference:

$$g(\overline{K}) = 1 - \varepsilon\left(\overline{Q^C} - \overline{Q^B}\right) = (N_{BV} - \varepsilon)\left(\frac{1+\overline{K}}{\overline{K}}\right) - N_{BV}\left(1 - \frac{1}{r}\right)\left(\frac{r+\overline{K}}{\overline{K}}\right) \tag{S61}$$

We then differentiate with respect to $\overline{K}$:

$$\frac{dg(\overline{K})}{d\,\overline{K}} = (N_{BV} - \varepsilon)\left(\frac{-1}{\overline{K}^2}\right) - N_{BV}\left(1 - \frac{1}{r}\right)\left(\frac{-r}{\overline{K}^2}\right) \tag{S62}$$

$$= \left(\frac{-1}{\overline{K}^2}\right)\left[N_{BV} - \varepsilon - N_{BV}(r-1)\right] \tag{S63}$$

$$= \left(\frac{-1}{\overline{K}^2}\right)\left(2N_{BV} - \varepsilon - N_{BV}r\right) \tag{S64}$$

$$= \left(\frac{-N_{BV}}{\overline{K}^2}\right)\left(2 - \varepsilon/N_{BV} - r\right) \tag{S65}$$

From Eq. (S65) we see the sign of $\frac{dg(\overline{K})}{d\,\overline{K}}$ is independent of $\bar{K}$ and solely depends on the sign of $2 - \varepsilon/N_{BV} - r$. Specifically:

$$\frac{dg(\overline{K})}{d\,\overline{K}} > 0 \quad \text{if} \quad r > 2 - \varepsilon/N_{BV} \tag{S66}$$

$$\frac{dg(\overline{K})}{d\,\overline{K}} = 0 \quad \text{if} \quad r = 2 - \varepsilon/N_{BV} \tag{S67}$$

$$\frac{dg(\overline{K})}{d\,\overline{K}} < 0 \quad \text{if} \quad r < 2 - \varepsilon/N_{BV} \tag{S68}$$

Most interestingly, $r = 2 - \varepsilon/N_{BV}$ is the boundary between type 1 and type 2 behavior. The sign of the derivative is interpreted as follows:

- $\frac{dg(\overline{K})}{d\,\overline{K}} < 0$ implies the relative benefit of the batch system increases as $\bar{K}$ increases. This is verified in Figures S6 - S9 that show type 1 behavior.
- $\frac{dg(\overline{K})}{d\,\overline{K}} = 0$ implies the relative difference between batch and semi-continuous systems remains constant for all $\overline{K}$.
- $\frac{dg(\overline{K})}{d\,\overline{K}} > 0$ implies the difference $\overline{Q^C} - \overline{Q^B}$ increases as $\overline{K}$ increases. This is seen in Figures S10 - S29 which exhibit type 2 and type 3 behaviors.

Furthermore, these derivatives help establish the necessary conditions Eqs.(S30), (S40), and (S57) are also sufficient.

For type 1 behavior, $\lim_{\bar{K}\to 0} \frac{\overline{Q^C}}{\overline{Q^B}} > 1$ establishes that the batch process is superior at infinitesimally small $\overline{K}$ and $\frac{dg(\overline{K})}{d\,\overline{K}} < 0$ implies the relative benefit of the batch system increases with $\overline{K}$. Thus $\overline{Q^C} - \overline{Q^B} > 0 \; \forall \, \overline{K} \in (0, \infty)$.

For type 2 behavior, $\overline{Q^C} - \overline{Q^B} < 0$ for $\overline{K} \approx 0$ and $\overline{Q^C} - \overline{Q^B} > 0$ for $\overline{K} \to \infty$. Both $\overline{Q^C}(\overline{K})$ and $\overline{Q^B}(\overline{K})$ are continuous and at least once differentiable, therefore there must exist at least one crossover point where $\overline{Q^C}(\hat{K}) = \overline{Q^B}(\hat{K})$ for finite $\hat{K} \in (0, \infty)$. Moreover, Eq. (S42) is linear in $\hat{K}$ and has only one root implying there is exactly one crossover point.

For type 3 behavior, $\lim_{\overline{K}\to 0} \frac{\overline{Q^C}}{\overline{Q^B}} < 1$ establishes that the semi-continous process is

superior at infinitesimally small $\overline{K}$. Although $\frac{dg(\overline{K})}{d\overline{K}} > 0$ implies the relative benefit of the semi-continuous system decreases with $\overline{K}$, $\lim_{\overline{K}\to\infty} \overline{Q^C} - \overline{Q^B} < 0$ establishes the semi-continuous remains superior in the limit. Thus $\overline{Q^C} - \overline{Q^B} < 0 \; \forall \, \overline{K} \in (0, \infty)$.

Sorbent Isotherm

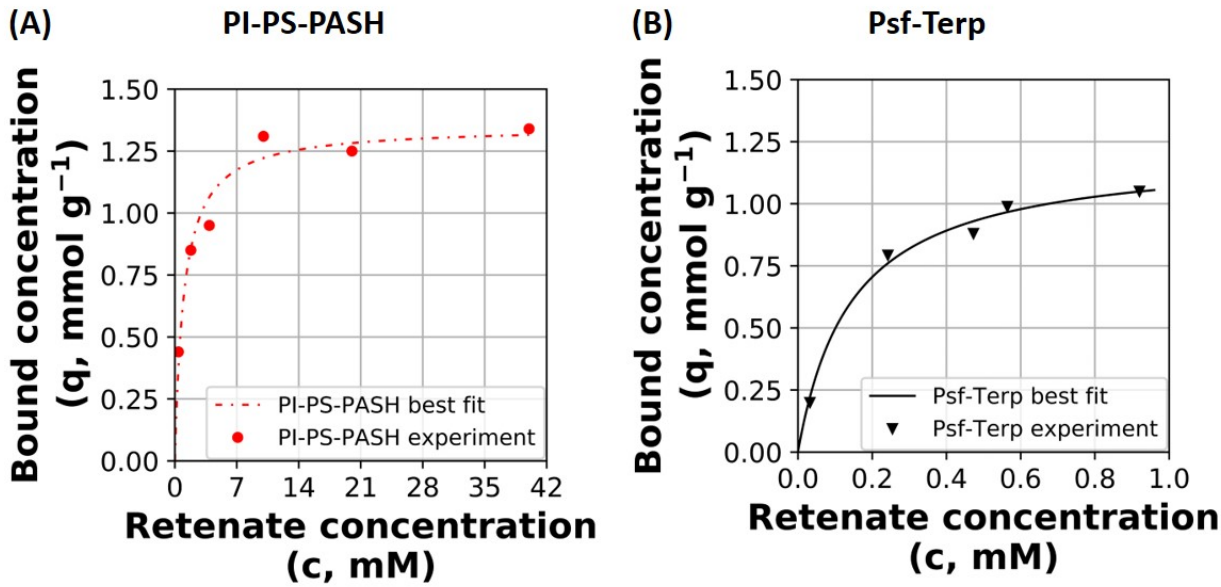

Figure S3: The Langmuir isotherm fits experimentally observed behavior of adsorptive nanoporous membranes well and is used to define the process equilibrium. Experimental observations and best fit Langmuir isotherm are shown for the **(A)** PI-PS-PASH[1] membrane in red and **(B)** Psf-Terp[2] membrane in black.

Breakthrough time analysis for point-of-use adsorptive water treatment system to treat lead contamination

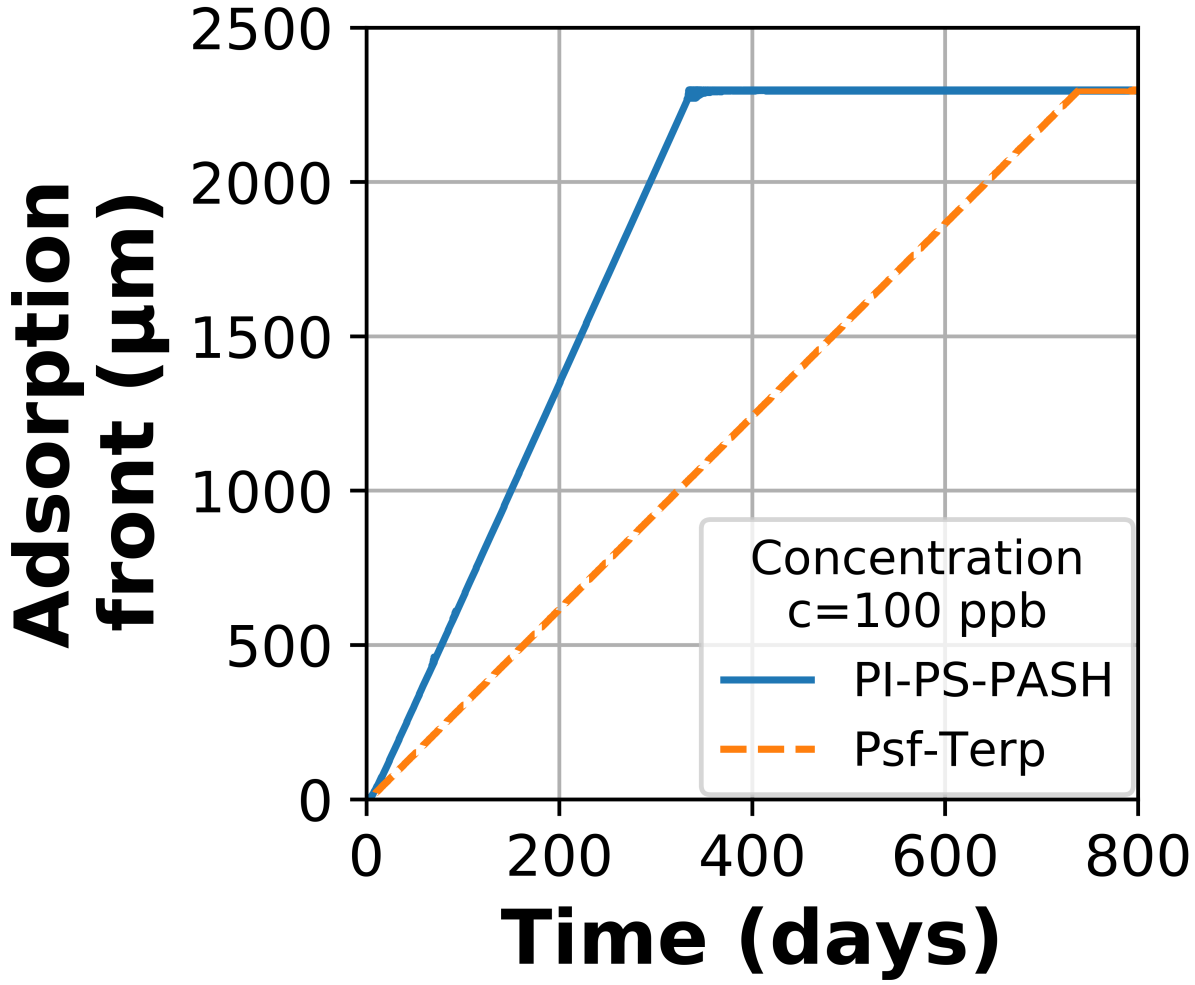

Figure S4: At breakthrough, the concentration of water leaving the adsorption module will be equal to the inlet concentration, i.e., c_{in} = 100 ppb, and the membrane will have to be regenerated. The solid blue and dashed orange contours correspond to a concentration of 100 ppb (lead) for the PI-PS-PASH and Psf-Terp membranes, respectively. Breakthrough time analysis shows that a water treatment system for $\mathrm{POU}_{24}^{\mathrm{C}}$ which uses 46 kg of Psf-Terp membrane (orange dashed curves) will have to be regenerated in 739 days (25 months). For the same application, 46 kg of PI-PS-PASH membrane (solid blue curves), whose binding affinity K is one order of magnitude smaller, will achieve breakthrough in 335 days (11 months). Since mass transfer resistances are neglected, the breakthrough curve is a step function.

Material property targets for point-of-use water treatment using adsorptive membranes operated in batch mode

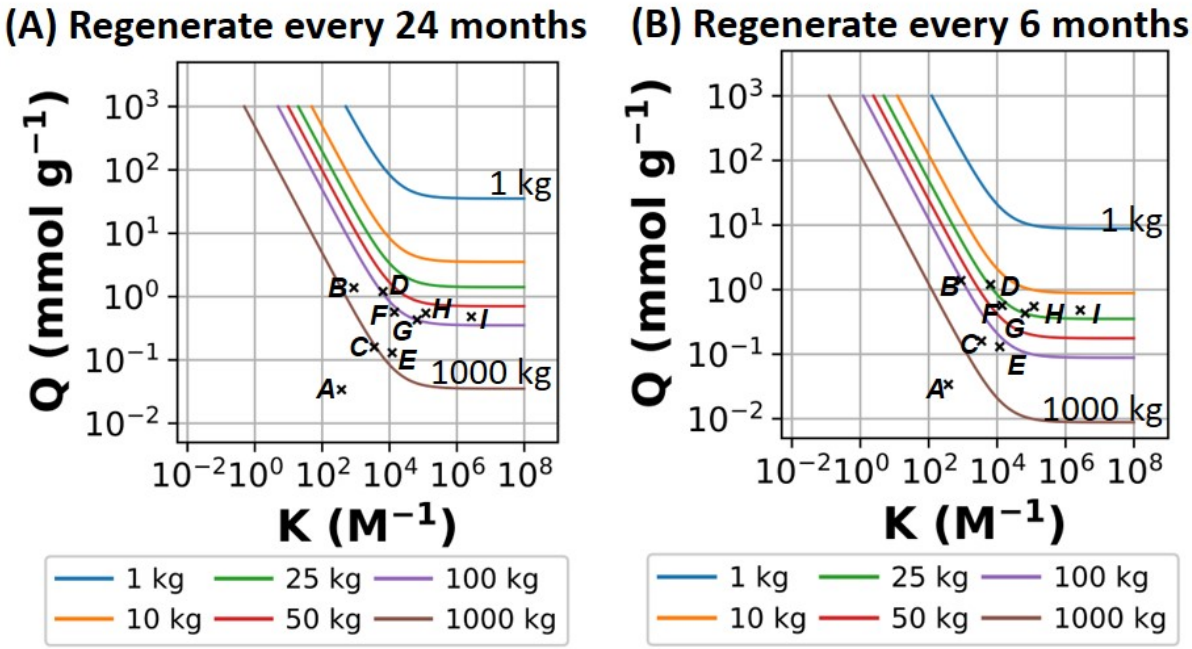

Figure S5: Material property targets for **batch adsorption** $\mathrm{POU}_{24}^{\mathrm{B}}$ (left, A) and $\mathrm{POU}_{6}^{\mathrm{B}}$ (right, B) systems for lead removal. Binding affinity K and saturation capacity Q are material properties in the Langmuir isotherm Eq. (1). The **solid colored contours** show the required Q and K to meet the separation specifications with 1 kg to 1000 kg of total adsorbent mass. These curves were computed by sensitivity analysis of Eq. (3) with respect to the binding affinity K and membrane quantity v_{mem}. The **letters *A* to *I*** correspond with the existing materials in Table **??**. **(A)** For example, 93 kg of material ***D*** is required for $\mathrm{POU}_{24}^{\mathrm{B}}$ whereas only 46 kg of ***D*** is required for $\mathrm{POU}_{24}^{\mathrm{C}}$ as seen in Fig. 3 and Table **??**. The characteristics of ***D*** classify it into **Type 2** regime before crossover, because of which the implicit staging effect in the semi-continuous process outweighs the penalty from over-treatment. This results in the semi-continuous process requiring less of the same material than the equivalent batch process. From Table **??**, it is clear that the crossover occurs at $K = 6.6 \times 10^4$ because of which ***H*** and ***I*** require less material for the batch process (71 and 73 kg, respectively) when compared to the semi-continuous process (77 and 86 kg, respectively). **(B)** In addition to the trends observed in (A), it is seen that the faster regeneration time of $\mathrm{POU}_{6}^{\mathrm{B}}$ makes the use of materials with lower saturation capacity Q for this application feasible.

Descriptive names of existing sorbents studied

The descriptive names of existing sorbents used in the lead and arbitrary adsorbent (arsenic) case studies listed in Table **??** and Table **??**, respectively are listed below.

Table S1: Descriptive names of lead sorbents used in the point-of-use water treatment system case study.

Legend identifier	Material	Descriptive name	Reference
A	SI-APTS-EDTA	Silica-3-aminopropyltriethoxysilane-ethylenediaminetetraacetic acid	Gomes et al.[3]
B	PI-PS-PASH	Polyisoprene-b-polystyrene-b-poly[N-(2-mercaptoethyl)acrylamide] membrane	Weidman et al.[1]
C	PS-EDTA resin	Polystyrene-ethylenediaminetetraacetic acid resin	Wang et al.[4]
D	Psf-Terp	Polysulfone-terpyridine membrane	Zhang et al.[2]
E	EDTA-PCF	Magnetic ethylenediaminetetraacetic acid (EDTA) modified Preyssler/chitosan/Fe_3O_4 nanoparticles composite	Tanhaei et al.[5]
F	EDCMS	Magnetic ethylenediaminetetraacetic acid-modified chitosan/SiO_2/Fe_3O_4	Ren et al.[6]
G	Magnetic Fe_3O_4 yeast treated with EDTA dianhydride	Magnetic Fe_3O_4 yeast treated with ethylenediaminetetraacetic acid dianhydride	Xu et al.[7]
H	Fe_3O_4@SiO_2–EDTA	Ethylenediaminetetraacetic acid functionalized Fe_3O_4@SiO_2 (Note 3)	Liu et al.[8]
I	Mag-Ligand	A regenerable magnetic ligand which includes metal binding ethylenediaminetetraacetic acid attached to an iron oxide nanoparticle	Huang and Keller[9]

Note 3: The @ symbol indicates that the EDTA-functionalized iron oxide particles are on the surface of silicon dioxide.

Table S2: Descriptive names of arsenic sorbents used in the case study for an arbitrary adsorption process.

Legend identifier	Material	Descriptive name	Reference
a	H90	H-MFI-90 zeolite	Chutia et al. [10]
b	MAHS	Magnetite iron oxide (Fe_3O_4) nanoparticles sequestered on sulfonated Amberlite XAD-2 ion-exchange resin	Beker et al. [11]
c	HAX1	Iron (hydr)oxide nanoparticles inside strong base anion exchange (Note 4)	Gifford et al. [12]
d	ARM	Red much activated with 1M HCl	Altundoğan et al. [13]
e	Copper (II) oxide nanoparticles	Copper (II) oxide nanoparticles	Goswami et al. [14]

Note 4: Properties K and Q for material ***d*** was obtained by fitting the data from the Freundlich isotherm reported by Gifford et al. to the Langmuir isotherm using nonlinear regression.

Calculation of the upper bound on saturation capacity

The upper bound on saturation capacity is calculated using an optimization problem wherein the objective is to maximize the saturation capacity Q subject to the constraints of the semi-continuous material property target model Eq. (10) and material limitations Eqs. (13) and (14). The detailed derivation and optimization model formulation follow.

Material property constraint

Recall the semi-continuous material property target model from Eq. (10):

$$Q = \frac{1}{1-\varepsilon} \times (N_{BV} - \varepsilon) \times \frac{1 + Kc_{in}}{K} \qquad \forall\ N_{BV} > \varepsilon \tag{S69}$$

Note that the superscript ^{C} was dropped from Eq. (S69) for simplicity since the capacity upper bound calculation is done only for an adsorptive process operating in semi-continuous mode.

Introducing the definition of N_{BV} from Eq. (3) and rearranging to avoid divisions and gives the material property constraint for the maximization of the saturation capacity:

$$Q\ \ (1-\varepsilon)\ \ K = \left(\frac{v_{total}}{v_{mem}} - \varepsilon\right) \times (1 + Kc_{in}) \tag{S70}$$

$$\implies Q\ \ (1-\varepsilon)\ \ K\ v_{mem} = (v_{total} - \varepsilon\ v_{mem})\ \ (1 + Kc_{in}) \tag{S71}$$

Eq. (S71) is the material property constraint for the capacity upper bound maximization problem.

Material constraint

The contaminant adsorbed is limited by the amount of solute that can fit in its pores based on monolayer coverage and molar volume of the solute, Eq. (13):

$$Q \leq \frac{4\varepsilon}{d_p} \frac{1}{(\pi N_A)^{\frac{1}{3}}} \left(\frac{4}{3\,\overline{v_s}} \right)^{\frac{2}{3}} \tag{S72}$$

Rearranging Eq. (S72) to avoid divisions and replacing the inequality with an equality gives the material constraint:

$$Q\ d_p\ \ (\pi N_A)^{\frac{1}{3}}\ \ (3\,\overline{v_s})^{\frac{2}{3}} = \varepsilon\ 4^{\frac{5}{3}} \tag{S73}$$

Pore diameter constraint

Eq. (14) defines the pore diameter limitations dictated by available pressure drop:

$$d_p \geq \left(\frac{N_{BV}}{t_{total}} \frac{128\mu l_{mem}^2}{N\pi\Delta P} \right)^{\frac{1}{4}} \tag{S74}$$

To obtain the saturation capacity constraint, first, the definitions for N_{BV}, Eq. (3), and l_{mem}, Eq. (16), are introduced into. Eq. (S74) and the inequality is replaced with an equality:

$$d_p = \left(\frac{v_{total}}{t_{total}} \frac{128\mu v_{mem}}{N\pi\Delta P A_{mem}^2 n_{mod}^2} \right)^{\frac{1}{4}} \tag{S75}$$

Next, the requirement for integral number of parallel modules in the treatment system is relaxed to avoid solving a mixed integer nonlinear programming (MINLP) problem. Instead, fractional membrane modules are considered:

$$n_{mod} = \frac{v_{mem}}{A_{mem} l_{mem}} \tag{S76}$$

In Eq. (S76), l_{mem} is the thickness of the membrane in a module and is constant across

all modules. Introducing the expression for n_{mod} from Eq. (S76) into Eq. (S75) gives:

$$d_p = \left(\frac{v_{total}}{t_{total}} \frac{128 \mu l_{mem}^2}{N \pi \Delta P v_{mem}} \right)^{\frac{1}{4}} \tag{S77}$$

Finally, to ensure that Eq. (S77) is well scaled, a logarithmic transformation of the expressions is performed, after which it is rearranged to avoid divisions to give the pore diameter constraint:

$$4 \log(d_p) = \log(128 \ \mu \ v_{total}) + 2 \log(l_{mem}) - \log(\pi \ N \ \Delta P \ v_{mem} \ t_{total}) \tag{S78}$$

Optimization problem

Eqs. (S71), (S73), and (S78) are combined to form the optimization problem to maximize the saturation capacity:

$$\begin{aligned}
\max_{d_p, l_{mem}, Q, v_{mem}} \quad & Q \\
\text{s.t.} \quad & Q \ (1-\varepsilon) \ K \ v_{mem} = (v_{total} - \varepsilon \ v_{mem}) \ (1 + K c_{in}) \\
& Q \ d_p \ (\pi N_A)^{\frac{1}{3}} \ (3 \, \overline{v_s})^{\frac{2}{3}} = \varepsilon \ 4^{\frac{5}{3}} \\
& 4 \log(d_p) = \log(128 \ \mu \ v_{total}) + 2 \log(l_{mem}) - \log(\pi \ N \ \Delta P \ v_{mem} \ t_{total}) \\
& \underline{d_p} \leq dp \leq \overline{d_p} \\
& \underline{l_{mem}} \leq l_{mem} \leq \overline{l_{mem}} \\
& \underline{Q} \leq Q \leq \overline{Q} \\
& \underline{v_{mem}} \leq v_{mem} \leq \overline{v_{mem}}
\end{aligned} \tag{S79}$$

In Eq. (S79), underbars and overbars are used to denote lower and upper bounds on the decision variables, respectively. The bounds $\underline{d_p} = 1 \times 10^{-10}$ m, $\overline{d_p} = 2 \times 10^{-6}$ m, $\underline{Q} = 0.3$ mmol cm^{-3}, $\overline{Q} = 75$ mmol cm^{-3}, $\underline{v_{mem}} = 1 \times 10^{-3}$ m^{-3}, and $\overline{v_{mem}} = 120$ m^{-3} were used in calculating the upper bound on saturation capacity. To calculate the upper bound for a 1

mm thick membrane, the bounds on membrane thickness were set to $\underline{l_{mem}} = \overline{l_{mem}} = 1 \times 10^{-3}$ m. Similarly, for the 0.1 mm thick membrane, $\underline{l_{mem}} = \overline{l_{mem}} = 1 \times 10^{-4}$ m was used.

Dimensionless material property targets

The following pages contain dimensionless material property target plots for all combination of removal ratio r = 1.5, 5, 10, 50, 100, and 1000, and sorbent porosity ε = 0.1, 0.2, 0.3, and 0.4. Each plot shows contours for N_{BV} = 50, 500, 1000, 5000, 10000, and 50000. These plots may be used to rapidly screen emerging nanomaterials to assess their performance at the systems level. The number of bed volumes N_{BV} for a given sorbent, or, for fixed N_{BV}, the increment in material properties $\overline{K}$ and $\overline{Q}$ required for an application may be easily read from these plots.

In Figs. S6-S29, the solid contours correspond to an adsorptive separation process operated in semi-continuous mode and were obtained by the sensitivity analysis of Eq. (11) with respect to N_{BV} and $\overline{K}$. The dashed contours are for the same separation when operated in batch mode and were calculated from a sensitivity analysis of Eq. (5) with respect to N_{BV} and $\overline{K}$. The predicted crossover point calculated using Eqs. (S41) and (S47), if applicable, is marked with a circle.

Recall that at moderate removal ratios the relative behavior of the batch and semi-continuous processes fall into the Type 2 regime characterized by a crossover point. However, some crossover points occur at very large values of $\overline{K}$, making Type 2 contours visually indistinguishable from Type 3 contours. For example, in Fig. S26 the contour for $N_{BV} = 50$ falls in the Type 3 regime, while the contours for $N_{BV} = 500$ to $N_{BV} = 50000$ fall under the Type 2 regime with crossover occurring at K $> 10^6$. The user is cautioned to use Eq. (**??**) to verify the regime into which the contours are classified, especially if no crossover point has been marked in the figure.

If the user wishes to obtain a dimensionless property target plot that is not in this

document, they may use the code available at the following link to generate the same: `https://github.com/dowlinglab/multiscale-adsorption-targets`

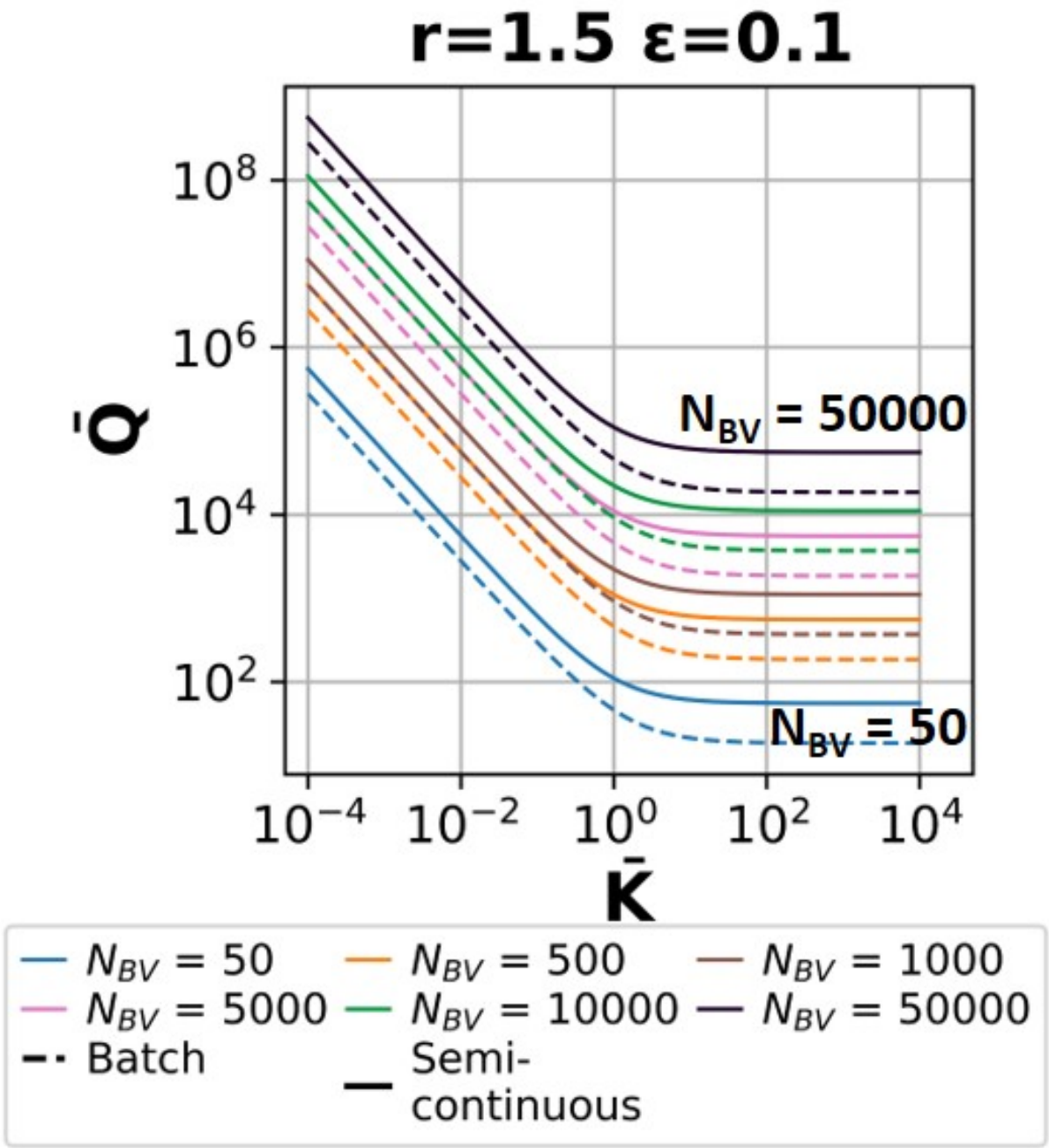

Figure S6: Dimensionless material property targets for removal ratio $r = 1.5$ and $\varepsilon = 0.1$.

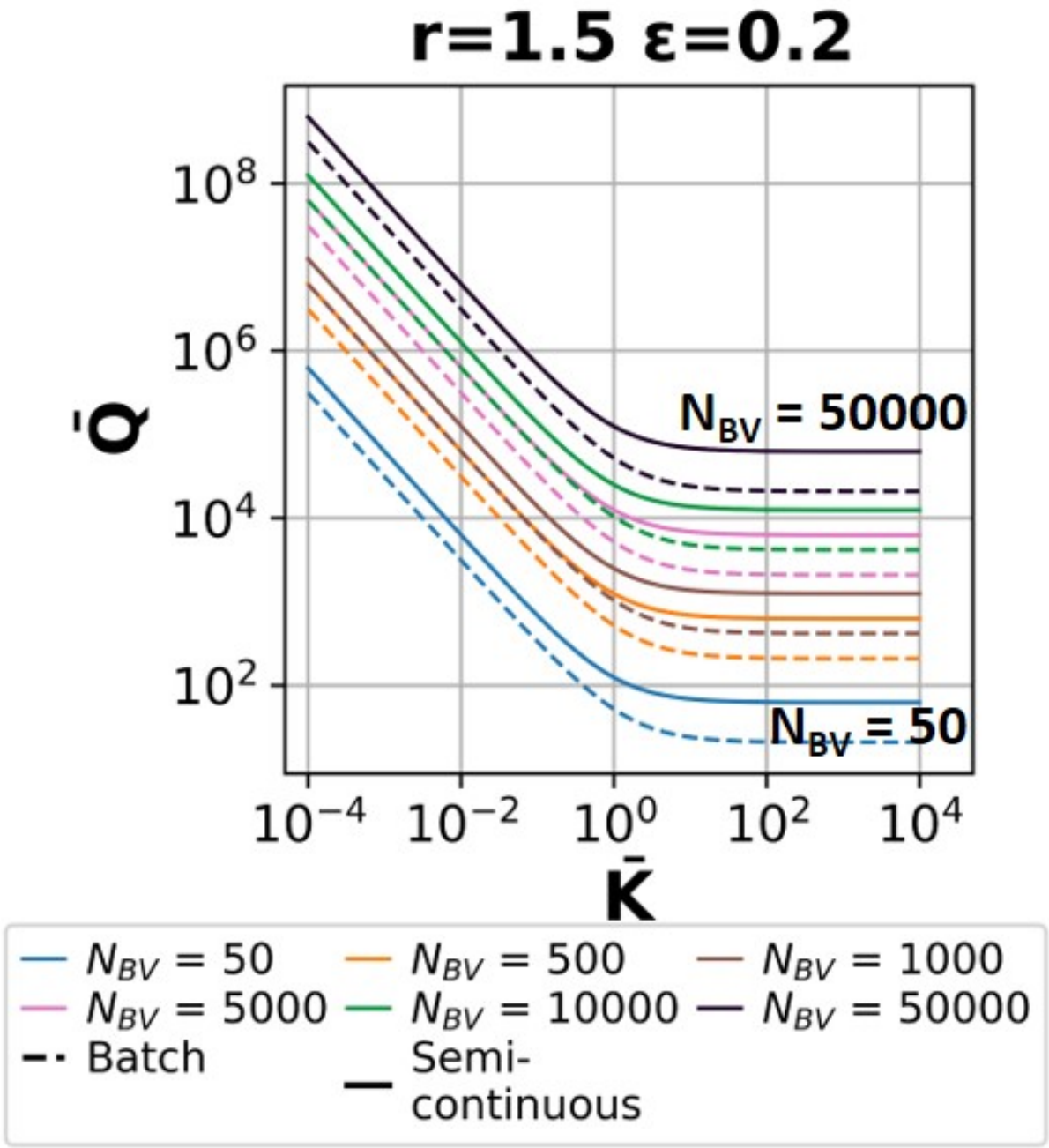

Figure S7: Dimensionless material property targets for removal ratio $r = 1.5$ and $\varepsilon = 0.2$.

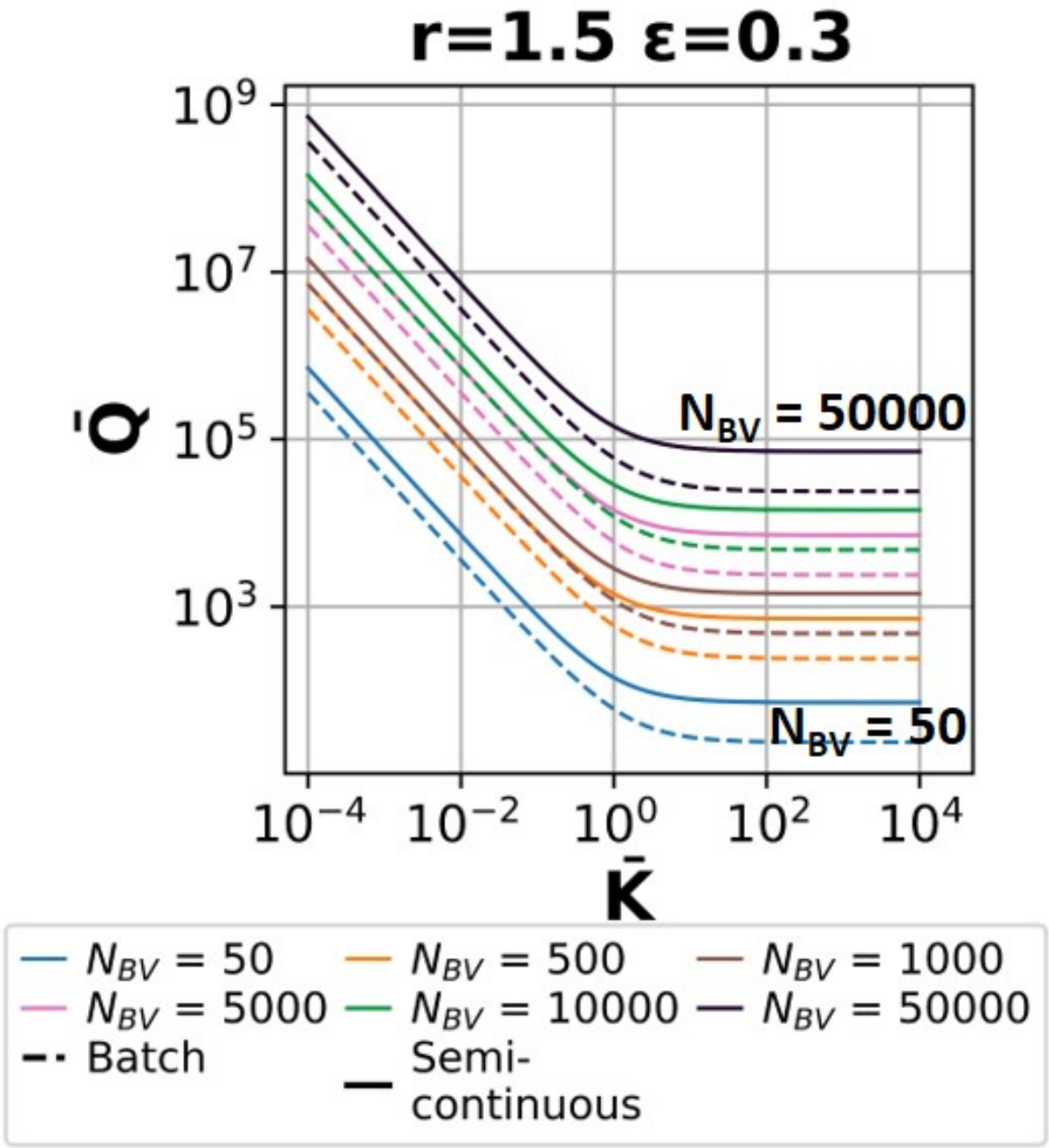

Figure S8: Dimensionless material property targets for removal ratio $r = 1.5$ and $\varepsilon = 0.3$.

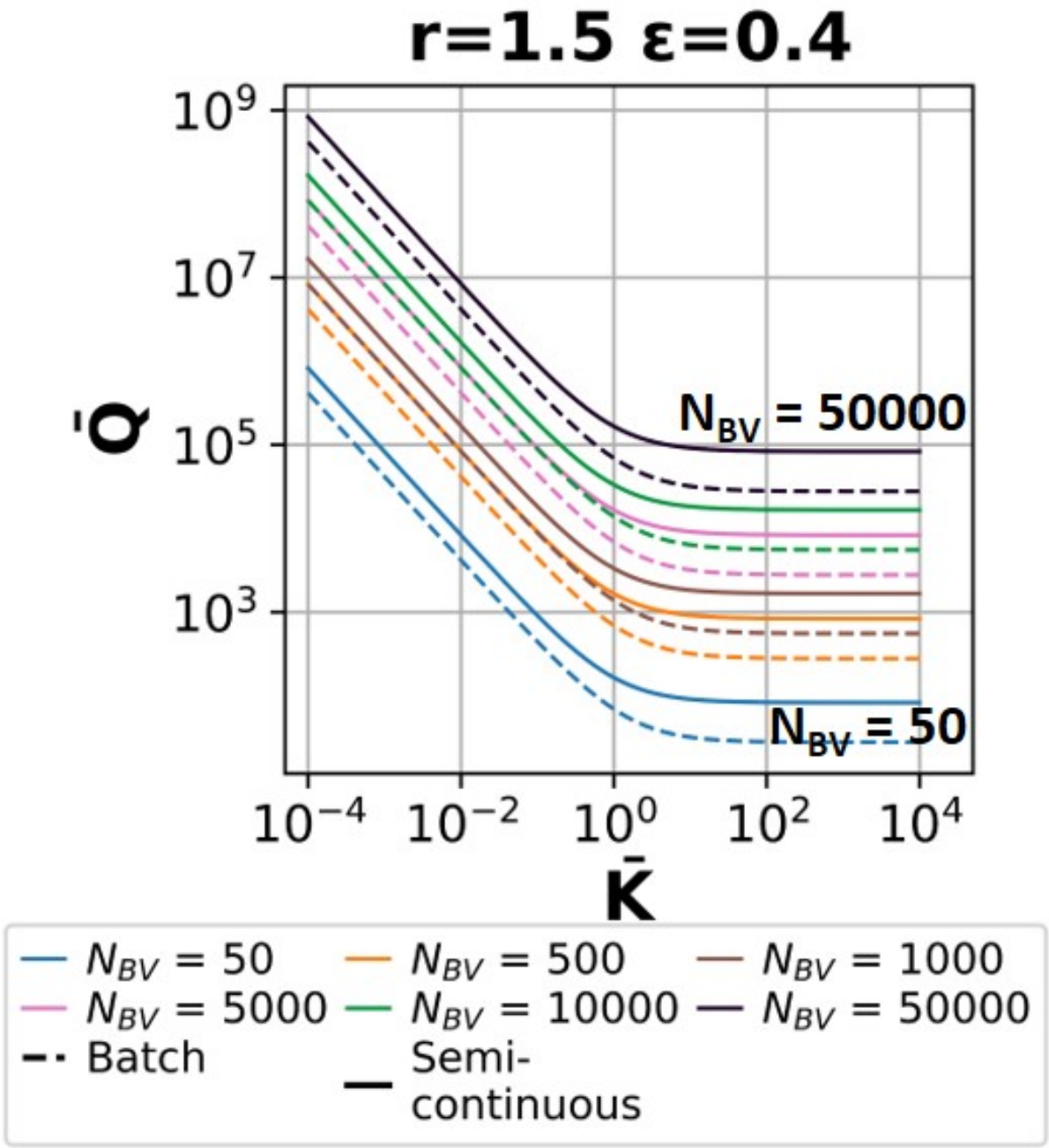

Figure S9: Dimensionless material property targets for removal ratio $r = 1.5$ and $\varepsilon = 0.4$.

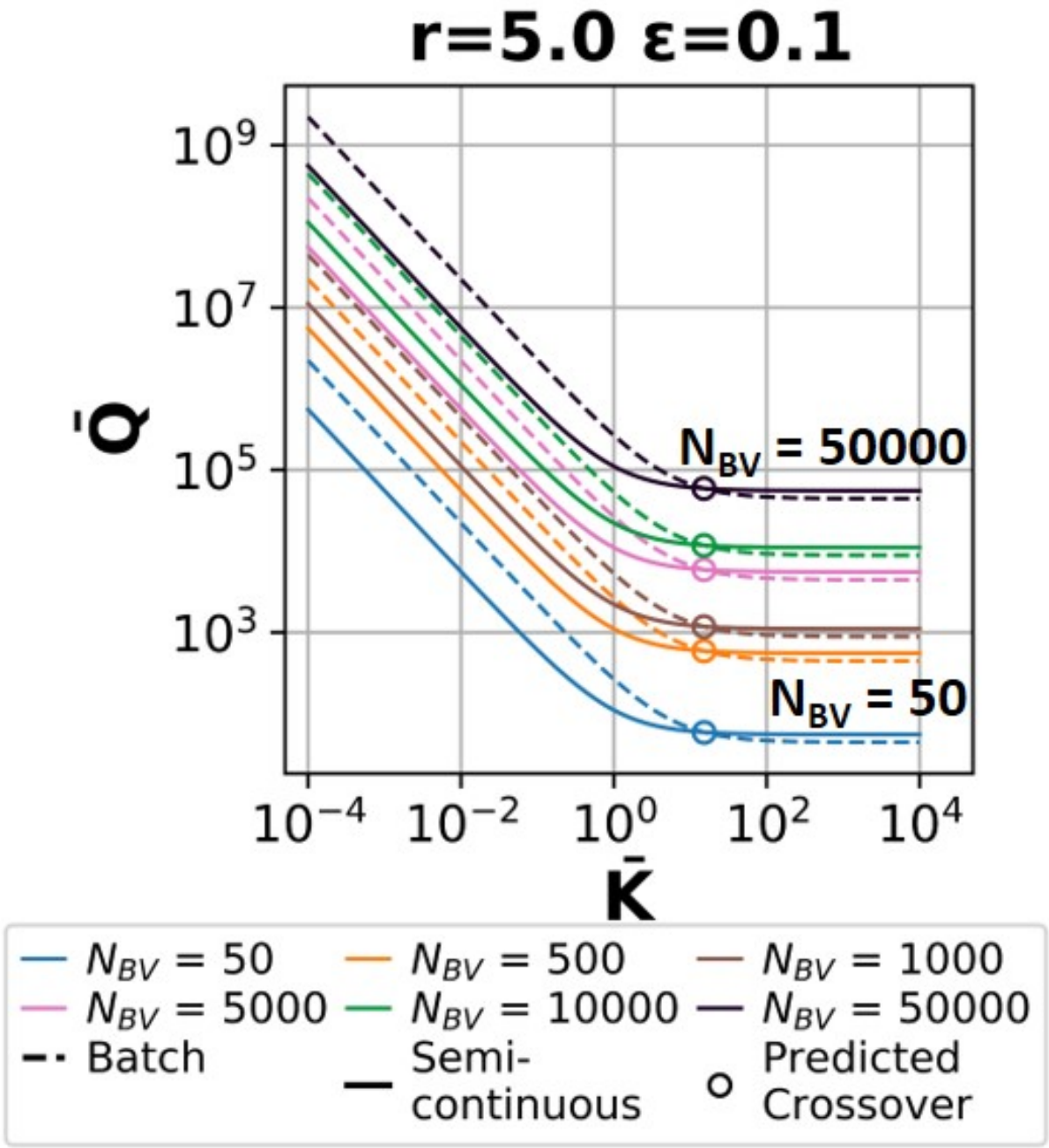

Figure S10: Dimensionless material property targets for removal ratio $r = 5$ and $\varepsilon = 0.1$.

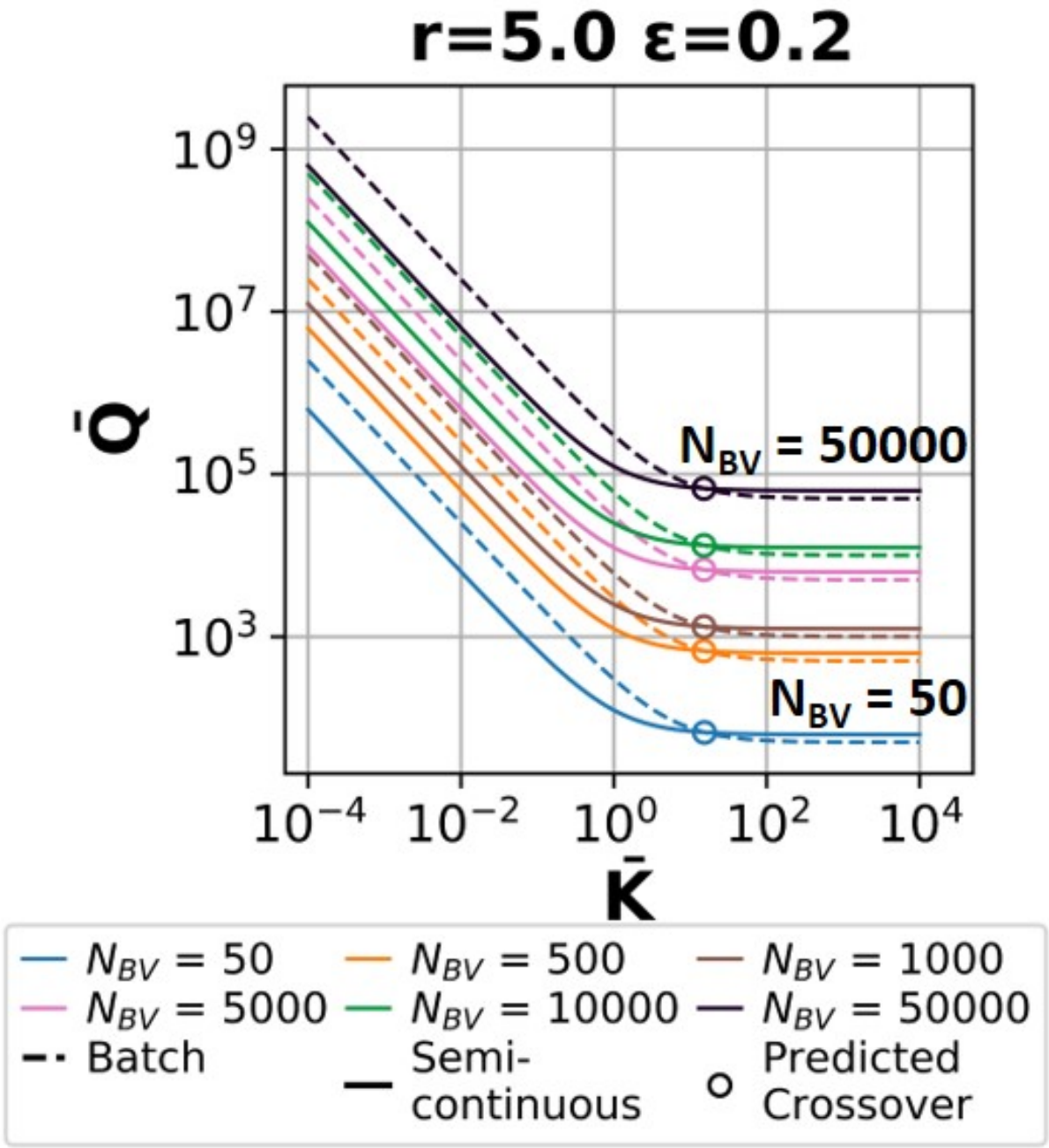

Figure S11: Dimensionless material property targets for removal ratio $r = 5$ and $\varepsilon = 0.2$.

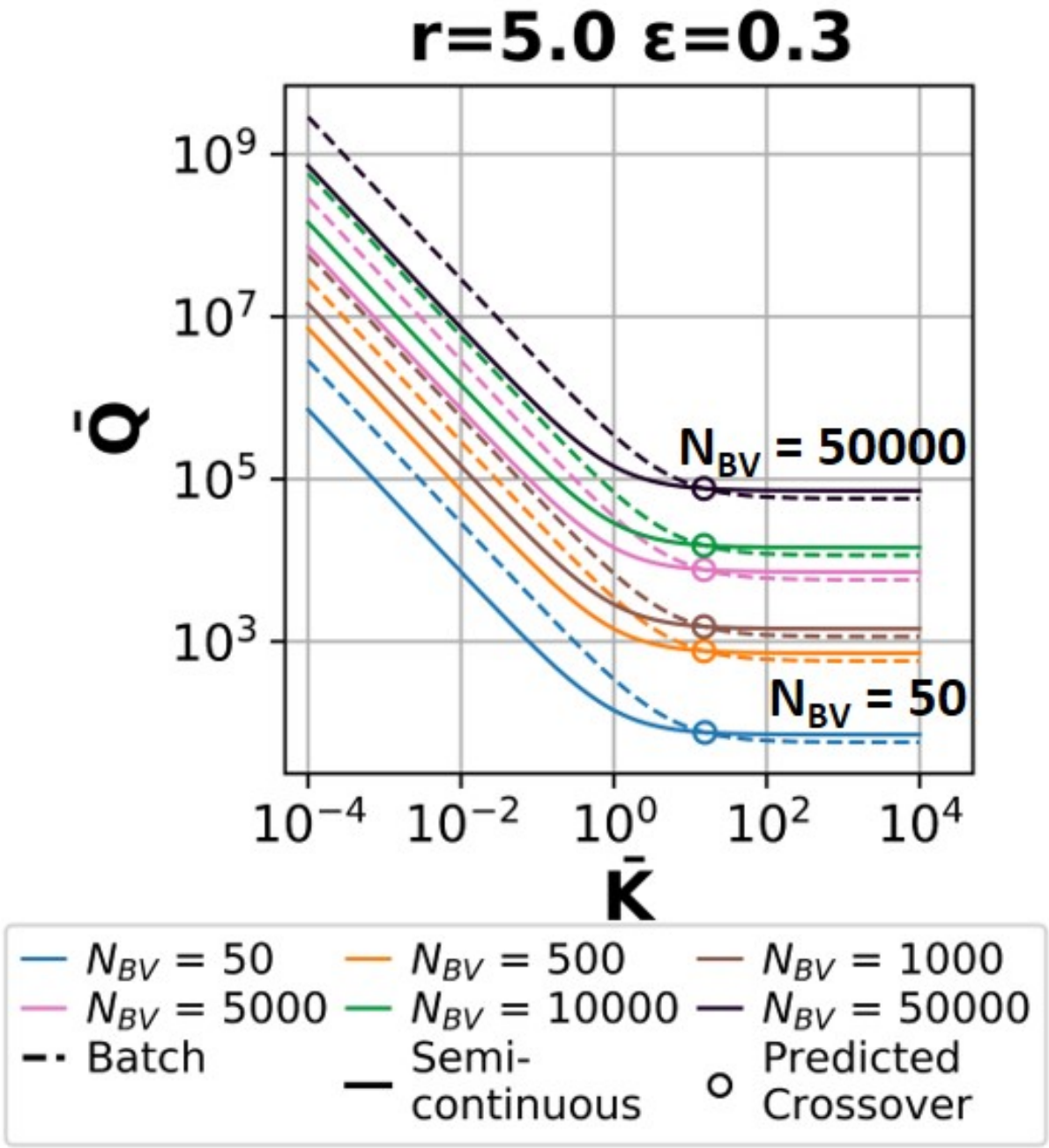

Figure S12: Dimensionless material property targets for removal ratio $r = 5$ and $\varepsilon = 0.3$.

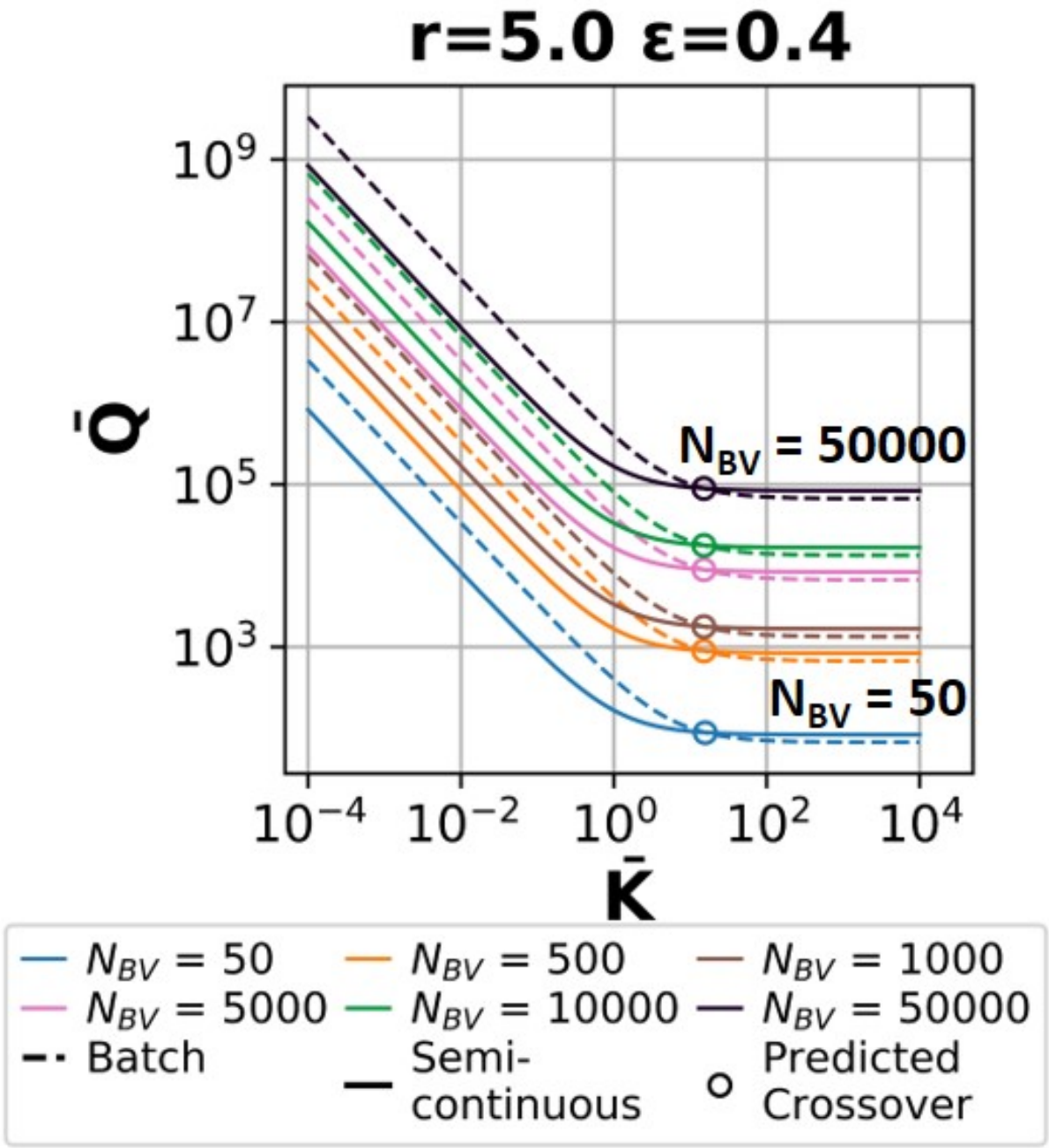

Figure S13: Dimensionless material property targets for removal ratio $r = 5$ and $\varepsilon = 0.4$.

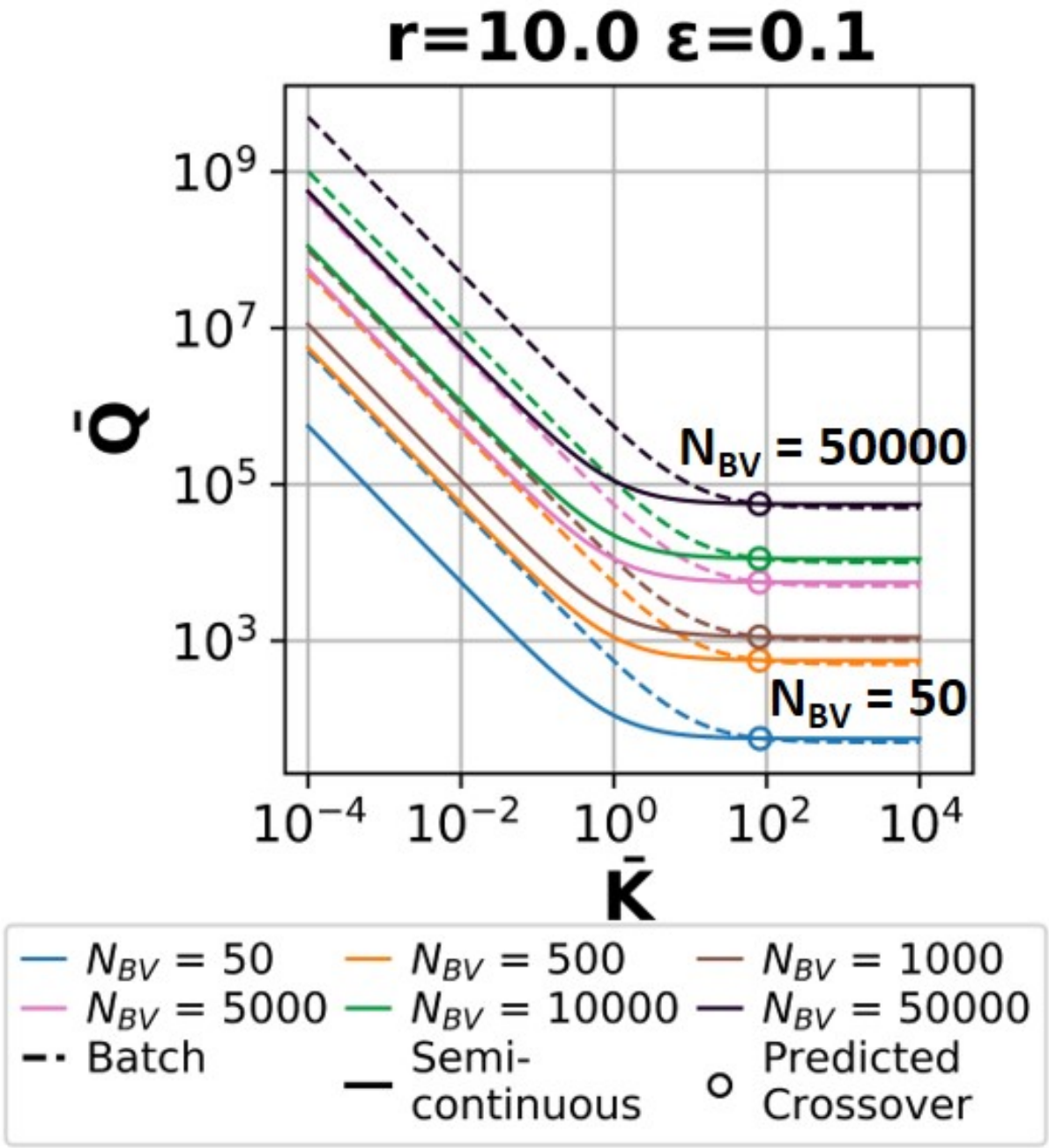

Figure S14: Dimensionless material property targets for removal ratio $r = 10$ and $\varepsilon = 0.1$.

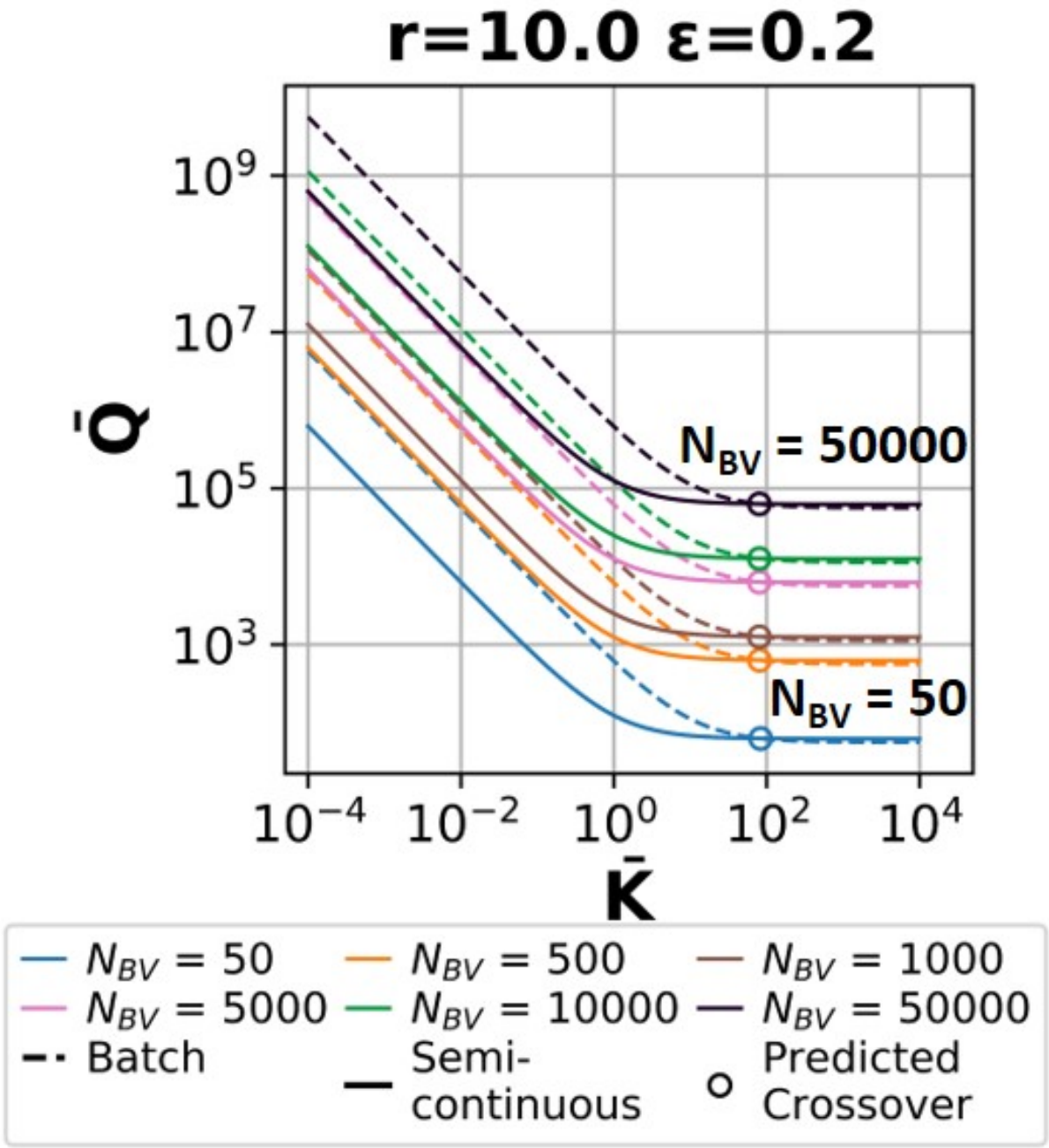

Figure S15: Dimensionless material property targets for removal ratio $r = 10$ and $\varepsilon = 0.2$.

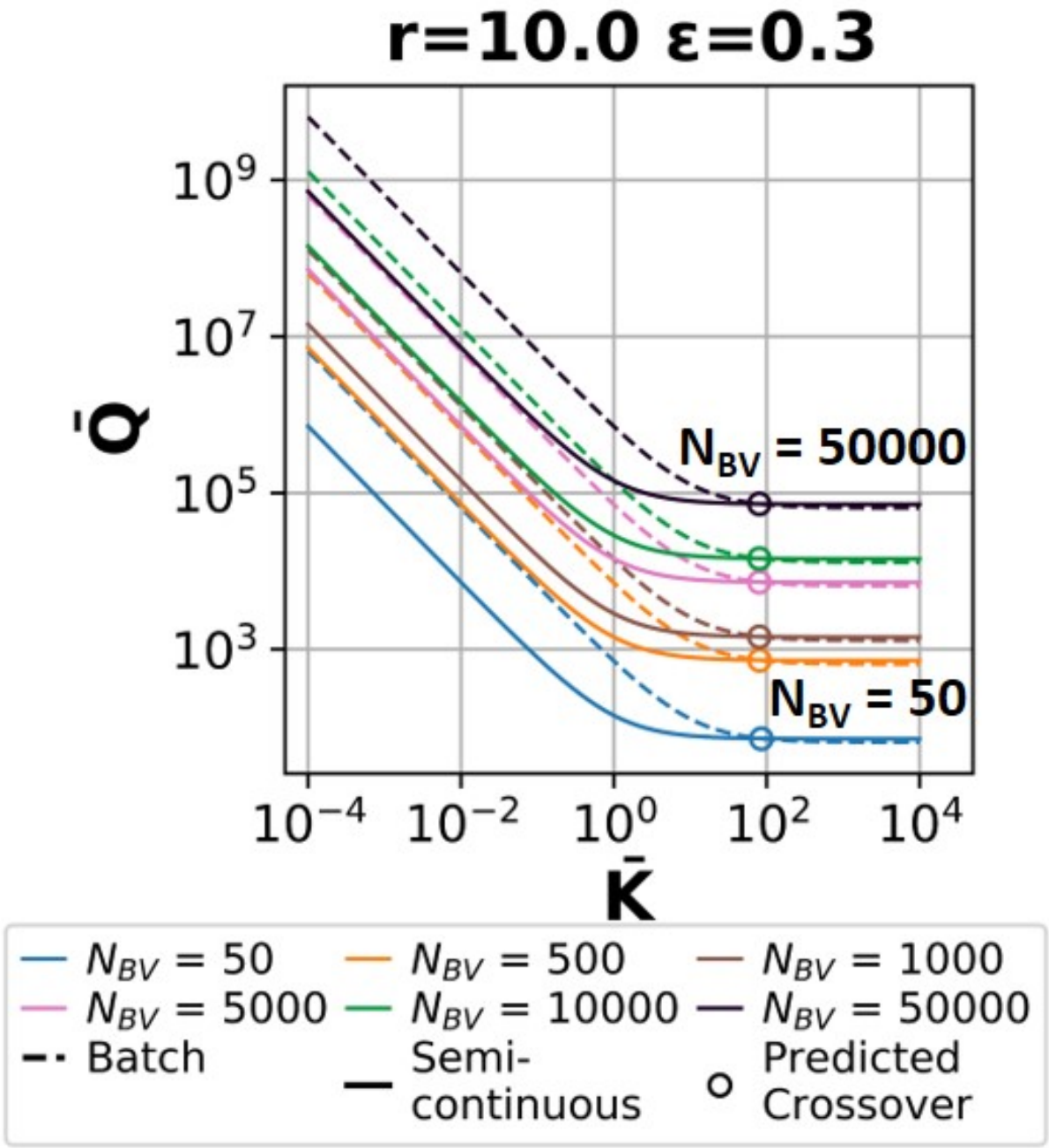

Figure S16: Dimensionless material property targets for removal ratio $r = 10$ and $\varepsilon = 0.3$.

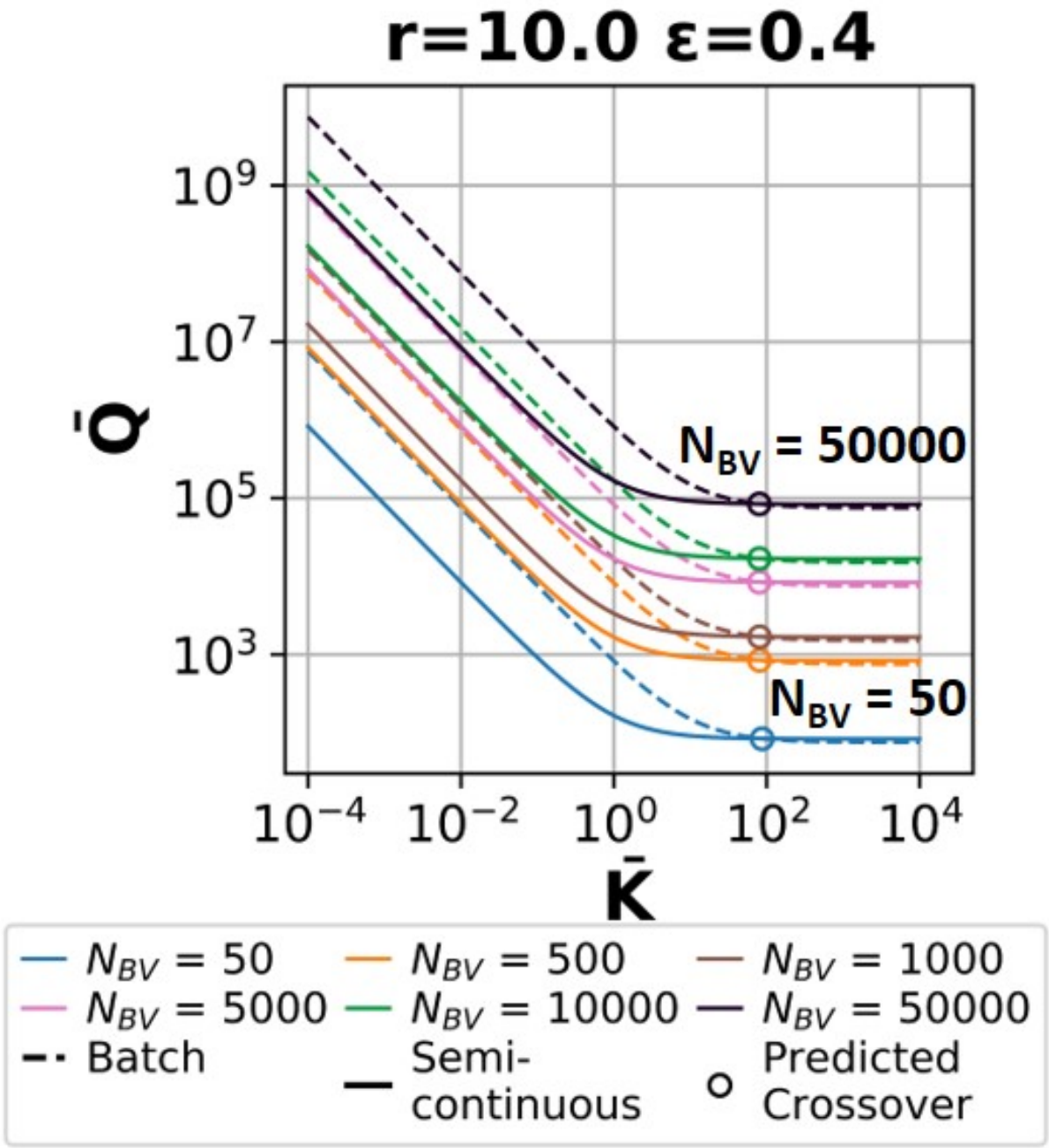

Figure S17: Dimensionless material property targets for removal ratio $r = 10$ and $\varepsilon = 0.4$.

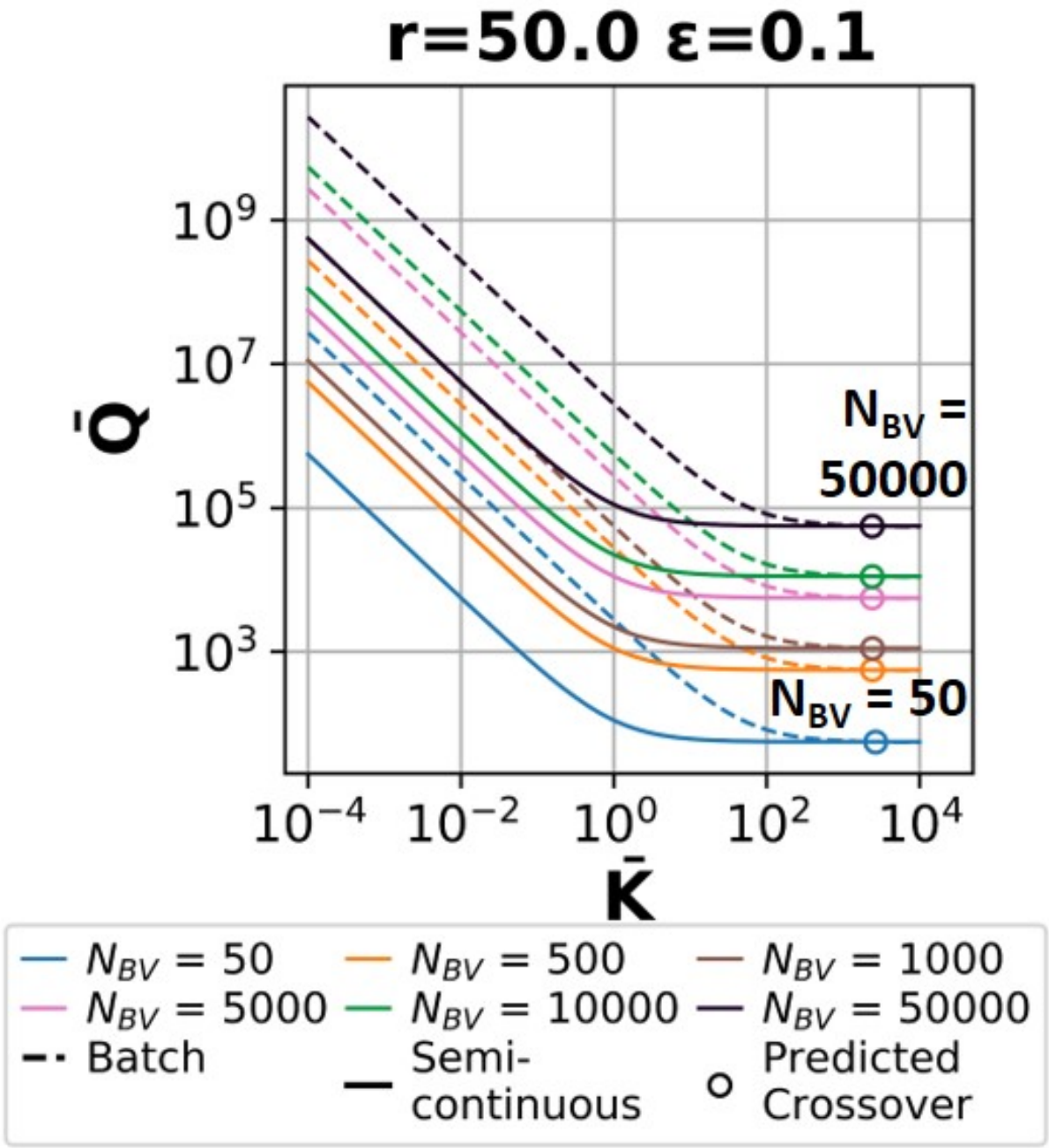

Figure S18: Dimensionless material property targets for removal ratio $r = 50$ and $\varepsilon = 0.1$.

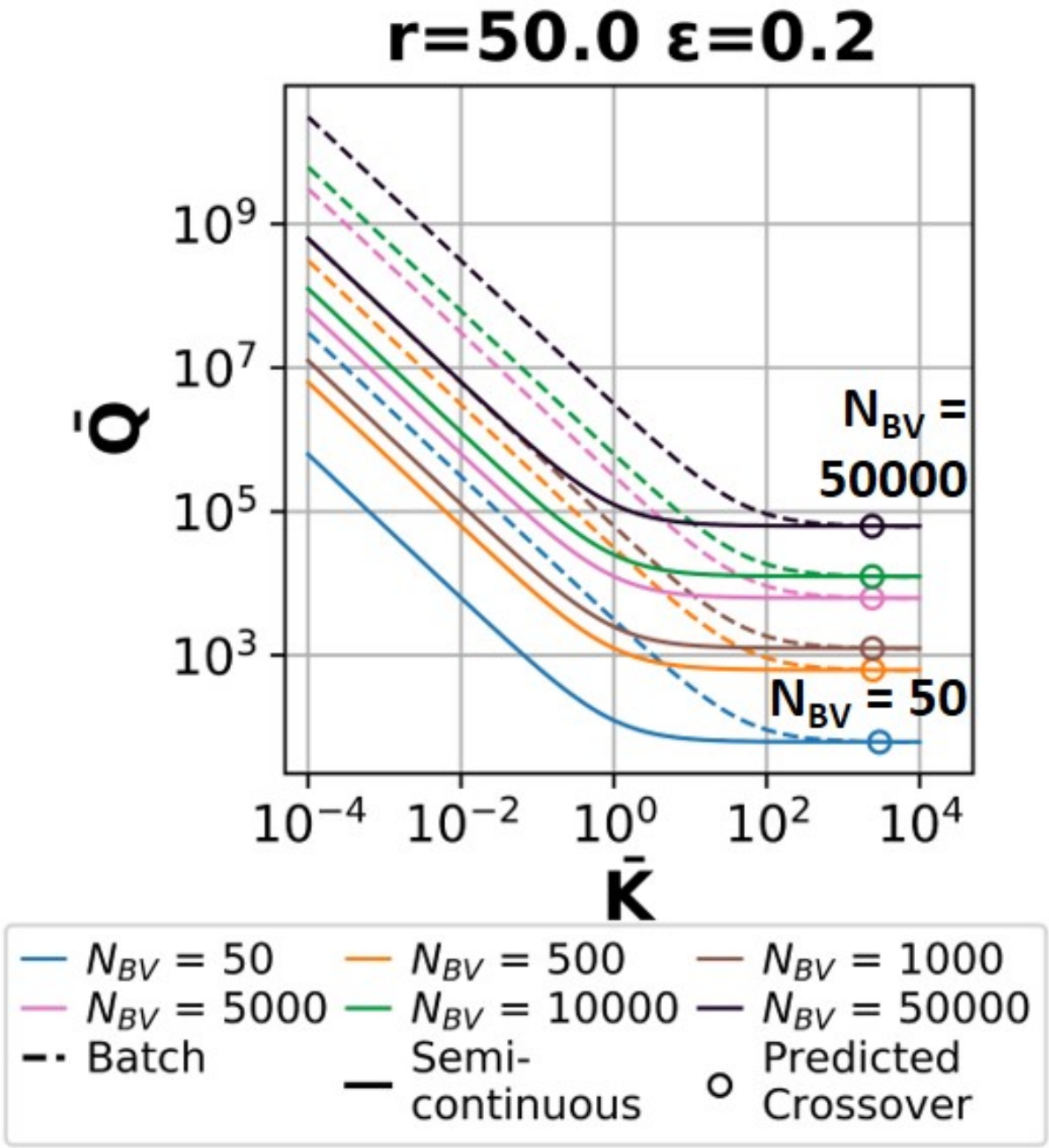

Figure S19: Dimensionless material property targets for removal ratio $r = 50$ and $\varepsilon = 0.2$.

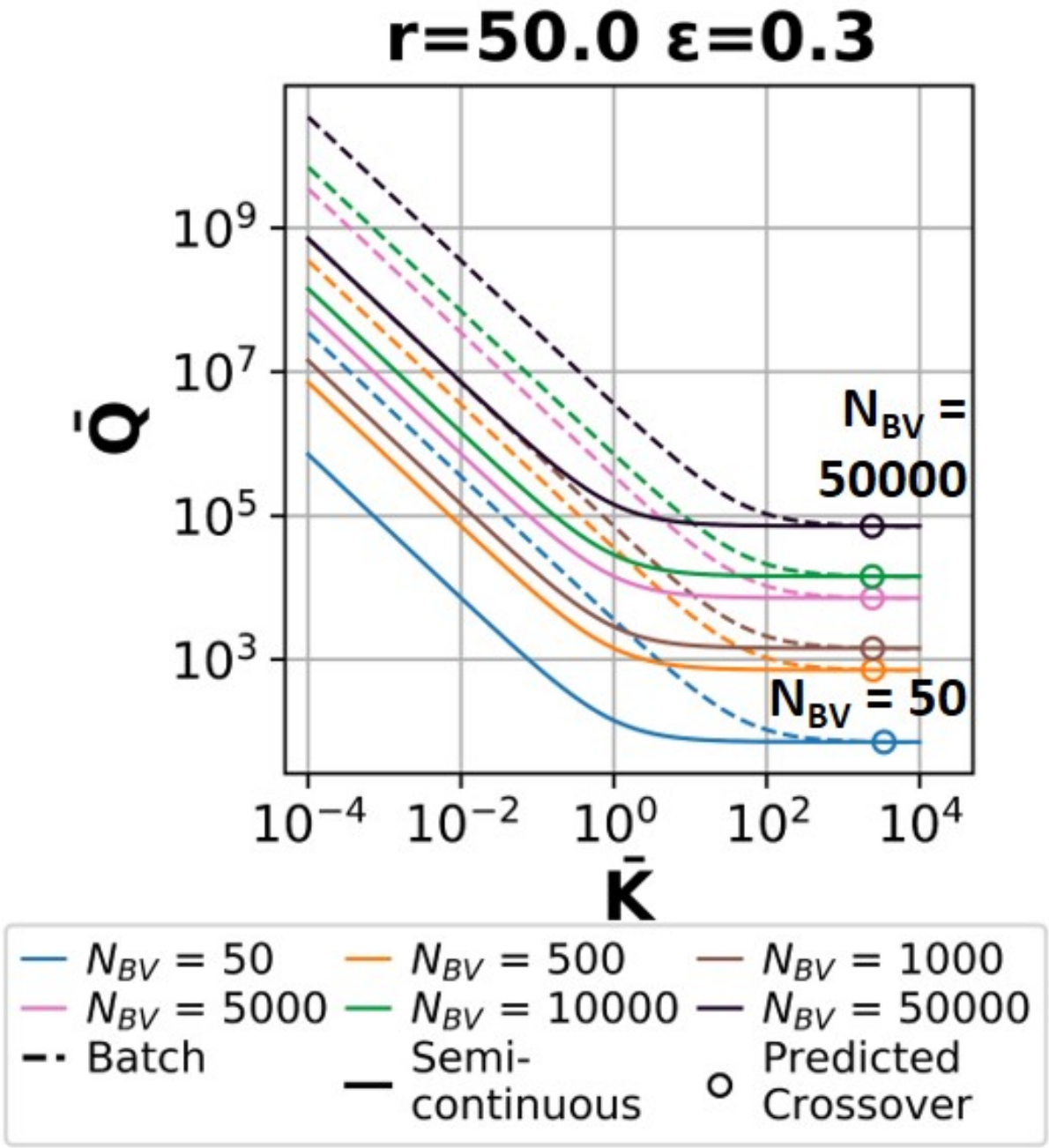

Figure S20: Dimensionless material property targets for removal ratio $r = 50$ and $\varepsilon = 0.3$.

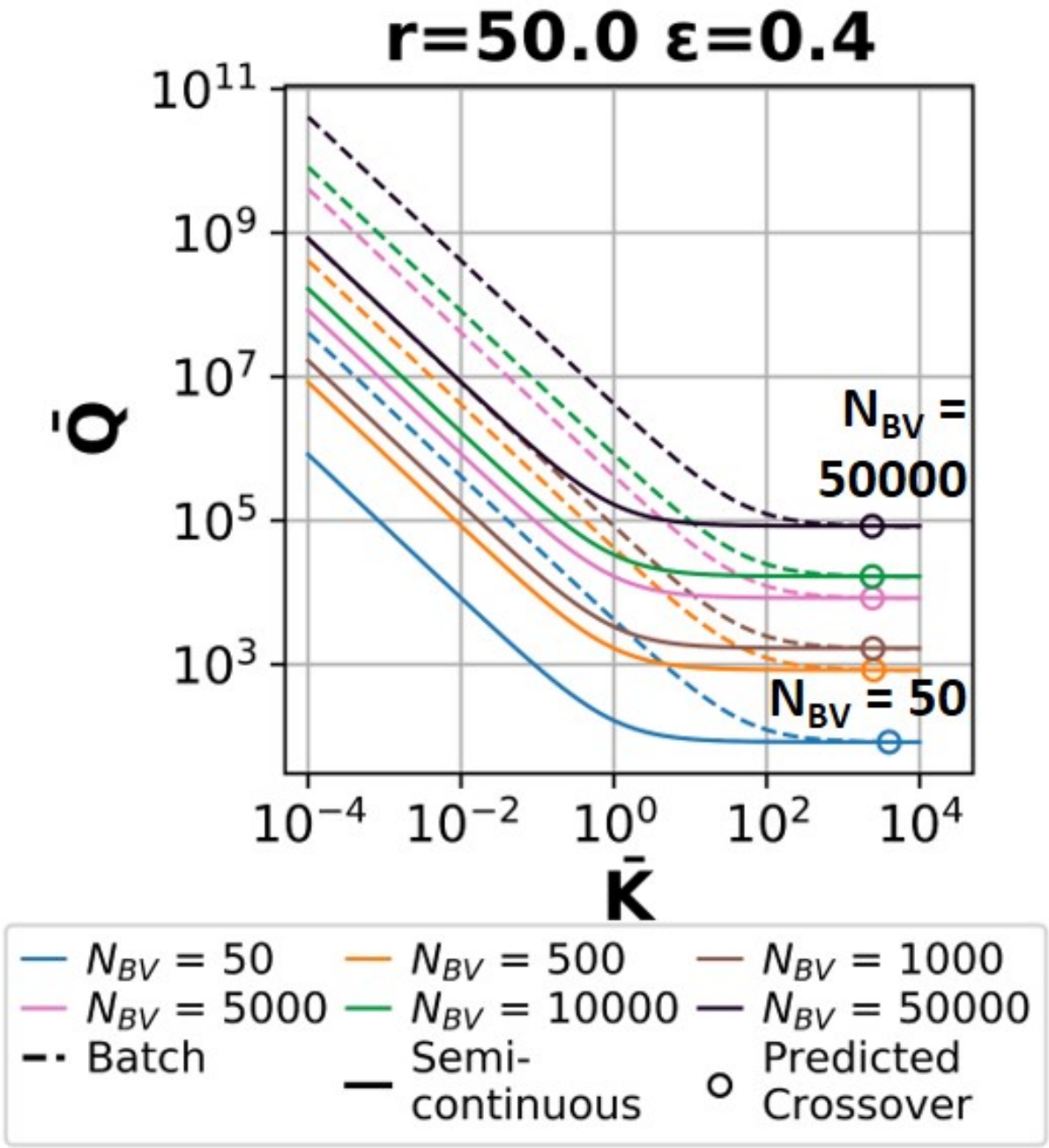

Figure S21: Dimensionless material property targets for removal ratio $r = 50$ and $\varepsilon = 0.4$.

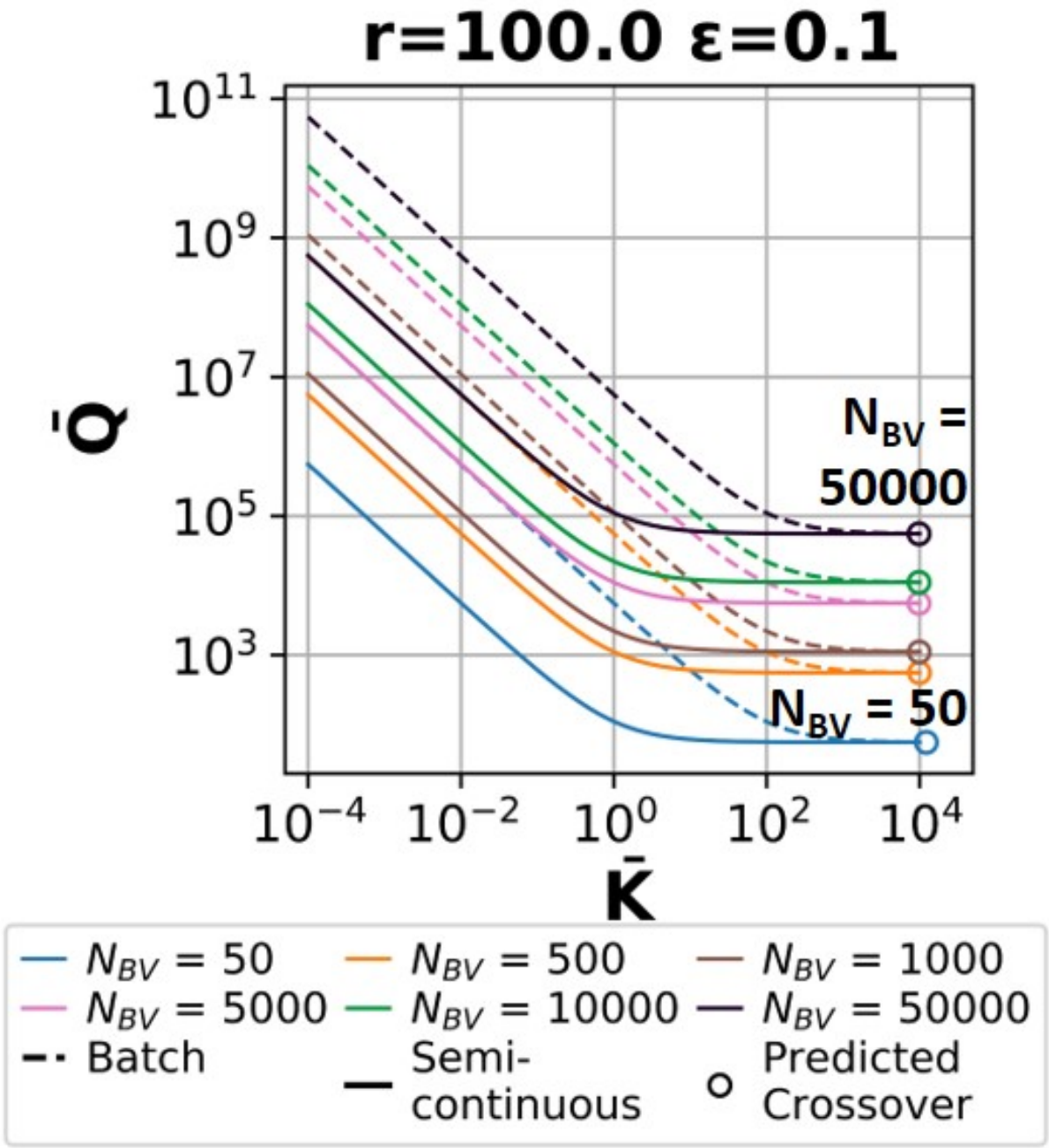

Figure S22: Dimensionless material property targets for removal ratio $r = 100$ and $\varepsilon = 0.1$.

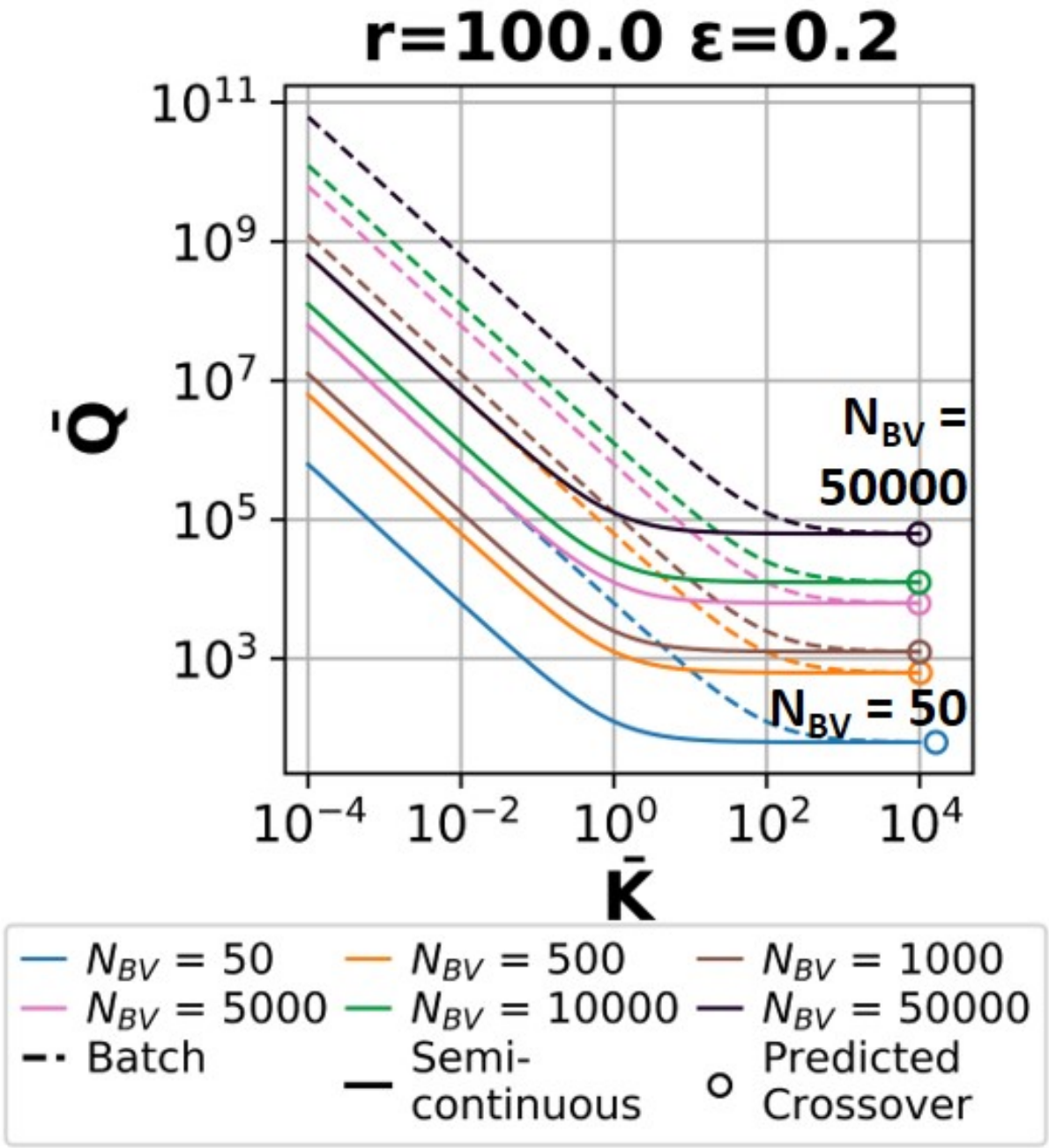

Figure S23: Dimensionless material property targets for removal ratio $r = 100$ and $\varepsilon = 0.2$.

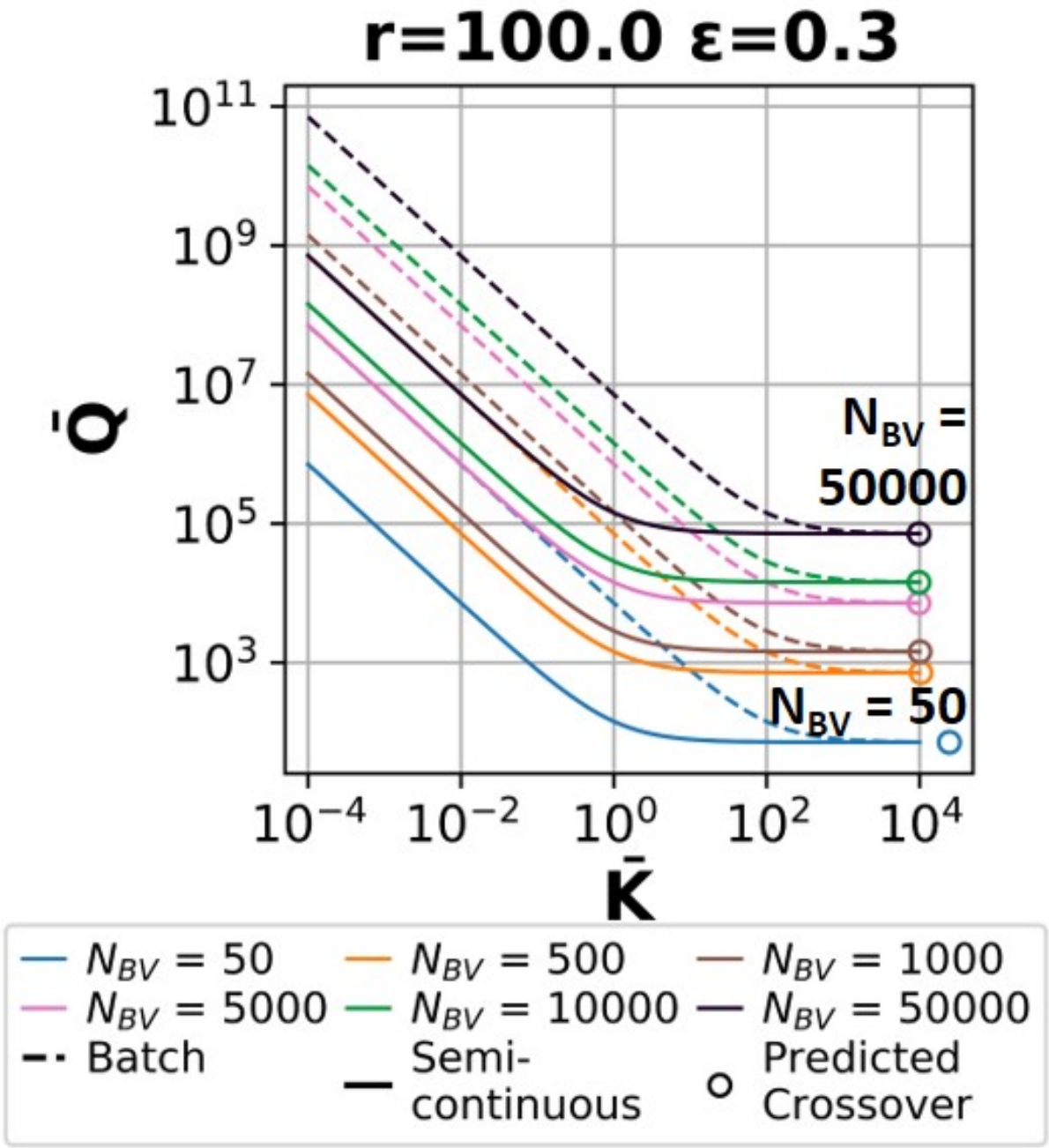

Figure S24: Dimensionless material property targets for removal ratio $r = 100$ and $\varepsilon = 0.3$.

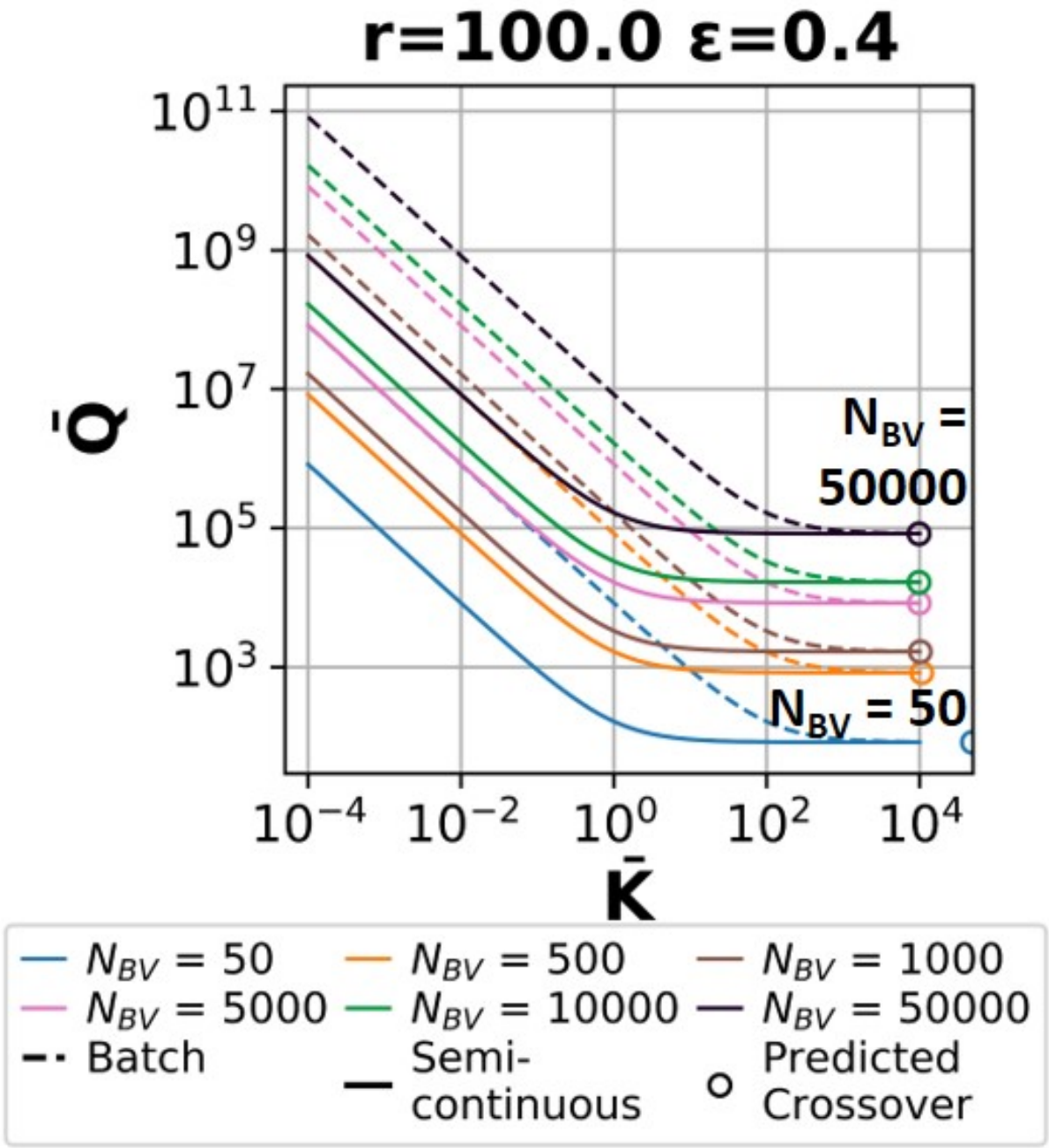

Figure S25: Dimensionless material property targets for removal ratio $r = 100$ and $\varepsilon = 0.4$.

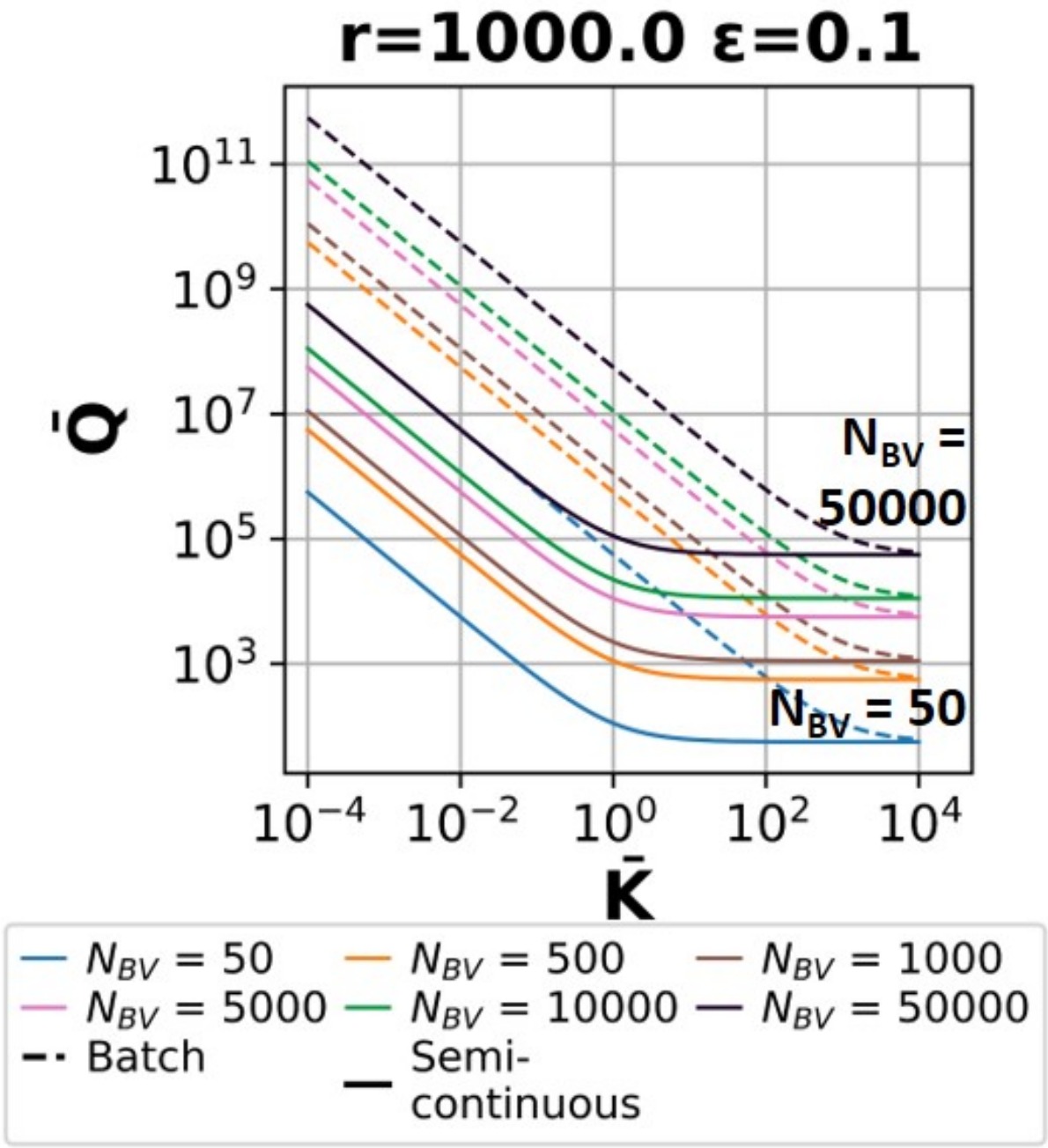

Figure S26: Dimensionless material property targets for removal ratio $r = 1000$ and $\varepsilon = 0.1$. Note that the contour for $N_{BV} = 50$ falls in the Type 3 regime as calculated from Eq. (**??**), while the contours for $N_{BV} = 500$ to $N_{BV} = 50000$ fall under the Type 2 regime with crossover occurring at $\mathrm{K} > 10^6$. These contours are visually indistinguishable, and Eq. (**??**) should be used to verify the regime into which the contours are classified. Eqs. (S41) and (S47) may be used to find the exact crossover point.

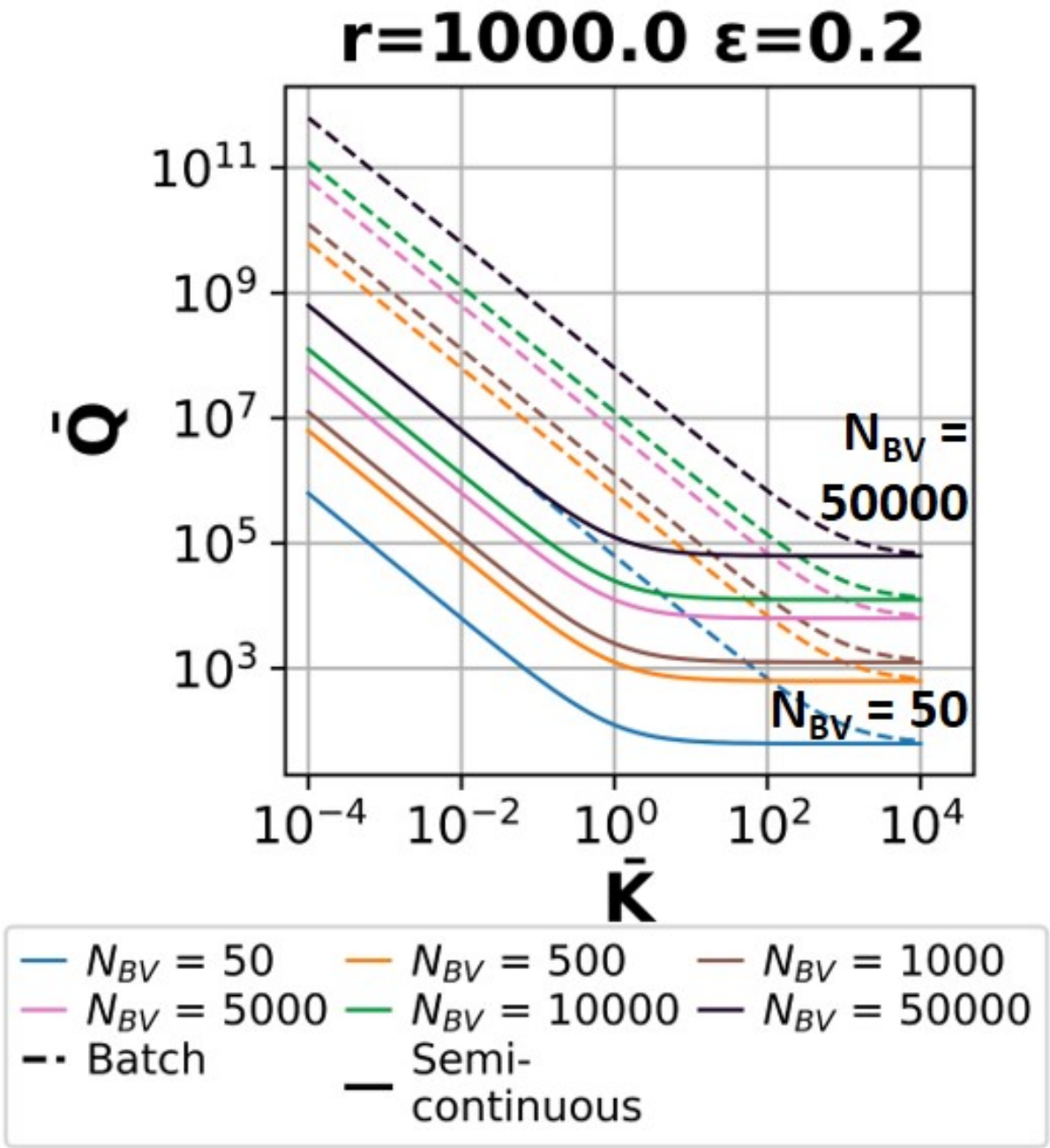

Figure S27: Dimensionless material property targets for removal ratio $r = 1000$ and $\varepsilon = 0.2$. Note that the contour for $N_{BV} = 50$ falls in the Type 3 regime as calculated from Eq. (**??**), while the contours for $N_{BV} = 500$ to $N_{BV} = 50000$ fall under the Type 2 regime with crossover occurring at $\mathrm{K} > 10^6$. These contours are visually indistinguishable, and Eq. (**??**) should be used to verify the regime into which the contours are classified. Eqs. (S41) and (S47) may be used to find the exact crossover point.

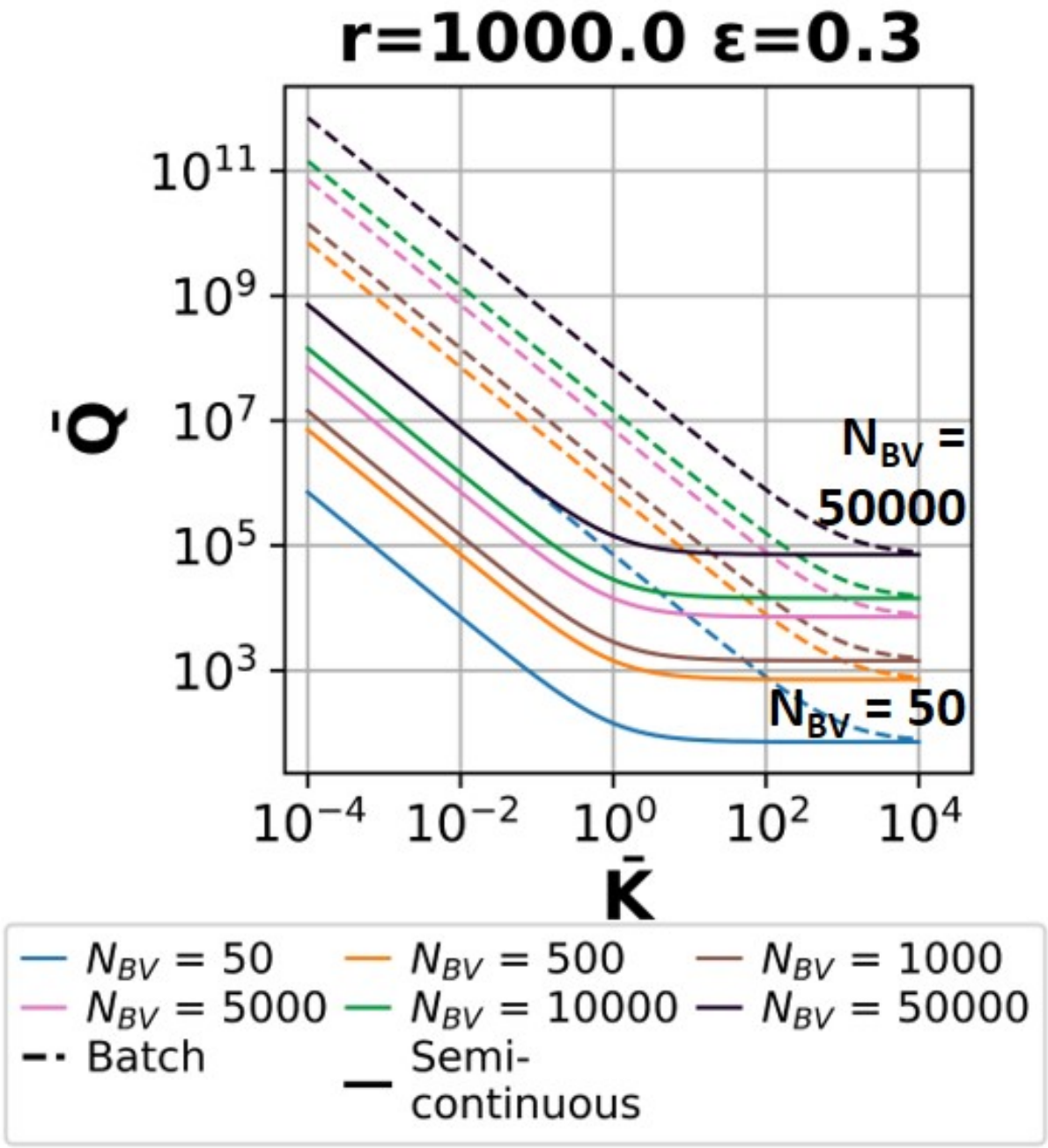

Figure S28: Dimensionless material property targets for removal ratio $r = 1000$ and $\varepsilon = 0.3$. Note that the contour for $N_{BV} = 50$ falls in the Type 3 regime as calculated from Eq. (**??**), while the contours for $N_{BV} = 500$ to $N_{BV} = 50000$ fall under the Type 2 regime with crossover occurring at $\mathrm{K} > 10^6$. These contours are visually indistinguishable, and Eq. (**??**) should be used to verify the regime into which the contours are classified. Eqs. (S41) and (S47) may be used to find the exact crossover point.

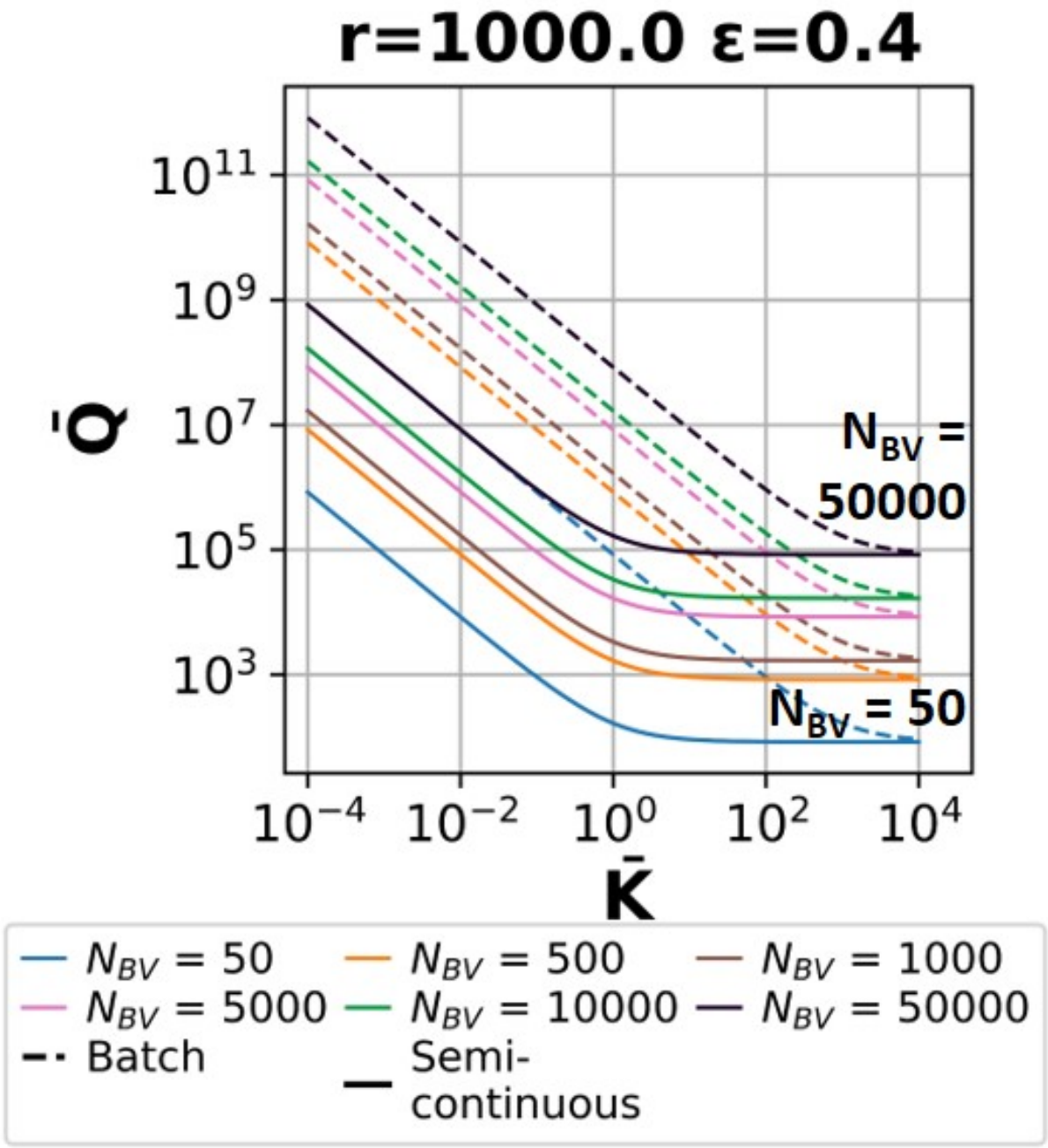

Figure S29: Dimensionless material property targets for removal ratio $r = 1000$ and $\varepsilon = 0.4$. Note that the contour for $N_{BV} = 50$ falls in the Type 3 regime as calculated from Eq. (**??**), while the contours for $N_{BV} = 500$ to $N_{BV} = 50000$ fall under the Type 2 regime with crossover occurring at $\mathrm{K} > 10^6$. These contours are visually indistinguishable, and Eq. (**??**) should be used to verify the regime into which the contours are classified. Eqs. (S41) and (S47) may be used to find the exact crossover point.

References

(1) Weidman, J. L.; Mulvenna, R. A.; Boudouris, B. W.; Phillip, W. A. Nanoporous block polymer thin films functionalized with bio-inspired ligands for the efficient capture of heavy metal ions from water. *ACS Applied Materials and Interfaces* **2017**, *9*, 19152–19160.

(2) Zhang, Y.; Vallin, J. R.; Sahoo, J. K.; Gao, F.; Boudouris, B. W.; Webber, M. J.; Phillip, W. A. High-affinity detection and capture of heavy metal contaminants using block polymer composite membranes. *ACS Central Science* **2018**, *4*, 1697–1707.

(3) Gomes, E. C. C.; Sousa, A. F. D.; Vasconcelos, P. H. M.; Melo, D. Q.; Diógenes, I. C. N.; Sousa, E. H. S. D.; Ronaldo, F.; San, R. A. S.; Longhinotti, E. Synthesis of bifunctional mesoporous silica spheres as potential adsorbent for ions in solution. *Chemical Engineering Journal* **2013**, *214*, 27–33.

(4) Wang, L.; Yang, L.; Li, Y.; Zhang, Y.; Ma, X.; Ye, Z. Study on adsorption mechanism of Pb(II) and Cu(II) in aqueous solution using PS-EDTA resin. *Chemical Engineering Journal* **2010**, *163*, 364–372.

(5) Tanhaei, B.; Ayati, A.; Bamoharram, F. F.; Sillanpää, M. Magnetic EDTA functionalized preyssler cross linked chitosan nanocomposite for adsorptive removal of Pb(II) ions. *CLEAN-Soil, Air, Water* **2017**, *45*, 1700328.

(6) Ren, Y.; Abbood, H. A.; He, F.; Peng, H.; Huang, K. Magnetic EDTA-modified chitosan/SiO_2/Fe_3O_4 adsorbent : Preparation , characterization , and application in heavy metal adsorption. *Chemical Engineering Journal* **2013**, *226*, 300–311.

(7) Xu, M.; Zhang, Y.; Zhang, Z.; Shen, Y.; Zhao, M.; Pan, G. Study on the adsorption of Ca^{2+} , Cd^{2+} and Pb^{2+} by magnetic Fe_3O_4 yeast treated with EDTA dianhydride. *Chemical Engineering Journal* **2011**, *168*, 737–745.

(8) Liu, Y.; Fu, R.; Sun, Y.; Zhou, X.; Ali, S.; Xu, X. Multifunctional nanocomposites Fe_3O_4@SiO_2-EDTA for Pb(II) and Cu(II) removal from aqueous solutions. *Applied Surface Science* **2016**, *369*, 267–276.

(9) Huang, Y.; Keller, A. A. EDTA functionalized magnetic nanoparticle sorbents for cadmium and lead contaminated water treatment. *Water Research* **2015**, *80*, 159 – 168.

(10) Chutia, P.; Kato, S.; Kojima, T.; Satokawa, S. Arsenic adsorption from aqueous solution on synthetic zeolites. *Journal of Hazardous Materials* **2009**, *162*, 440–447.

(11) Beker, U.; Cumbal, L.; Duranoglu, D.; Kucuk, I.; Sengupta, A. Preparation of Fe oxide nanoparticles for environmental applications: arsenic removal. *Environmental Geochemistry and Health* **2010**, *32*, 291–296.

(12) Gifford, M.; Hristovski, K.; Westerhoff, P. Ranking traditional and nano-enabled sorbents for simultaneous removal of arsenic and chromium from simulated groundwater. *Science of the Total Environment* **2017**, *601-602*, 1008–1014.

(13) Altundoğan, H.; Altundoğan, S.; Tümen, F.; Bildik, M. Arsenic adsorption from aqueous solutions by activated red mud. *Waste Management* **2002**, *22*, 357–363.

(14) Goswami, A.; Raul, P.; Purkait, M. Arsenic adsorption using copper (II) oxide nanoparticles. *Chemical Engineering Research and Design* **2012**, *90*, 1387–1396.